1. Report No. RailTEAM VT-6	2. Government Accession No.	3. Recipient's Catalog No.
4. Title and Subtitle Methods for Qualitative and Quantitative Measurement of Top of Rail Friction Modifiers (TORFM) in Revenue Service		5. Report Date September, 2022 6. Performing Organization Code:
7. Author(s) Mehdi Ahmadian https://orcid.org/0000-0003-1171-4896 and Timothy E. Mast		8. Performing Organization Report No. VT-6
9. Performing Organization Name and Address Virginia Tech Department of Mechanical Engineering 445 Goodwin Hall, 635 Prices Fork Road - MC 0238 Blacksburg, VA 24061		10. Work Unit No. 11. Contract or Grant No. 69A3551747132
12. Sponsoring Agency Name and Address Office of Research, Development and Technology (RD&T) US Department of Transportation 1200 New Jersey Avenue, SE Washington, DC 20590		13. Type of Report and Period 14. Sponsoring Agency Code
15. Supplementary Notes		

16. Abstract

This research serves to evaluate the ability of optical detection techniques for ascertaining the lubricity of revenue service track from a moving platform. A literature review is presented that covers the rail vehicle dynamics that drive the need of Top-of-Rail lubrication and directly affect the manner in which the Top-of-Rail Friction Modifiers (TORFM) and flange grease both spread down rail and eventually wear away.
The research then overviews previous rail lubricity sensors developed by the Railway Technologies Laboratory at Virginia Tech and the lessons learned from their application. The preceding field testing conducting with a modified second generation rail lubricity sensor and a rail push car is briefly summarized with emphasis on the drawbacks and issues that were used to develop the third generation sensor used for this research. The development of the third generation sensor is covered including the issues that it attempts to solve from its predecessor and the governing optical principals that govern the operation of the sensor. The laboratory evaluations conducting to commission the sensor are also covered in preparation for deploying the new third generation sensor in medium speed, medium distance revenue service testing. This includes a shakedown run on a siding in Riverside, VA prior to conducting mainline in-service testing.
Finally, this study covers the revenue service testing on in-service track conducted with the new third generation rail lubricity sensor and the accompanying remote control (RC) rail cart. The two components, when combined, create a Lubricity Assessment System which is capable of being operated at speeds upwards of 10 mph remotely from a follow Hyrail truck. The data collected from this field test is analyzed for the lubricity assessments that are able to be drawn from this initial phase of field service testing. The conclusions from this testing affirm the ability of optical methods to determine and evaluate Top-of-Rail (TOR) lubricity at higher speeds from a moving platform. Based on the continuous moving data collected for this test, several new signal traits such as the frequency associated with the passing freight cart wheels in the lubricity signal and the phantom applicator effect of transient lubricity conditions at the entrances and exits of curves can be detected and investigated.

17. Key Words	18. Distribution Statement
Top-of-Rail lubrication, new generation sensor in medium speed, medium distance revenue service testing	No restrictions. This document is available to the public through the National Technical Information Service, Springfield, VA 22161. http://www.ntis.gov

19. Security Classif. (of this report)	20. Security Classif. (of this page)	21. No. of Pages	22. Price
Unclassified	Unclassified	147	

Form DOT F 1700.7 (8-72) **Reproduction of completed page authorized.**

USDOT Tier 1
University Transportation Center
on Improving Rail Transportation
Infrastructure Sustainability and Durability

Final Report VT-6

METHODS FOR QUALITATIVE AND QUANTITATIVE MEASUREMENT OF TOP OF RAIL FRICTION MODIFIERS (TORFM) IN REVENUE SERVICE

Mehdi Ahmadian, J. Bernard Jones Chair and Director

and

Timothy E. Mast, Graduate Research Assistant

Center for Vehicle Systems and Safety
Railway Technologies Laboratory
Virginia Tech
3103 Commerce Street
Blacksburg, VA 24060

September, 2022

Grant Number: 69A3551747132

DISCLAIMER

ABSTRACT

This research serves to evaluate the ability of optical detection techniques for ascertaining the lubricity of revenue service track from a moving platform. A literature review is presented that covers the rail vehicle dynamics that drive the need of Top-of-Rail lubrication and directly affect the manner in which the Top-of-Rail Friction Modifiers (TORFM) and flange grease both spread down rail and eventually wear away. This literature review also highlights previous research in the field of rail lubrication and the benefits that rail lubricants, specifically TORFM, provide for the railroads. Finally, the literature review covers the governing optical principals inherent to the synchronous spot radiometer that has been developed for use in the research and also addresses the drawbacks and challenges inherent to applying this type of instrument to the railroad industry.

The research then overviews previous rail lubricity sensors developed by the Railway Technologies Laboratory at Virginia Tech and the lessons learned from their application. The preceding field testing conducting with a modified second generation rail lubricity sensor and a rail push car is briefly summarized with emphasis on the drawbacks and issues that were used to develop the third generation sensor used for this research. The development of the third generation sensor is covered including the issues that it attempts to solve from its predecessor and the governing optical principals that govern the operation of the sensor. The laboratory evaluations conducting to commission the sensor are also covered in preparation for deploying the new third generation sensor in medium speed, medium distance revenue service testing. This includes a shakedown run on a siding in Riverside, VA prior to conducting mainline in-service testing.

Finally, this study covers the revenue service testing on in-service track conducted with the new third generation rail lubricity sensor and the accompanying remote control (RC) rail cart. The two components, when combined, create a Lubricity Assessment System which is capable of being operated at speeds upwards of 10 mph remotely from a follow Hyrail truck. The data collected from this field test is analyzed for the lubricity assessments that are able to be drawn from this initial phase of field service testing. The conclusions from this testing affirm the ability of optical methods to determine and evaluate Top-of-Rail (TOR) lubricity at higher speeds from a moving platform. Specifically, the new sensor is able to identify several local phenomenon that demonstrate the high potential for errant evaluation of rail lubricity evaluation from spot check based methods that are solved by evaluating the track in a continuous, moving fashion. Based on the continuous moving data collected for this test, several new signal traits such as the frequency associated with the passing freight cart wheels in the lubricity signal and the phantom applicator effect of transient lubricity conditions at the entrances and exits of curves can be detected and investigated. The success of this research implores the continued evaluation of lubricity signals from a moving platform and suggests the potential of introducing one of these systems to various track metrology cars deployed throughout the United States railroads.

CONTENT

LIST OF FIGURES

LIST OF TABLES

1. Introduction

For all the benefits it provides, friction management is still not as well understood as other aspects of track maintenance. “Railroads don’t question whether friction management is good for their overall track maintenance program,” [Vennie Dyavanapalli, Loram Maintenance of Way’s Director of Friction Management] said. “But the industry is at a point where it needs to figure out how to measure its return on investment [1].

Railroads have utilized different forms of lubrication since their inception to minimize the high cycle counts and heavy loads associated with their operation. Top-of-Rail Friction Modifiers (TORFM), while a relatively new fixture in railway maintenance-of-way programs, has still been in use in some form since the early 2000’s if not before. At the time of writing TORFM has been in use in some form on United States Railroads for about two decades! In that time, numerous different experiments and reports have proven and documented the benefits of TORFM from reduced wheel and rail asset wear to reduced fuel consumption and in-train forces. There still remains the need for an instrument to accurately detect and measure the presence of TORFM to benchmark the performance of rail lubrication programs and determine the effective carry distance from wayside applicators. Because tools for evaluating track lubricity are limited, visual inspection plays a critical role in track inspection including the effectiveness of wayside lubricators [2]. This is a big challenge for the railroads as the Association of American Railroads (AAR) estimates that ineffective lubrication costs the US Railroads in excess of $2 billion each year [3].

Researchers at the Railway Technologies Laboratory (RTL) at Virginia Polytechnic Institute and State University (Virginia Tech, VT) have been studying a wide array of railroad projects for over 15 years: many of which have involved the use of optics. In contrast to the contacting methods of TORFM detection currently used by the railroads, optics provide a non-contact method that directly correlates scattered optical power with the physical presence of TORFM and Flange Grease at a micro level. Past work on the RTL Track Lubricity project has investigated the performance of off-the-shelf optical sensors and designed and prototyped custom optical systems catered to the specific requirements of collecting lubricity measurements with optics. The optical methods presented directly identify the presence of TORFM rather than attempt to intuit the track lubricity which presupposes a deeper understanding of the exact thicknesses a stochastic nature of revenue service traffic than has been found in published reports. To be sure, future research will be required to precisely identify the level of lubricity needed to optimally treat the top-of-rail surface. The commercial tools required to do so currently do not exist providing the motivation for this research project.

This research expands upon the work done by previous researchers. The existing second generation Lubricity Assessment System was modified to be mounted in a push cart and equipped with a tachometer to collect continuous spatial lubricity down track from a wayside applicator. This resulted in both laboratory assessment of the device at collecting data while moving as well as a preliminary field test on revenue service track to determine its suitability to real-world rail applications. Following the lessons learned and conclusions drawn from this 2018 field test [4], a new third generation Lubricity Assessment System was developed, benchmarked, and used in a 2019 field test again on revenue service track. Along with a new sensor, a remote-controlled rail cart was also designed and constructed allowing the test to be conducted at speeds up to 10 mph

from a follow Hyrail truck rather than at walking speeds as with the original pushcart. As a result, the November 2019 field tests with the third generation Lubricity Assessment System were able to cover approximately 5 times as much track as previous field tests.

In its current iteration, the most recent version of the Rail Lubricity Sensor offers significantly improved reliability and performance over previous iterations. The remote-control rail cart was developed to eliminate the need for a specific Hyrail truck to be provided by the railroad increasing the flexibility and availability for testing. The system is ready for immediate application for additional revenue service testing. Because the assessment is non-contact and uses light, it is anticipated that the traverse speed can be increased with little effect so long as the impact on sampling rate is considered and unnecessary vibrations are effectively mitigated. As with any emerging technology, the veracity of the Rail Lubricity Sensor will only increase as more track is tested.

1.1 Motivation

Effective rail lubrication is important to the railroads for a variety of reasons the first of which is reduced asset wear. Railroads experience large wheel-rail contact forces especially in curves. To mitigate wear, lubricants are deployed at the contact surfaces. Flange grease is applied to the wheel flange and, when flanging occurs in curves, the goal of the grease is to reduce the coefficient of friction, and therefore the wear, as much as possible. By greatly reducing the friction, flange wear is mitigated but the lateral force keeping the train on the track is preserved. At the top-of-rail surface, the load of the weight is applied to the rail by the wheel. Lateral motion of the wheelsets and longitudinal braking and tractive forces all cause wear at the top-of-rail surface. Unfortunately friction is needed here for braking, traction, and some curving forces are needed to properly orient the conical wheelsets so an ordinary grease cannot be used. Top-of-Rail Friction Modifiers (TORFM) are specifically engineering to adjust the coefficient of friction at the top-of-rail surface to an ideal amount, usually around μ=0.25 to 0.4 [5]. This preserves the necessary traction needed for good train handling and rail vehicle dynamics but significantly reduces the wear. Both Flange Grease and TORFM, when deployed correctly, reduce wear on the rail and wheels extending the life of those assets and reducing the frequency of needed maintenance. This extends the uptime of both the rail vehicles and the rail lines which is a huge benefit for the railroads logistically.

Rail lubrication also reduces the in-train forces for rail vehicle while navigating turns. TORFM reduces the force needed as the wheel sets shift laterally and flange grease reduces the grinding that occurs when the flange makes contact with the rail in curves. Reducing both of these road loads reduces the amount of energy needed to move the train. This has direct benefits for fuel consumption and the maximum tonnage that can be pulled. The FRA estimates lubrication can reduce fuel consumption by about 10% for loaded trains and 5% for unloaded. This is an average fuel savings of about 7.7% [6, 7]. Additionally, as the United States railroads embrace Precision Scheduled Railroading (PSR), they endeavor to maximize train lengths and tonnages while minimizing the amount of locomotives needed to pull the train. Proper lubrication allows for longer trains by reducing the in-train forces.

The driving component to these benefits is a reduction in lateral forces which also contributes to less rail noise, squealing, flanging, and “roaring rail,” which is a benefit for communities

surrounding the railroad [8, 9]. Noise generation is also directly caused by energy being expended through wasteful modes so a reduction in noise is also a positive indication that the lubrication is effective. The reduction in lateral forces also lowers the risk of derailment increasing the safety of the railroads as well [10].

With all of the above benefits of proper lubrication, there is a strong need for an instrument to properly evaluate the effectiveness of the wayside applicators dispensing the lubricant. The wayside applicators dispense rail lubricant onto the passing train wheels and the passing train wheels carry the lubricant down track. This method is effective and widely used throughout the United States Class 1 railroads but the effective carry distance of the lubricants is difficult to measure.

Figure 1-1: A gage face wayside applicator applies flange grease to the gage corner of the rail and the wheel flanges of passing wheels.

Existing methods for detecting rail lubricants include strain gages and tribometers. Strain gages are mounted to the web of the rail and calculate the lateral forces in the track from the strain of the rail. They are effective at identifying train curving performance and correctly intuit the presence of track lubricants when through suppression of lateral forces but can also be uncertain as different train traffic conditions can affect the loads generated in the curves. Strain gage sites are expensive to install and are not portable [11]. For Class 1 railroads with tens of thousands of miles of track it is cost prohibitive to deploy these sites widely throughout their system. Further, a large percentage of the track is in remote conditions difficult to access both for installation and for collecting and / or transmitting test data remotely.

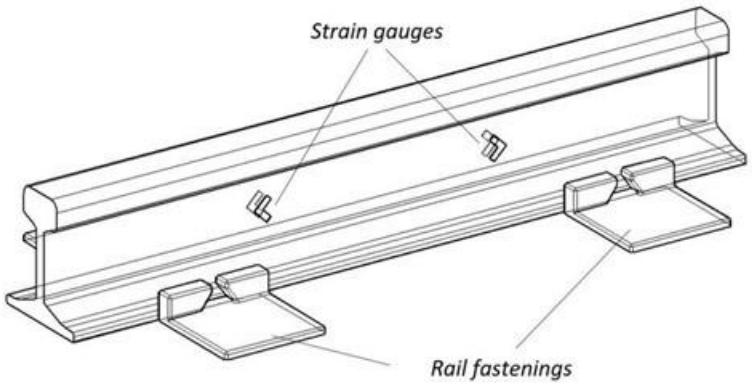

Figure 1-2: Diagram of strain gages installed on the web of the rail [12]

Tribometers use a metal wheel in contact with the rail to measure the friction at the rail head. Many are push operated requiring a maintenance-of-way engineer to walk trackside and collect measurements. This severely limits the amount of track that can be inspected and the accuracy of the data collection is also dependent on the skill of the individual inspector. The tribometer also does not impart the same forces as a fully loaded train would thus approximating the contact behavior at a smaller scale. Different tests with the tribometer have identified some issues with the repeatability and accuracy of their readings [13]. Neither of these methods directly measure the presence of track lubricants, rather they measure lateral forces (strain gages) or friction (tribometers) and intuit the presence and effectiveness of track lubricants by desired performance. There exists the need for another tool for evaluating rail lubricity.

Figure 1-3: Hand pushed tribometer for measuring the coefficient of friction on the rail surface [14]

1.2 Objectives

The objective of this project is to fill the industry-identified need for a sensor to evaluate track lubricity. As with any sensor designed for railroad application, there is a need for the sensor to be able to be used safely, accurately, and quickly. The goals for this project are to:

- Expand on previously conducted research with additional laboratory and field testing with a focus on moving testing
- Continue hardware development to improve repeatability of sensor and increase robustness against adverse environmental conditions
- Conduct longer distance field testing over multiple wayside TORFM applicators
- Provide analysis of presence / absence of TORFM and Flange Grease from instrument data
- Estimate TORFM carry distance from field testing data and provide a preliminary diagnosis of the track condition from field test
- Demonstrate the ability of the sensor and rail cart to conduct lubricity testing while in motion

1.3 Research Approach

There are three distinct, separate elements of research presented. The first is laboratory evaluation of Rail Lubricity Sensors. The Railway Technology Laboratory has a 40 foot track panel located in at the Center for Vehicle Systems and Safety (CVeSS). The track panel was removed from revenue freight service so the top-of-rail surface is sufficiently worn and accurately represent the bare metal condition of revenue service track. During laboratory evaluation, different top-of-rail lubricity conditions are prepared and optical measurements are taken from the cart running over the track panel surface. The track panel is indoors and isolated from weather related effects. Using a 3 step cleaning process, the track can be cleaned to return it to a bare metal condition and then a variety of sample TORFM and Flange Grease materials can be applied to the rail. This allows for clean rail comparisons that are not typically possible in field service testing allowing for clear identification of the optical effects of lubricating the rails when only the presence or absence of TORFM is altered. Laboratory results are analyzed in MATLAB and semi-permanent start and stop marks can be freely placed on the track panel allowing for the isolation of localized surface features.

The second element of research involves testing the Rail Lubricity Sensor on revenue service track in collaboration with our industry partner. While rail lubricity conditions can be artificially manufactured in a laboratory setting, the primary goal of the research is to develop a sensor to measure accurate rail lubricity conditions. The lack of such a sensor makes accurate replication of the stochastic application of track lubricants by passing trains impossible in a laboratory setting. In particular, it is often found that far thinner layers of TORFM that have been packed into the surface figure of the steel by heavy axle loads are still effective and detectable even though those conditions are almost impossible to create in the lab. Field testing requires transporting the instrument and cart to the test site and, with the oversite of maintenance-of-way personnel, conducting a moving sweep of the cart and sensor over the track while following all safety protocols and managing the test inside of the track authority window from the dispatcher.

Both of the previous research methods require post processing of the raw data in MATLAB following the data collection phase. This involves averaging and low pass filtering to identify long term trends, high pass filtering and variance calculations to investigate dynamic features of the data, and frequency domain analysis to isolate specific frequency content. It is understood that the data signals contain far more information than just the lubricity component. The scope of this study is directed at conducting lubricity evaluation while the sensor is in motion and verifying that the

sensor is still able to perform. If this is demonstrated, future steps can involve collecting additional sections of data and will involve a deeper level of signal processing. Data analytics of a larger selection of test data will increase the accuracy of lubricity detection and for the investigation of other trends that may be predictive of other track conditions.

Figure 1-4: Remote Control (RC) Rail Cart and Third Generation Rail Lubricity Sensor setup on track and ready to begin field testing on revenue service track

1.4 Contributions

The results of this study demonstrate both the ability of custom optical devices to detect the presence of rail lubricants and the viability of implementing these optical detection methods in moving testing on revenue service track. This is a significant step in creating an instrument that is available for widespread application across the United States railroads and abroad.

Figure 1-5: Field Testing with Rail Push Cart and Second Generation Rail Lubricity Sensor in the summer of 2018

Using the lessons learned from the trial field test with the push cart and the second generation sensor, a third generation sensor was developed with moving testing in mind. To aid in the development of the third generation sensor, several laboratory evaluations were done with different wavelength laser diodes and other optical devices including some LIDAR based sensors. In parallel, a new remote controlled rail cart was designed and constructed to allow for faster traversing speeds for moving testing. Once the rail cart and sensor were assembled, commissioning testing and a shakedown run were performed on the two new test instruments now combined into a Lubricity Assessment System.

Following successful commissioning testing, the Lubricity Assessment system was evaluated on revenue service track with assistance and guidance from our industry partner. This 5 mile field test represents a medium range field test: far longer than the preceding short distance field testing and far shorter than future high speed system wide evaluation. This data was processed and evaluating in consult with industry experts to validate the ability of the instrument to perform in-service testing on revenue service track. Successful initial field testing with the Lubricity Assessment System demonstrates its viability as a test unit for expanded medium to long distance testing in the future.

1.5 Report Outline

In this study, chapter 2 will offer a more comprehensive literature review of the rail vehicle dynamics that drive the need for rail lubricants and the effects of rail lubrication. It will also cover

the fundamental properties of optical measurement methods, and the prevailing track surface condition and geometry and their effects on optical methods.

Chapter 3 will cover the conclusions from testing conducted with previous rail lubricity sensors that drove and informed the design for the third generation rail lubricity sensor. It will include the laboratory benchmarks conducted for the third generation Rail Lubricity Sensor prior to being deployed for the intermediate distance Field Testing. This includes a shakedown run at a passing siding in Riverside, VA.

In November of 2019, an intermediate distance field test was conducted with the third generation Lubricity Assessment System. This intermediate test is so-called because with the implementation of a remote controlled rail cart the field test was able to cover about 5 miles of track, significantly more distance than any previous field test. “Intermediate” was chosen with a future “long distance” field test in mind that would conceivably involve the sensor mounted to a track metrology car capable of traveling track speeds and covering hundreds of miles in a test. This November field test significantly improved upon previous field tests in the quality of instrument deployed and the evaluation of multiple wayside lubricators. Chapter 4 covers the design of the remote control (RC) rail cart, the planning and logistics of the field testing, and the actual field test itself and the resulting raw data.

Chapter 5 covers the data processing of the November field test including the signal processing, averaging, and frequency analysis of the lubricity data. Some analysis and conclusions will also be covered in this section with final conclusions of the overall project covered and summarized in Chapter 6.

2. Literature Review and Background

This chapter contains a comprehensive literature review covering the background information needed to understand the research being conducted. There is an overview of the wheel and rail features that are necessary for supporting the vertical load of the train and creating the steering forces needed to navigate through curves. This demonstrates the forces that provide the need for rail lubrication to reduce the wear forces caused by train traffic. Some issues and challenges identified during the history of applying rail lubricants is then presented. This issues raise questions about the rail lubricity condition of the rails and presents the need for a sensor to identify lubricity conditions and inform decisions needed to improve wayside lubricators on the railroads.

Based on this need, an overview of optical systems is presented to provide background on the principals that are integral to the operation of the optical sensors developed for this research. With these fundamentals explained, it is possible to revisit the application of optical instruments on railroad applications. Several conditions inherent to railroad application are uncommon to classical laboratory based optical methods. Several factors relating to the surface condition and wear angles of railroad tracks make repeatable optical measurements challenging when these optical methods are applied to railroad applications. Knowledge and understanding of some of these complications is necessary to understand the results and methods employed in this research.

2.1 Rail Vehicle Dynamics Overview

At a fundamental level, railway vehicles are largely unchanged since the early seventeenth century. A wheelset is comprised of two wheels mounted onto a common rigid axle and rides on a pair of rails. A cross section of a 136 pound per yard AREMA rail is shown below with some reference zones added.

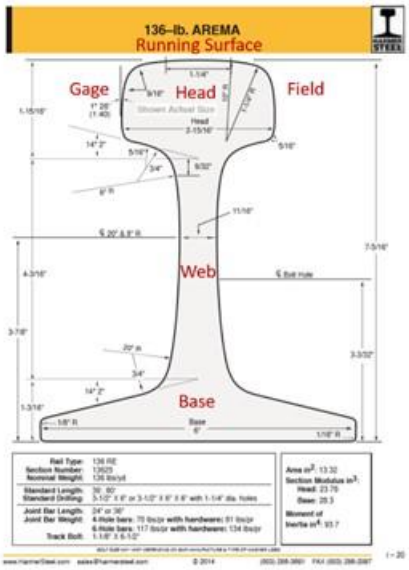

Figure 2-1: 136lb/yd AREMA Rail Cross section from Harmer Steel with annotations [15]

The distance between the inside of the two rails is called the track gage. It is measured 5/8 inch below the head of the rail. US standard gage track is 56.5 inches or 4 foot and 8.5 inches. A comparison of various track gages used throughout the world is shown below.

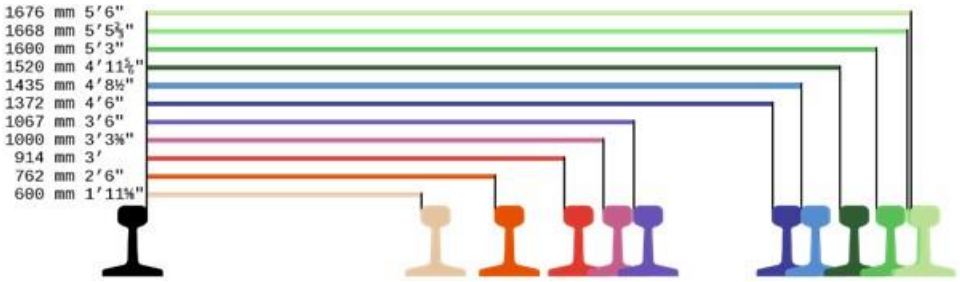

Figure 2-2: Comparison of various railway track gauges [16]

The wheel rides along the top of the rail as shown in the figure below. A wheel flange is inside the track gage to keep the wheelset on the rails. The primary load is supported by the wheel tread on the running surface of the rail. Over time this wears as shown by the red line compared to the new, unworn wheel profile in blue.

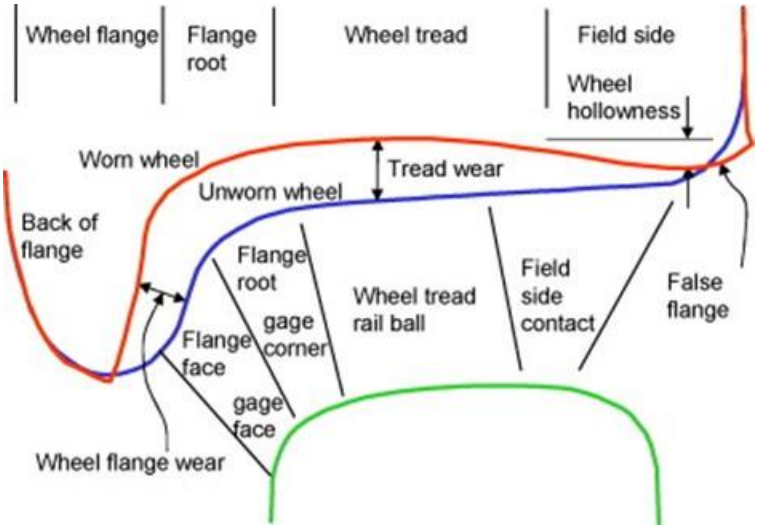

Figure 2-3: Worn and unworn wheel profiles [17]

Flanged cylindrical wheels are capable of navigating track structures and are still acceptable on low speed and / or low tonnage applications. Many wooden roller coasters use cylindrical flanged wheels. With this configuration, the flange is the only element applying a guiding force to the rail vehicle through contact with the gauge face of the rail. In curves, cylindrical wheels face another issue: the outside wheel is required to cover a farther distance than the inside wheel in the same number of revolutions because they are connected with a rigid axle. This leads to a high wear situation not only from the high force at the wheel flange but also at the top-of-rail surface because the wheels want to spin at different speeds.

Tapering or coning the wheels allows the wheel set to shift left or right and create a rolling radius difference. This is demonstrated by Redtenbacher's formula [18] and the figure below:

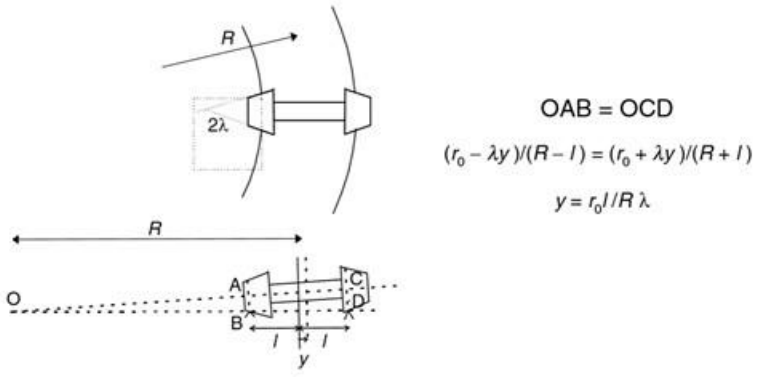

Figure 2-4: Redtenbacher's formula for the rolling of a coned wheelset through a curve [19]

The rolling radius difference allows the outside wheel to have a larger diameter and the inner wheel to have a smaller diameter causing them to now travel different distances every revolution. This allows rigid wheelsets to steer through curves and allows for greatly reduced wheel-rail contact forces. In wide curves, there is adequate lateral shift to allow for curving without flange contact. In tighter curves, the lateral shift is eventually exhausted when the wheel flange makes contact with the outside rail. This is called "flanging" and results in added contact and wear forces. The rolling radius difference caused by the lateral shift of the conical wheels generates a portion of the curving forces needed with the flange contact providing the rest while keeping the wheel on the rail. The figure below shows the forces on the wheelsets in a centered (a) position and a maximum lateral shift with flange contact (b).

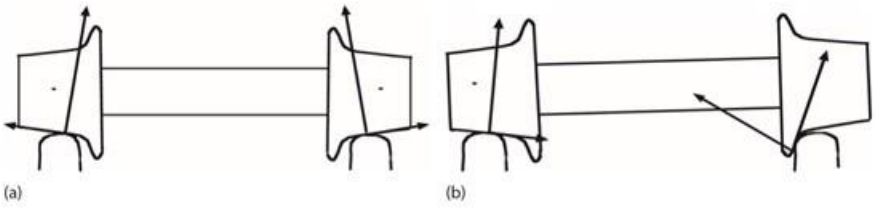

Figure 2-5: Forces on a conical wheelset in neutral and curving positions [19]

Coning of the wheels has a large impact on reducing rail and wheel wear in heavy haul rail applications and is widely adopted by railroads world-wide. There is, however, a cost associated with tapered wheelsets in terms of dynamic stability. Adding taper to the wheels introduces lateral oscillations. Klingel derived the relationship for the kinematic oscillation wavelength (Λ) for a wheelset in 1883 [20]. Klingel's equation requires as input parameters the wheel rolling radius (r_o), ½ of the lateral distance between contact points (l), and the effective conicity of the wheel (λ).

$$\Lambda = 2\pi\left(\frac{r_o l}{\lambda}\right)^{\frac{1}{2}} \quad (1)$$

This dynamic instability is referred to as "hunting" and is represented in the figure below. Hunting is bad for a couple reasons. Because hunting is a dynamic instability it is directly affected by the train velocity and can present harmonic oscillations that can amplify and cause a derailment. The lateral motion also saps energy from the train and results in a larger amount of tractive force to be applied by the locomotives. This increases fuel usage and reduces the amount of tonnage a locomotive can pull. Finally, the energy loss from the hunting is transferred into the wheels and rails in the form of contact forces and wear.

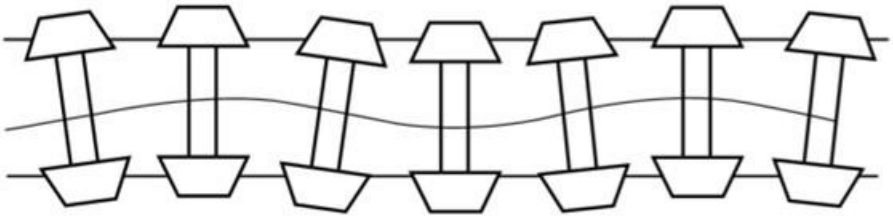

Figure 2-6: Kinematic Oscillations of a hunting wheelset [19]

For railroad applications, traditional physics assumptions of rolling without slipping are often not valid. Creep occurs when the speed of the wheel and the rail is not equal. The concept of creep was introduced by Osbourne Reynolds and applied to power transmission from belts [21]. The same concept was applied by Carter in the effort to identify the source of hunting [22]. Creep is defined along three vectors: longitudinal which is forward along the direction of travel, lateral which is perpendicular to the direction of travel, and spin which is a rotational creep around the vertical or normal axis [23].

$$Longitudinal\ Creepage\ \gamma_1 = \frac{V_x^{Wheel} - V_x^{Rail}}{V} \quad (2)$$

$$Lateral\ Creepage\ \gamma_2 = \frac{V_y^{Wheel} - V_y^{Rail}}{V} \quad (3)$$

$$Spin\ Creepage\ \omega_1 = \frac{\Omega_z^{Wheel} - \Omega_z^{Rail}}{V} \quad (4)$$

$$Mean\ Velocity\ V = \frac{\mathrm{V}_x^{Wheel} - \mathrm{V}_x^{Rail}}{2} \quad (5)$$

In more practical terms, in a free rolling scenario a wheel revolving 100 times would cover a longitudinal distance down the rail of 100 circumferences. If instead there was a 1% positive creep the wheel would now rotate 101 time but only cover a distance of 100 circumferences. The distance

lost would be the result of incremental slippage at the contact patch. The ratio of stick to slip decreases until pure slipping takes over. At this point the behavior is driven by pure Coulomb friction of two bodies sliding past each other. Any point between pure rolling and full slip contact is an amalgam of those two contact behaviors and affects the shape of the contact patch [5].

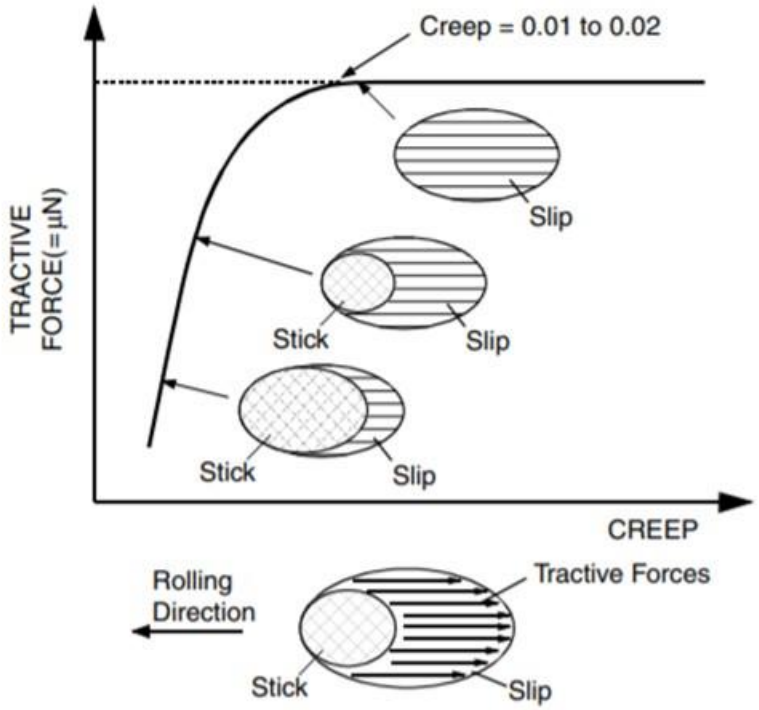

Figure 2-7: Plot of Tractive Forces vs Creep and Stick/Slip regions of rolling contact [19]

The figure and example above is in terms of longitudinal creep forces but lateral creep forces and spin creep forces also occur during the lateral shift of wheelsets into curves. For the context of this study, it is important to understand that increasing amounts of creep result in higher amounts of wheel and rail wear at the top-of-rail surface.

2.2 Rail Lubrication Motivation

In the previous section, numerous points of wear and energy loss were identified from train dynamics. Each point of contact is an opportunity for energy to be expended while the train is moving decreasing the train efficiency. Track lubricants are proven to be effective and as a result are widely adopted by railroads in North America. The key benefits of lubrication include extended asset life or the wheels and rails, increased fuel efficiency or pulling capability for motive power, and a reduction in lateral forces which can decrease the risk of derailment [5].

Rail lubricants are divided into two primary different types: flange greases and top-of-rail friction modifiers (TORFM). Flange greases are a type of lubricant applied by a gage face wayside applicator to the gage corner of the rail. Gage face applicators are also commonly referred to as flange greasers. They act as a lubricant between the wheel flange and the gage face of the rail to

reduce friction in curves. Flange greases are designed to have frictional coefficients of less than 0.2 [5]. Top-of-rail friction modifiers (TORFM) are applied to the top-of-rail surface and act as a friction modifier rather than a traditional lubricant. A friction modifier is an engineering substance that is designed to alter the coefficient of friction to an optimal amount. TORFM is applied to the rail head to act as a third body layer and modulate the coefficient of friction to an ideal amount, usually between 0.25 and 0.4, for traction and adhesion while also reducing contact forces and wear that unnecessarily deplete the service life of the wheel and rail [5]. The TORFM creates a third body layer between the wheel and the rail and transmits longitudinal tractive forces while acting as a protective interface against wear forces from sliding. TORFM is applied at a TOR (top-of-rail) wayside applicator and the wiper bars for such an applicator are located on the field side of the rail rather than the gage side as with a flange greaser or gage face applicator.

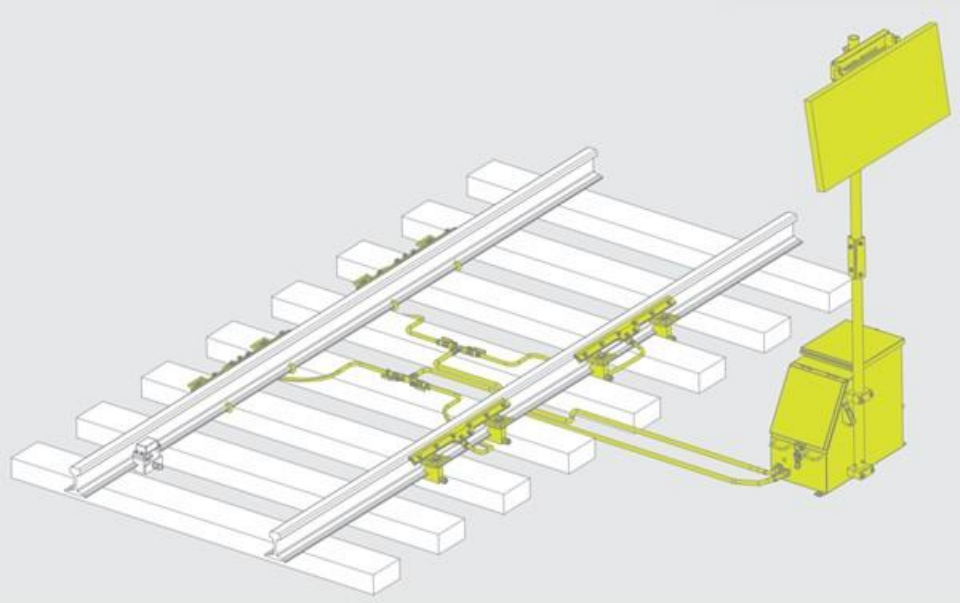

Figure 2-8: TOR Wayside Applicator diagram [24]

The strongest and most direct motivation of applying lubricants to the track is the immediate reduction in wheel and rail wear. Track maintenance is a significant expense for the railroads. A 2013 Association of American Railroads Annual Spending document shows that American railroads spent $8.9 billion maintaining infrastructure and equipment [25]. A significant reduction in rail and wheel wear can have a significant impact on the maintenance spending for the railroads. Field deployments of TORFM from wayside applicators have demonstrated reductions of rail wear between 30-60% [26]. Reducing rail wear also has the secondary effect of reducing rail grinding requirements. Rail grinding requirements may also reduce from deeper corrective rail grinding to lighter preventative rail grinding further reducing the rail grinding costs. Rail grinding is estimated to cost the American railroads about $130 million per year [25, 27]. From a safety perspective, this also reduces the maintenance intervals for maintenance-of-way crews reducing the amount of railroad personnel that need to be in potentially hazardous situations in the field. From an operations perspective, this increases the service life of the rail lines and decreases the amount of downtime needed to perform maintenance. This increase in rail line uptime reduces traffic congestion and allows trains to move more freely.

The reduction in asset wear will have a secondary impact on the logistics side of the railroads business. Reduction in stops, slow orders, and traffic restrictions will increase the network throughput and decrease the dwell time of trains on the road. This will reduce idling and unnecessary starting and brake applications. Adequate rail lubrication also reduces the amount of energy needed to move the train. This further increases the train efficiency which can be used to lower fuel consumption or increase the train tonnage per locomotive. United States Department of Transportation (DOT) and Federal Rail Administration (FRA) testing found on average TORFM application could provide 7.7% fuel savings during testing with CSX in June 2000 with higher savings on loaded trains than empty trains. At a reported $3.2 billion spent on fuel every year, a 7.7% reduction in costs provides a significant opportunity to reduce costs [6, 7, 28] This is all a result of the decrease in the amount of energy required to move the train. Especially in territories where there are a large number of curves, application of TORFM can significantly reduce the amount of power consumed while moving the train [10].

The major component in reducing energy consumption is the reduction in lateral forces. The FRA reports a reduction between 30-40% in lateral forces from the application of TORFM from a test in 2006 at the FRA's Facility for Accelerated Service Testing (FAST) at the Transportation Technology Center (TTC) in Pueblo, Colorado [11]. Reduced forces improves the curving performance of railroad trucks. More interestingly, research presented in Wear in 2005 by Akira Matsumoto et al. shows that the reduction in lateral force from TORFM can also reduce the risk of derailment. Matsumoto et al. found that the derailment coefficient was reduced to about 1/3 with TORFM compared to without in a 200m (656 ft) radius curve [29]. As previously mentioned in the introduction, the reduction in forces can also reduce the amount of noise [8, 9]. Some of the energy lost when the rail is not adequately lubricated is dissipated through noise so a reduction in noise indicates that less energy is being lost. Increasing safety and decreasing noise is also desirable for the surrounding communities that the railroads operate through.

2.3 Challenges and Issues with Rail Lubrication

Clearly, it is accepted that, despite the high investment cost, rail lubricity programs are overwhelmingly beneficial. The implication that follows is that there is a significant penalty to the railroads if they fail to lubricate their rails adequately. Sweden installed about 3000 wayside lubricators in 2000, an investment cost of about 7.9 million United States Dollars. It was determined that the alternative was to allow excess rail wear and more frequent rail replacement which would be far more costly [27, 30]. This can be as simple as failing to capitalize on the significant investment in wayside lubricator infrastructure to more indirect issues relating to poor train handling and unnecessary waste in excess wear in the wheels and rail and extraneous dispensing of track lubricants.

The fundamental failure mode for a track lubricity system is failing to dispense enough, or any, track lubricants. As a direct result, detecting and understanding inadequate disbursement of track lubricants is a major metric that railroads need to be able to measure. Clogged nozzles, failed wheel sensors, empty reservoirs, and broken pumps are all catastrophic failures that need to be identified and fixed quickly for the investment lubricating infrastructure to be beneficial [5, 27]. Tuzik reports that uptime is the key metric for wayside lubricators and that uptime falling below 50% as not uncommon on United States Class 1 railroads. The need for useful tools for determining

lubricity conditions is even direr when coupled with the strong demand for track time between revenue service trains and maintenance-of-way operations. “NRC’s Rob Caldwell [points] out: The most effective lubrication / friction management program can go for naught, if it’s interrupted by something as simple as letting the reservoir run empty” [1]. When lubrication systems fail, the entirety of the capital investment of the infrastructure becomes effectively worthless until the system is running again. During this time, rail wear and wheel wear all dramatically increase and the return on investment drops to zero.

Once the issue with reliability and uptime is addressed, the next issue that arises is dispensing the correct amount of lubricant. The penalty for dispensing too little lubricant is the same as dispensing no lubricant only to a lesser magnitude. Insufficient lubrication allows for higher than necessary wheel and rail wear and decreases the efficiency of the trains operating on that section of track. The other case would be dispensing excess lubricant. Although rail lubricants are typically environmentally neutral and some operators are using biodegradable lubricants, residue from extraneous lubrication can be harmful to the environment. Over dispensing lubricant at the applicator is very expensive. The Association of American Railroads estimates that $2 billion is spent in improper lubrication [3, 27, 31].

Excessive lubrication can lead to adhesion loss for the locomotives. This affects both physical train dynamics and operator behavior. Adhesion loss may cause the operator to turn on the sanding system on the locomotive as a traction enhancer which counteracts the benefits of the modified friction at the top-of-rail surface. Adhesion loss may also cause wheel slip, rail burns, and potentially even stalling of the train [5]. Wheel slip or stalling of the train can cause operational delays for the rail network. This can have a cascading effect where the loss of adhesion for one train can cause delays for all of the train traffic on the same line. A stalled train would block the rail line until a rescue train can be dispatched to clear the line.

Adhesion loss can also affect braking performance for trains [5]. Tuzik points out that this is most certainly a red flag for railroad operators and should be particularly true for passenger operators [1]. The actual consensus on whether TORFM affects braking performance is contested. In the United States, several Federal Railroad Administration reports claim no issues with braking or train handling [7, 28]. Deutsche Bahn (DB), the German railroad infrastructure owner, reported low friction conditions affecting braking performance [13]. DB conducts both passenger and freight operations.

Tractive forces at the running surface are also essential for correctly orienting railroad wheelsets through curves. The longitudinal creep forces steer the wheelset into the curve and laterally outward so that the rolling radius offset can compensate for the difference in distance travelled by the outer rail and the inner rail.

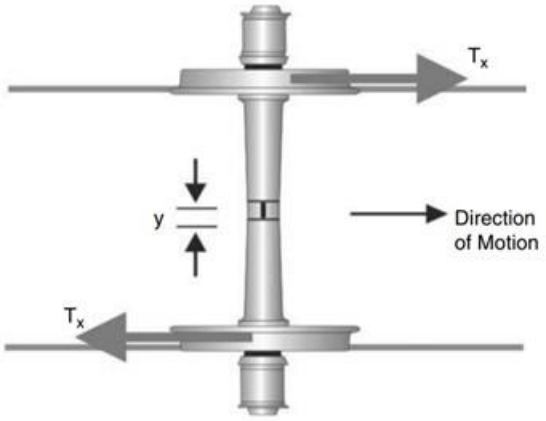

Figure 2-9: Steering Forces on a wheelset [19]

If the top-of-rail longitudinal tractive forces are removed, a couple undesirable vehicle dynamic characteristics occur. Without steering forces, the wheelset will continue forward until the leading axle in the truck makes flange contact with the outer rail. This causes a high contact force on the wheel that is flanging since the flange contact is the only force steering the wheelset around the curve. The opposite side wheel on the trailing axle will also fail to steer and be forced towards the inside rail gage corner as the curve turns in. This is called anti-steering because the bogie is turned counter to the direction of the curve. In this condition, the inside wheel is flanging and has a higher rolling radius than the outside wheel which, because it is shifted laterally inwards, now has a smaller rolling radius. This results in large longitudinal creep forces also driving the anti-steering moment and drives poor curving dynamics. The high longitudinal creep on the rear axle in particular is a large increase in wear conditions. This will first decrease the carry distance of the TORFM as it is sheared off from high creep and then increase the wear condition at the top-of-rail surface. In addition, the rear wheelset on the truck is now flanging with the inside rail creating additional contact [23, 32].

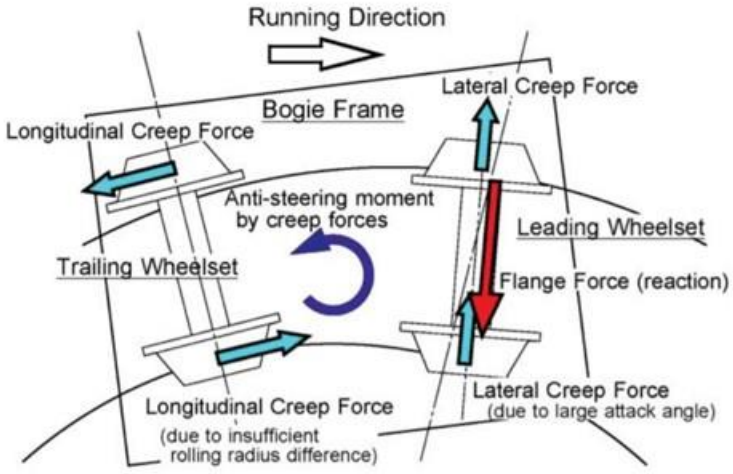

Figure 2-10: Anti-steering forces and moment on a three piece truck [33]

Finally, flange grease contamination on the top-of-rail surface can counteract the benefits of the TORFM. Excessive flange grease can flood the track structure and allow the grease to migrate to unwanted areas. It is also thought that high flanging forces can pump excess flange grease onto the top-of-rail surface. The presence of flange grease on the top-of-rail surface can alter the surface adhesion of the TORFM films and cause poor wetting of the running surface. This can cause uneven coverage of the TORFM on the rail head limiting the effectiveness of the friction modifier. Once the grease is mixed with the TORFM, the coefficient of friction drops because of the flange grease lowering the adhesion of the wheels and resulting in all of the previously mentioned issues related to adhesion loss [34]. Keeping the appropriate rail lubricants in the correct regions of the rail surface is a careful balancing act and demands that the dispense rates of the wayside applicators be set correctly. Setting these parameters will, no doubt, be an iterative process with parameters that need to be tailored in accordance with the specific and unique track geometry conditions for each curve. With large rail systems and a wide variety of track layouts, this demands accurate and fast tools to be useful for track engineers.

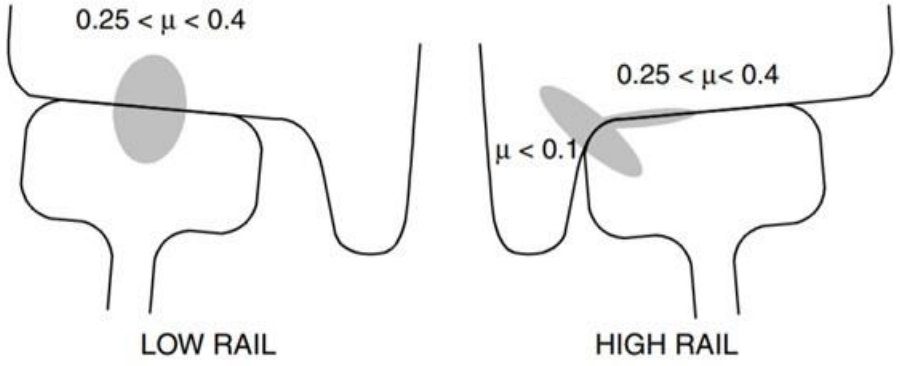

Figure 2-11: Ideal friction coefficients for different wheel-rail contact points [19]

From a financial perspective, there is a significant challenge in justifying the costs associated with the upkeep of a track lubrication program when the benefits are spread between multiple operating groups. Tuzik notes that the different functional groups, Track Maintenance, Mechanical and Rolling Stock, and Operations, are often separate entities in a large organization. This drives a need to precisely define a return on investment to present to higher level figures in the rail organizations to justify the added expenses in materials and maintenance for the wayside lubricators to lower the overall cost of maintenance and operations [1]. This in turn drives the need for precise measurements on the effectiveness of TORFM and the wayside applicators.

The March 2004 FRA report on "Locomotive-Based Top of Rail Friction Control Implementation Results and Issues" concludes a couple of issues to this effect. The first issue raised was the variance in lateral force readings. There was significant variance on raw force readings based on train speed, tonnage, and track curvature. This was also true between trains equipped with TORFM systems and those without. This indicates that a single force site measurement cannot absolutely determine lubricity with a single reading. This was expended on by the need to conduct longer term monitoring of each curve on a route. This further demonstrates that the placement of wayside lubricators will likely not be a one-size-fits-all approach [7].

An April 2006 FRA report on using Dynamics Rail Deflection also helps to illustrate the challenges with detecting TORFM. The TORFM applications on the rail head are very thin films that are often not visible to the human eye [11]. Strain gage sites are certainly able to measure the reductions in lateral forces that provide the benefits of rail lubrication but remain expensive to install and maintain. Likewise, tribometers can be effective tools of measuring ideal friction coefficients at the rail head but cannot exactly recreate the contact forces associated with true wheel-rail contact of passing trains [13, 34, 35]. FRA reports from June 2000 and March 2004 even disagree as to whether TORFM is entirely consumed by the passing train [7, 28]. This of course strongly depends on the amount of TORFM applied and the number of axles, tonnage, train speed, and other train metrics as well. This suggests that accurate evaluation of a rail lubricity program will likely require a holistic approach. A vehicle mounted system that could be applied to a track metrology vehicle presents a compelling opportunity where historical data can be captured and synthesized with rail profile measurements, rail replacement intervals, annual train tonnages, wayside applicator uptimes, and any other relevant metrics to make informed decisions and track iterative adjustments. This also highlights the significant challenge in accurately detecting the presence of TORFM, especially with the existing contacting methods.

2.4 Overview of Optical Measurements

All optical methods begin with a light source. In this case, a laser diode was selected to take advantage of the single wavelength and spatial coherence properties unique to lasers. The single wavelength allows for narrow optical interference filters to be used to tightly control the light allowed to pass to the photodetectors. The spatial coherence constrains the optical signal to a single columnar spot. This allows the optical instrument to operate as a spot photometer adopted and investigate a specific spot on the rail surface instead of gathering optical reflectance information from all of the area illuminated by an unfocused light source. An illustration of planar, spatially coherent laser waves versus a diverging and converging spherical waves is shown below [36]. Note that even if a spherical wave is focused to converge at a single spot, the incoming light rays will be incident at a wide variety of incident angles which will have a strong effect on the optical reflections.

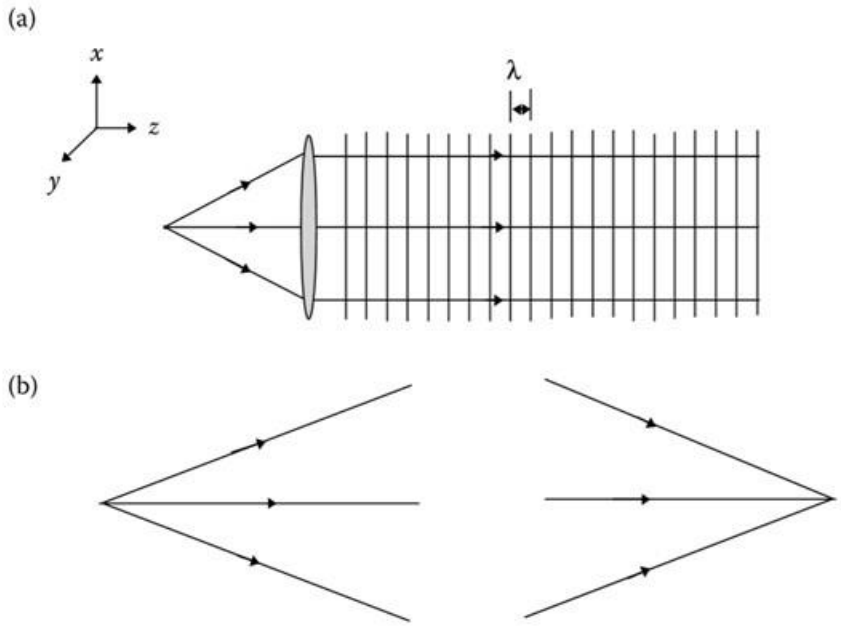

Figure 2-12: Planar wave (a) compared to diverging and converging spherical waves (b) [36]

For the optical measurements in an experimental setting that demands consistency, single wavelength and spatially coherent waves provide a significant increase in uniformity. This removes variance in scattering from the light source itself and instead allows all of the scattering to be a function of the incident surface that is being measured [31, 37].

When the light hits a surface, the light is scattered and reflected based on the material properties. For mirrors the light is reflected at near 100% based on the quality of the mirror. For highly polished steel surfaces, the reflectivity is above 90% [38]. Light that is not reflected can either be transmitted into the material or scattered. For solid, opaque materials, the transmissivity of incident light is incredibly low. The reflected and scattering effects are the key phenomenon exploited for optical detection on this project. There are two types of scattering: specular and diffuse. Specular scattering is the mirror like scattering where the reflected angle is equal to that of the incident angle. This specular scattering is very strongly angle dependent and the reflected intensity drops off significantly outside of the reflected angle. Diffuse scattering is driven by Lambert's cosine law where the scattered optical power is directly related to the angle [39]. A figure demonstrating the optical scattering lobe of diffuse, or Lambertian, scattering is shown below.

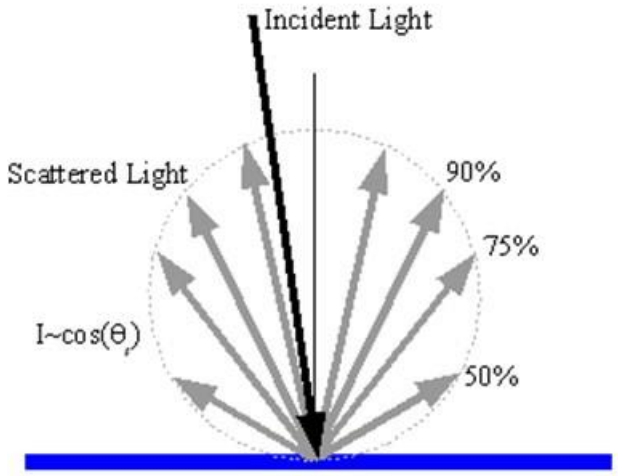

Figure 2-13: Lambertian Diffuse Scattering power at various angles [40]

In addition to optically scattered light, fluorescence is also used to detect changes in third body layers on the top-of-rail surface. Fluorescence is inherently different from optical scattering. The optical scattering is reflected light that rebounds off the incident surface without being absorbed. Materials with fluorescent properties absorb incident light, typically in the ultra-violet band, and reemit the light from vibrations inside the material structure of the fluorescent target [41]. The process of measuring the fluorescence of a sample is called "Fluorescence spectroscopy" and uses a fluorescence detector, or fluorimeter, to detect the optical power generated and emitted by the fluorescent sample [42]. The carriers and organic components of the track lubricants tend to have fluorescent properties that the bare rail steel does not. By pumping ultra-violet light into the target spot, resulting fluorescence signals can be identified as an indication of track lubricants on the top-of-rail surface.

The other half of the optical system is the photodetectors. For the fluorescence sensor, a fluorimeter is mounted in the sensor chassis for the sole purpose of detecting the fluorescence effect. Optical filters play an important role in isolating specific signals when multiple detectors are mounted in the same sensor chassis. For fluorescence, the wavelength of the reemitted light is typically a longer wavelength as the luminescence is lower power than the incident light. This allows optical filters to be installed that block the wavelength of the ultra-violet light that is exciting, or pumping, the fluorescent sample and isolate only the fluorescent signal that is emitted from the sample. Conversely, the monochromaticity of the laser allows for the scattering detectors to have optical filters with very narrow passbands. The narrow passband allows only light with a frequency very close to that of the incident light to be transmitted to the photodetectors. This limits the interference of light that was not introduced by the sensor. The scattering photodetectors are aligned relative to the target spot to receive scattered light at specific angles. The scattered power at these angles will be governed by the aforementioned Lambert's Cosine Law, the equation for which is presented below where I is the scattered intensity, I_0 is the intensity of the incident light, and θ_s is the angle of scattering [40].

$$I(\theta_s) = I_0 * \cos(\theta_s) \tag{6}$$

The optical instrument designed and used for this research is based on the concept of a spot photometer. The instrument is based on radiometry instead of photometry. Radiometry is grounded in measuring electromagnetic radiation in contrast to photometry which is grounded in the optical response to the human eye. As a result, radiometry uses watts as a base unit while photometry uses lumens. The key radiometric quantities are power, radiant intensity, and irradiance. Irradiance, H, is the power over the surface are measured in SI units as $Watts/m^2$. Radiant intensity, J, is instead a function of solid angle, Ω, and has SI units of *Watts / Steradian*. The power is in units of Watts [43].

When the laser light is emitted from the sensor to the target, it has a power in Watts and based on the beam size can be characterized by an Irradiance. When the laser hits the target, the Lambertian scatters the optical light radially from the incident spot. The hemisphere of scattered light rays is characterized by radiant intensity and the power in any direction is a function of the Steradian portion of the hemisphere that is collected. That is, the scattered light is a function of the spherical coordinate system of the aperture with respect to the scattering sphere. By calculating the solid angle, Ω, of the aperture, the collected optical power can be integrated.

2.5 Top-of-Rail Surface Condition and Track Geometry Complications

The rails and track structure are located in outdoor environments and as such are subjected to weather conditions year round. In addition, wheel/rail contact induces heavy forces onto the rail steel often exceeding the elastic limit and work hardening the metal [44]. By these wheel/rail interactions, surface roughness and defects can be present on the top-of-rail surface changing the scattering properties of the rail in a stochastic manner. This introduces an unknown surface roughness into the optical readings that can be difficult to filter out. Surface roughness has several definitions but for this research, surface roughness is defined by the root-mean-square, or RMS, roughness of the geometric microstructure of the surface [39].

Several papers have been published explaining methods of using optical measurements to determine surface roughness [45, 46]. Throughout the history of Rail Lubricity research at the Railway Technologies Laboratory, different metrics have been trialed for their versatility and detectability of rail lubricants [31, 37]. Early detection metrics relied on specular reflections which presented challenges that will be addressed in the next section. The most recent and successful metric has been a simple gloss ratio. Optical gloss is derived from the equations of Augustin-Jean Fresnel. The Fresnel equation for optical gloss, or specular reflectivity, is given below where I_0 is the incident intensity, I_R is the specular reflected intensity, and R_s is the specular reflectance or optical gloss [47].

$$R_s = \frac{I_R}{I_0} \tag{7}$$

Optical gloss is an ideal metric for determining TOR lubricity because layers of tend to cause a slight haze effect when compared to shiny, clean rail steel. This effect is very hard to determine without a direct comparison between clean and lubricated rail and only in very heavily lubricated conditions where the difference in surface friction can be easily felt tactilely on the rail head. This

slight hazing effect does illustrate the ability of optical gloss measurements to be used to ascertain rail lubricity. By replacing human vision with quantitative photodetectors, smaller variances in optical gloss can be observed and measured even if the difference in signal is minute.

Figure 2-14: Clean vs Lubricated Rail Comparison [4]

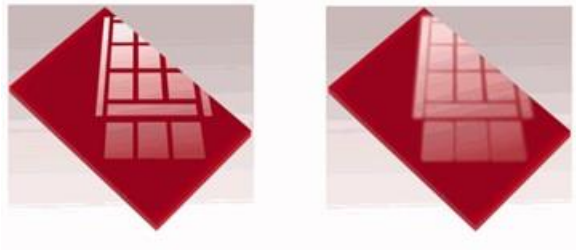

Figure 2-15: High Gloss Surface (Left) vs Low Gloss with Hazing (Right) [48]

All of the optical properties presented so far presume a level, flat incident surface. This is not the case for optical methods conducted on a rail surface. The figure below taken from an article written by Brad Kerchof on rail profiles shows that the surface normal on the top-of-rail surface is not level or flat [49]. In fact, the rail head is not necessarily flat and is often crowned or sloped from rail wear. This head slope introduces another stochastic variable the needs to be accounted for while making optical measurements of track structures.

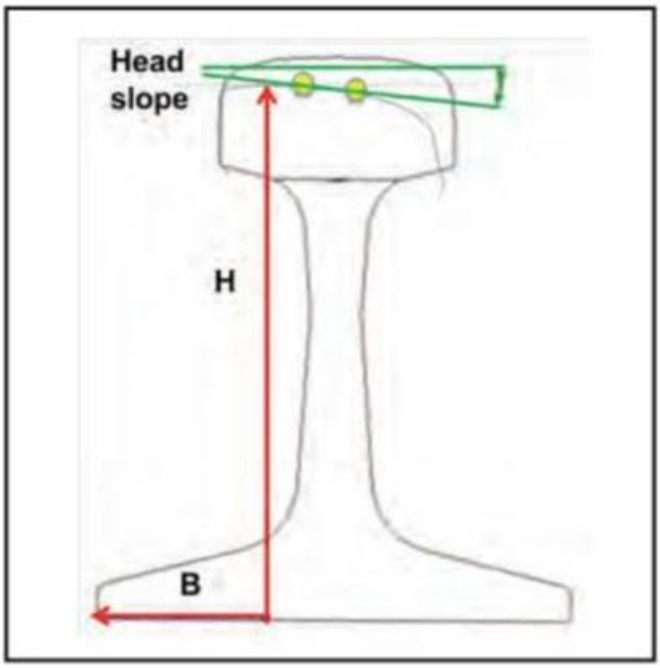

Figure 2-16: Worn Rail cross section with head slope annotation [49]

The figure below shows the orientation of the incident laser beam and the shape of the diffuse scattering lobes for laser measurements on the rail head. The lines as drawn assume a level planar surface for the beam to reflect off of but as shown above this is not necessarily true. An angle from the head slope of the rail will steer the specular signal out of the plane the incident light and sensor operate in.

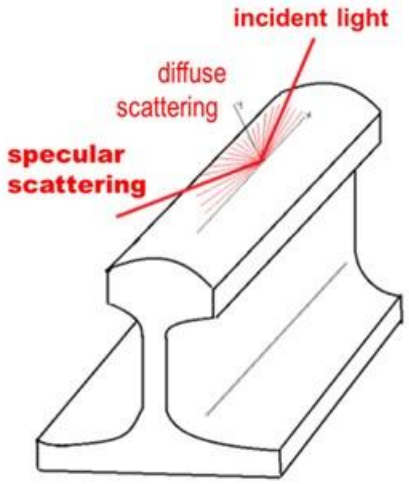

Figure 2-17: Light Reflections off the Top-of-Rail Surface [4]

Early testing with the second generation Rail Lubricity Sensor and push cart determined that specular misalignment was a large source of error, lost data, and ambiguity during field testing [4]. Based on this observation, a modified version of gloss ratio was implemented to remove the specular channel and high angle sensitivity associated with specular measurements. In this modified gloss ratio, the ratio of two diffuse scattering angles is used instead. The diffuse scattering is radial instead of columnar allowing for greater variance in angle before the intensity falls off. An off-angle diffuse scattering measurement is recorded as is a diffuse measurement normal to the rail in the vertical plane. This normal diffuse scattering channel is used to help normalize the gloss ratio against surface roughness conditions. The equation for the gloss ratio is presented below.

$$Gloss\ Ratio = \frac{Diffuse\ Scattering\ Intensity}{Normal\ Scattering\ Intensity} \tag{8}$$

The final series of challenges are directly associated with the dynamics of railway vehicles. The railway wheels are not rigidly constrained to a specific contact patch on the top-of-rail surface and, in fact, the wheels shift laterally a significant amount especially in curves and the transitions between tangent, or straight, track and curved track called a spiral. As such, taking lubricity measurements is depended on the stochastic performance of the railway vehicles as they travel down track. Taking optical measurements from a moving platform adds another degree of freedom as the sensor platform is likewise unable to be perfectly constrained and is also allowed to have some lateral movement across the rail head. None of these challenges are exclusive to optical methods and these challenges are not even directly related to the ability of optical methods to determine track lubricity. They simply provide another variable that needs to be carefully observed

and understood while conducting track lubricity experiments and interpreting optical data collected from railway applications.

3. Rail Lubricity Sensor Development and Laboratory Evaluation

This chapter will cover a brief overview of previous optical sensors applied to detecting rail lubricants and the lessons learned from those sensors that were applied in the development of the third generation Rail Lubricity Sensor. The third generation Rail Lubricity Sensor is the sensor that was used for the field testing reported in this study. This section will cover the basics of the spot photometer design this sensor is based off of and the optical and electrical elements used to create and capture optical measurements. This chapter will also include some laboratory baseline tests that were conducted to demonstrate that this device has similar capability to other optical sensors developed and tested for the rail lubricity project at RTL. These tests will demonstrate the sensor's ability to detect track lubricants and will serve as the basis for evaluating the field testing results collected in chapter 4 and analyzed in chapter 5.

3.1 Lessons Learned from Prior Deployment of Rail Lubricity Sensors

The primary optical instrument used for testing in this research project is the third generation of Rail Lubricity Sensors employed for track lubricity measurements by the Railway Technologies Laboratory. The first generation sensor system used an off-the-shelf Keyence laser and included a data acquisition system and tachometer to collected spatial lubricity down track [50].

Figure 3-1: First Generation Lubricity Assessment System [50]

The results of this indicated that optical detection methods were successful but a more advanced and custom sensor would significantly aid in creating metrics for evaluating rail lubricity. In response, the second generation Rail Lubricity Sensor was constructed with multiple optical detectors at different angles. At the time of its design and construction, the instrument was designed to be used for hand held spot checks at intervals down track from a wayside applicator. The user would approach the track and place the unit on the tracks. The box would be rotated around the rail head while monitoring a readout of the specular refection channel. When the signal maximum was found, this orientation was assumed to be normal to the rail surface normal as the specular reflection would be maximum when perfectly aligned. At this point an optical reading would be captured, the box would then be switched off and moved to the next check point. For this phase of testing, it was also possible to clean the rail surface to get and compare a clean and field condition for that section of rail [31].

Figure 3-2: Second Generation Rail Lubricity Sensor in operation during field testing [31]

It was decided that continuous moving data along the track would provide more detailed information and a much higher resolution to the actual lubricity content and carry distance down track. To this end, the second generation Rail Lubricity Sensor was mounted onto a rail push cart. The push cart featured wheels designed to clamp to the rail head to remove lateral variation from the sensor position. The wheels were also located such that they minimized their contact with the point of interest on the running band of the rail head. This was to avoid disturbing the track condition while taking measurements to the greatest extend possible. A tachometer was added to the cart and connected to the data acquisition unit (DAQ) on the Rail Lubricity Sensor. It is worth noting that while the moving data is sometimes referred to as “continuous” this is somewhat of a misnomer since the data is sampled at a discrete frequency by the DAQ and then further delineated by each tachometer pulse, or tach, of the wheel to determine distance. This cart was used for two field tests in the summer of 2018 and began the basis for all of the dynamic field testing moving forward [4].

Figure 3-3: Second Generation Lubricity Assessment System in operation during moving field testing [4]

This first round of field testing revealed several key issues with the current Lubricity Assessment System. The rigid fixturing of the second generation Rail Lubricity Sensor to the push cart proved to be a challenge when it came to the changing rail surface normal. As the track would shift from tangent track to spiral and curved track, the local wear angle, also called head slope [49], would change and the optical scattering would vary as a result to a greater magnitude than the presence of absence of lubricants. For the second summer 2018 field test, a new set of sensor mounts was designed and fabricated to allow for quick adjustment of the box angle. These mounts featured two concentric arcs to allow the box to be rotated while staying equidistant and concentric to the same point on the rail head. Even so, the time constraints of the track authority window coupled with the slow rate of traversal while walking strongly limited the ability to make frequent enough adjustments [4]. It is understood that this field test data has inconsistencies in different sections due to the change in head slope. A laboratory test below shows the strong signal variance as the roll angle of the device changes. The yellow line shows the point where the two signals overlap and become ambiguous for the tested laboratory condition [51].

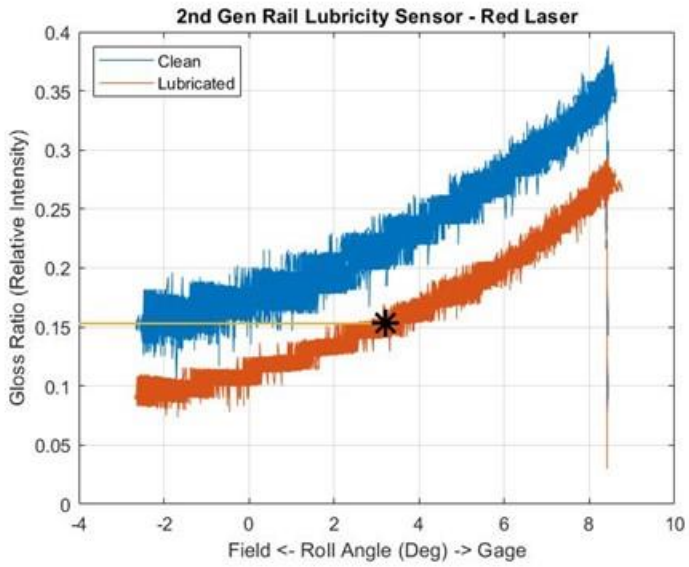

Figure 3-4: Gloss Ratio vs Roll Angle for different rail lubricity conditions demonstrating ambiguity due to roll angle [51]

A second issue that arose was from the elevated device temperature. In its original configuration, the second generation Rail Lubricity Sensor was not intended for a continuous duty cycle and was allowed to operate intermittently. During the hot July and August testing, the internal box temperature reached excessive temperatures of 110°F [4]. During laboratory follow-up evaluations, it was found that the response from the detectors would vary with temperature when left focused on the same target for a long period of time. A 3 hour static endurance test is shown below displaying significant thermal drift while left facing a constant target. After consulting with our resident electo-physicist, a couple culprits were identified. The first was the choice in optical components and electronics. For this phase of the project, the second generation Rail Lubricity Sensor was still entirely intended to be a development kit and lacked some features that would be found in a commercial unit. The laser itself would alter its performance based on temperature allowing fluctuations in wavelength and power output. These shifts in output are generally insignificant for less sensitive applications but the lubricity component of the optical scattering signal is minute causing the interference to be more pronounced. In addition, the optical filters installed over the optical detectors have a very narrow passband. For constant, steady-state performance, this would be fine as the narrow passband would eliminate the majority of unwanted light and decrease outside interference. In this case, the off-the-shelf filters selected were only marginally suited for the accompanying laser. This was fine in previous tests where the temperature and laser parameters were not allowed to deviate but in the more extreme field testing conditions, the shifting wavelength of the laser caused the light to shift out of the passband of the filters and attenuating the already small lubricity signal.

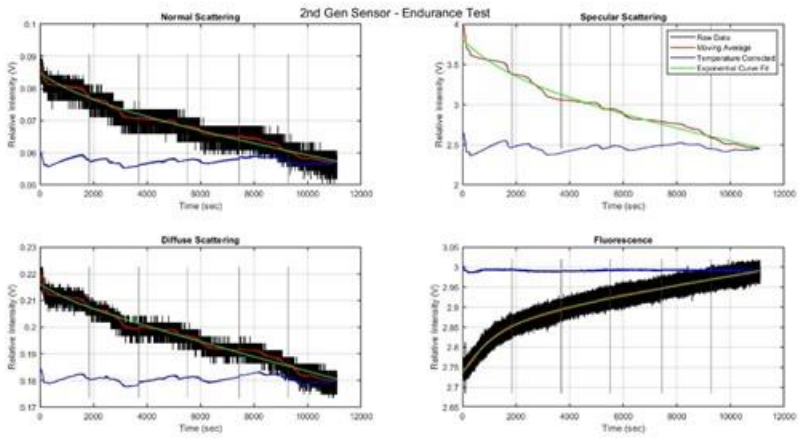

Figure 3-5: Sensor drift of optical channels during extended operation

"I feel the need… the need for speed" – Pete Mitchell "Maverick" and Nicholas Bradshaw "Goose," Top Gun

By far the most significant issue uncovered from this testing was the drawbacks of only testing at walking speed. This limited testing to 3 mph or less and restricted the total distance covered from the summer 2018 tests to just over 1 mile each. The prevailing assumption is that the carry distance of TORFM down track is in the region of 2-3 miles if not more so there was clearly the need to test more track. At the conclusion of the 2018 field testing it was clear that the path forward was a new instrument with more stable optical elements and a propelled rail cart to cover more distance in a single track authority window.

3.2 Design and Development of the Third Generation Rail Lubricity Sensor

With the lessons learned from the previous iterations, a third generation prototype Rail Lubricity Sensor was constructed over the summer of 2019. One of the primary changes is that this new sensor now uses a 405 nm laser wavelength which provides a 16 times increase in optical light scattering over the 633 nm laser used in previous iterations. Another changes is the inclusion of two cross polarized laser diodes that are combined into a single beam and then sent through a chopper. The cross polarization eliminates optical speckle from reflections off the rail head surface. The new interference filters are much wider than the narrow filters used in the second generation sensor. They are centered at 400 nm with a 40 nm bandwidth. This allows for much more fluctuation in the laser wavelength due to thermal effects before the signal can cross the cutoff wavelength and begin to be filtered out. With wider filters, more external light will also be allowed in. The chopper injects frequency content into the lubricity signal so that outside interference can be filtered out later. In particular, sunlight has no frequency associated with it so a high pass filter will be able to remove sunlight effects. The interference optical filters are still necessary to block the majority of the sunlight as to not overpower the photodetectors [52].

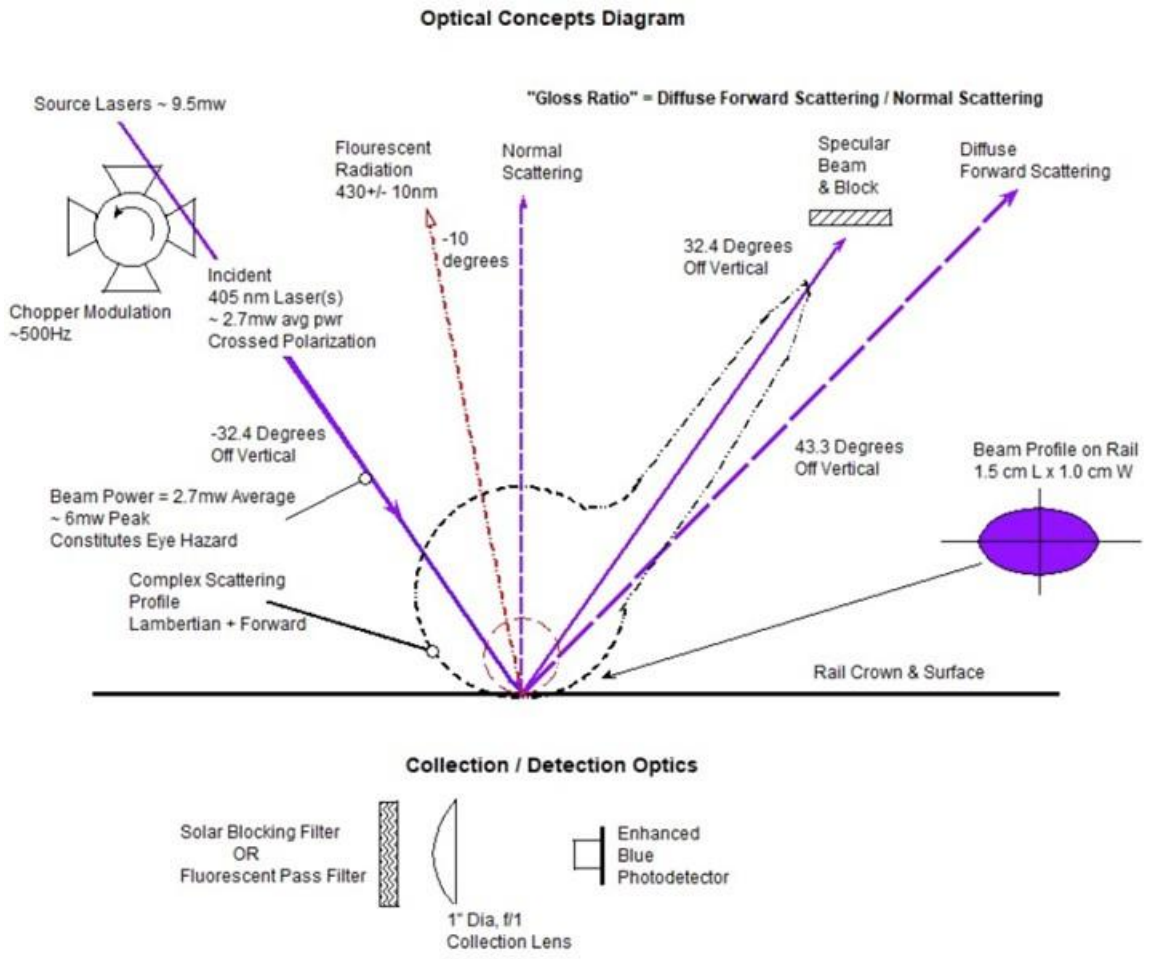

Figure 3-6: Third Generation Optical Concepts Diagram [52]

The 405 nm laser wavelength is near Ultraviolet and as a result can acts as a fluorescence pump for any fluorescent materials on the top-of-rail surface. As previously mentioned, the light reemitted by fluorescent materials has a wavelength shift. In this case, the fluorescence signal is shifted to around 430nm. This allows for interference filters to be applied to the fluorimeter that block the laser reflection and isolate the fluorescence signal. The figure below shows the spectroscope analysis of the fluorescence response with the interference filters installed over the detector. Notice that the signal at the 405 nm pump wavelength is negligible compared to the surrounding noise and the 430 nm fluorescence peak is between 3dB and 6dB above the noise.

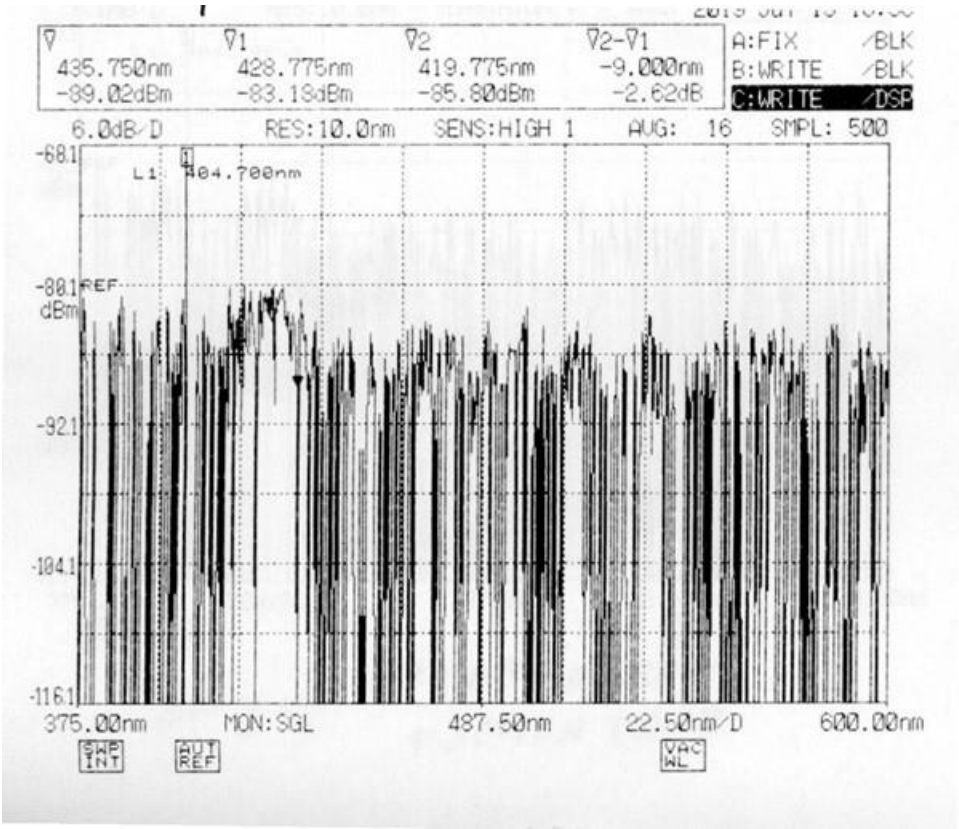

Figure 3-7: Spectrum analyzer plot of fluorescent performance for Third Generation sensor [52]

The resulting instrument is a synchronous spot radiometer that has been adapted for scattering measurements. The figure above shows a concept diagram of the different optical signals being generated from an incident light spot on the top-of-rail surface. The beam profile on the rail is approximately 1.5 cm x 1.0 cm. Traced out from the incident spot is the approximate Lambertian scattering sphere. The sphere itself follows Lambert's cosine law and, in general, has roughly uniform scattering with small changes in angle. Also shown with the scattered light rays is the specular reflection off the rail head. The specular reflection vector is a function of incident angle and the azimuth of the rail head. It is strongly dependent on device orientation and the head slope of the rail. From previous iterations, it was determined that the specular channel was far too volatile for reliable sensor performance during moving testing. As such, it is now blocked by the sensor chassis to ensure that it does not drift into other optical detectors and interfere with their measurements [52].

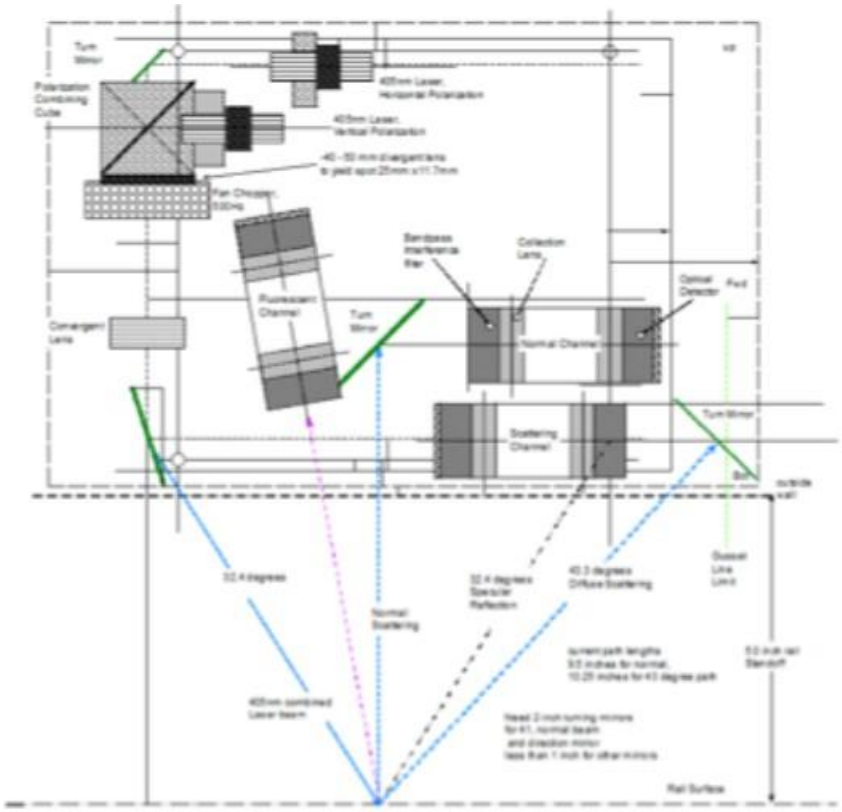

Figure 3-8: Third Generation sensor internal component layout [52]

The figure above shows the actual layout of the optical components inside of the sensor head. The first laser diode is reflected of turn mirror M4 and reflected down into the combining cube. The second laser enters the combining cube from the other aperture. Both lasers are combined in a cross polarized orientation to remove optical speckle from the scattered reflections off the steel surface. From here on, the two lasers follow the same path through a divergent lens, L1, the chopper, a convergent lens, L2, and then a final mirror down to the rail surface at a 32.4 degree angle. The optical gains for all of these steps is shown in the table below.

Table 3-1: Output optical power cascade gains and calculations

	Laser Diode	**Mirror 4**	**Combining Cube**	**Lens 1**	**Chopper**	**Lens 2**	**Mirror 1**	**Average Power**
Laser 1	4.7 mW	0.85	0.89	0.9858	0.405	0.9858	0.82	1.148 mW
Laser 2	4.8 mW	-	0.985	0.9858	0.405	0.9858	0.82	1.526 mW
Total	**9.5 mW**							**2.673 mW**

By multiplying the original laser power, shown in the laser diode column on the left, by each of the successive gains through the optical path a final incident optical power can be calculated in the last column on the right. The optical power is calculated for each laser independently and then the two optical powers are added together for a total average optical power of 2.673 mW incident to the rail surface. With the chopper in the optical path, the optical now has a 500 Hz frequency associated with the pulse rate of the light. The spot radiometer is now a synchronous spot radiometer.

The peak power of the incident laser is 5.941 mW as it exits the sensor head. The peak power of the combined lasers inside of the sensor head is 9.5 mW which constitutes a Class 3B laser as defined by IEC 60825. Class 3B is an eye damage hazard if directly viewed but diffuse reflections are generally not harmful. When the beam exists the sensor head it has been expanded to a spot size of 1.5 cm x 1.0 cm. The 2.673 mW average power would lower the classification to a Class 3R laser although the peak power of 5.941 mW exceeds the 5 mW cap on the Class 3R definition. When reflected off the rail, the laser should not constitute an immediate eye damage hazard, however, eye exposure to both the direct and reflected light should be avoided. The instrument is marked with appropriate warning labels [52].

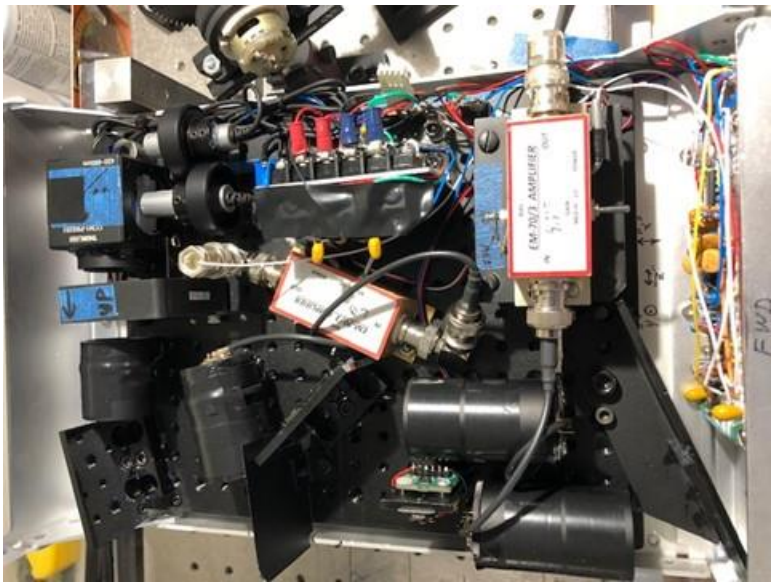

Figure 3-9: Inside view of optical sensor head [52]

The scattering signals collected are a normal scattering channel and a diffuse scattering channel. The normal scattering is located directly above the incident laser spot perpendicular to the longitudinal (forward) axis of the rail. This is considered to be located at 0 degrees and is 32.4 degrees off of the incident laser angle. The diffuse scattering channel is occasionally colloquially referred to as the 60 degree scattering. In the second generation Rail Lubricity Sensor, the diffuse off angle scattering channel was located at 60 degrees. For the third generation sensor, this off angle diffuse scattering channel is 43.3 degrees off the vertical axis. This was primarily due to space constraints to fit all of the components inside the off-the-shelf aluminum housing. The fluorescence channel is located 10 degrees counter clockwise from the vertical axis. This helps shield the fluorescence sensor from strong forward specular type reflections off of the rail head

which could overpower the small fluorescence signal. All of the lenses and detector positions were designed so that the detector would be capable of imaging the entire incident spot on the rail head. This eliminates the need for complex integrals of solid angles needed to determine the optical power scattered into the detector [52].

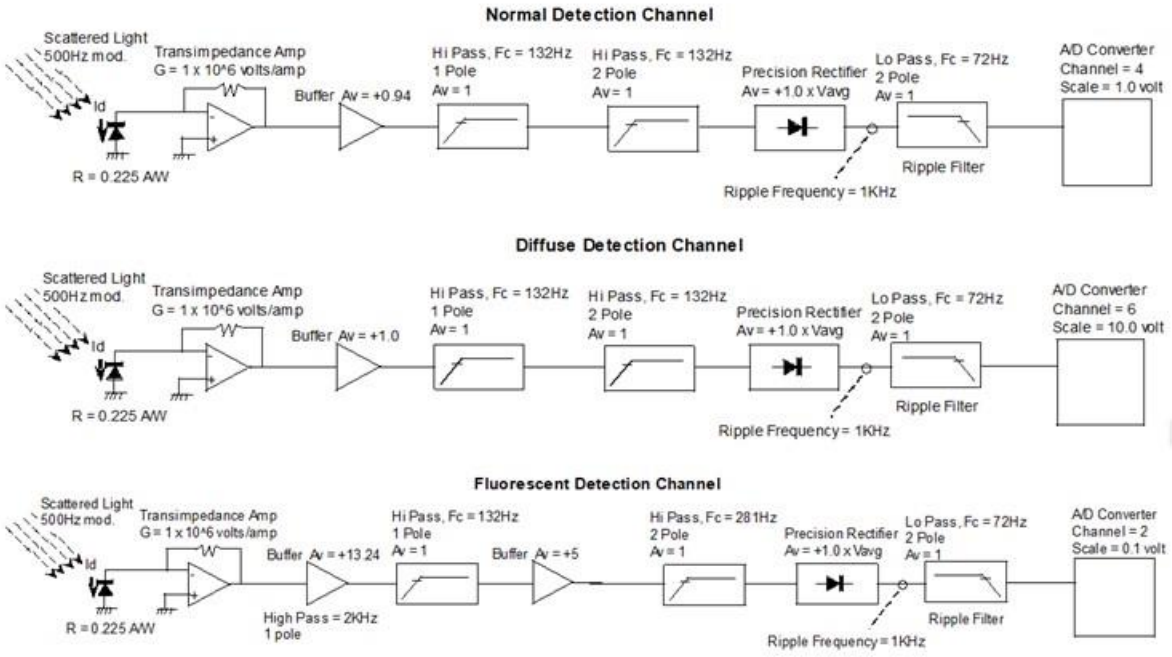

Figure 3-10: Block diagram of electronic components in the detection path [52]

Some typical optical rail lubricity measurements are shown in the table below. By calculating through the electrical circuit block diagrams shown above it is possible to find the optical power at the photodetectors. The raw component signals is shown for four different typical lubricity signals is shown in the table below. Each of those signals was divided by all of the gains in the appropriate channel diagram above to get to the raw voltage at the Transimpedance Amplifier. The Transimpedance amplifier converts the current from the photodetector into a voltage for the analog to digital converter. By dividing by the conversion factor specified for the Transimpedence Amplifier, the current out of the photodetector can be calculated. The photodetector also has a conversion factor to convert the current emitted from the detector to the optical power captured by the detector aperture measured in Watts. This final value is recorded in the table below. Note that while there is a significant difference in magnitude particularly between the scattered signals and the fluorescence channel, all of the optical powers are in the microwatt (10^{-6}) to nanowatt (10^{-9}) range. Recall that the incident laser light had an average power of 2.673 miliWatts. This demonstrates that the lubricity signals, while effective at identifying lubricity on the track surface, are very low in overall signal magnitude. As a result, the fluorescence channel in particular is very susceptible to some anomalies from small drift currents in the sensor electronics.

Table 3-2: Optical signal voltages and corresponding detector input power

	Calculated Gloss Ratio	Normal Signal (V)	Normal Power (nW)	Diffuse Signal (V)	Diffuse Power (nW)	Fluorescence Signal (mV)	Fluorescence Power (nW)
Clean – Shiny	6.9824	0.0842	398.11	0.5880	2613.33	-	-
Clean – Rough	2.2836	0.0928	438.77	0.2081	924.89	-	-
TORFM #1	6.9820	0.0804	380.14	0.3779	1679.56	1.6886	0.11
Flange Grease	4.5900	0.0608	287.47	0.2890	1284.44	19.9047	1.34

The third generation Rail Lubricity Sensor has a sensor head box and a control box. Both boxes are aluminum enclosures from Thor Labs. The optical backplanes of the boxes allow for precise mounting of the optical components and the smaller aluminum enclosures are better suited for mounting on railway equipment. The split between the sensor head and the control box also allow the unit to be mounted in various configurations where the sensor placement may not be ideal for the research engineer to access the controls for starting and stopping the recording of the data logging and accessing the other control elements on the control box.

The third generation Rail Lubricity Sensor was also designed with a form factor intended for being easily mounted to a rail vehicle. In this case, it was determined that a new remote control rail cart would be an ideal moving platform for conducting this phase of the moving testing on revenue service track. The new rail cart borrows its design concept and many off-the-shelf components from the growing market of do-it-yourself electric skateboard enthusiasts. An open source electronic speed controller (ESC), brushless outrunner electric motor, and a remote control throttle served as the basis of the carts propulsion system with the structural components all designed from aluminum extrusion to allow for future flexibility and sensor mounting. More on the construction and design of the remote controlled rail cart will be covered in the field testing in chapter 4. The combined Rail Lubricity Sensor and the remote controlled rail cart are referred to as a Lubricity Assessment System.

Figure 3-11: Third Generation Rail Lubricity Sensor and Remote Control (RC) Rail Cart in operation during field testing

3.3 Determination of Sensor Detectability of Rail Lubricants

The first step of evaluating the new sensor was to verify the ability of the third generation Rail Lubricity Sensor to detect the presence or absence of rail lubricants. This was done in a couple different phases the first of which on an optical bench by Carvel Holton, an electro-physicist and retired research faculty member from CVeSS, during its design and construction. The second phase was conducted on the lab track panel as a final verification as a Lubricity Assessment System. The optical bench tests involved a short section of track pulled from revenue service and donated to RTL.

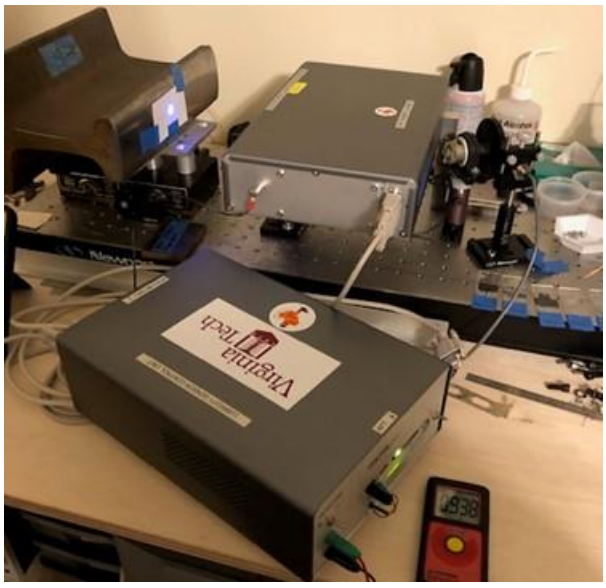

Figure 3-12: Third Generation sensor testing on optical bench [52]

These tests were all static tests and the results were compiled into an internal CVeSS report, the results of which are also recorded here. Using an optical probe, a measurement of a cleaned rail condition was measured and compared with the measurements from different lubricated conditions. This allows for the estimation of an approximate material thickness with the understanding that the surface roughness variation is significant with respect to the material thickness making an absolute thickness measurement impossible. Instead, an approximate estimated thickness is imposed on the x axis allowing for a rough quantification of the general material thickness compared to optical response [53]. The optical bench tests demonstrate that there is a response in the gloss ratio between a clean rail condition and one where an opaque lubricant has been added to the surface. The different fluorescent plots demonstrate the fluorescent behavior of the 3 tested lubricants. The flange grease and TORFM #2 fluoresce more than TORFM #1 does but the fluorescent behavior of any of these lubricants can aid in the detectivity of the sensor.

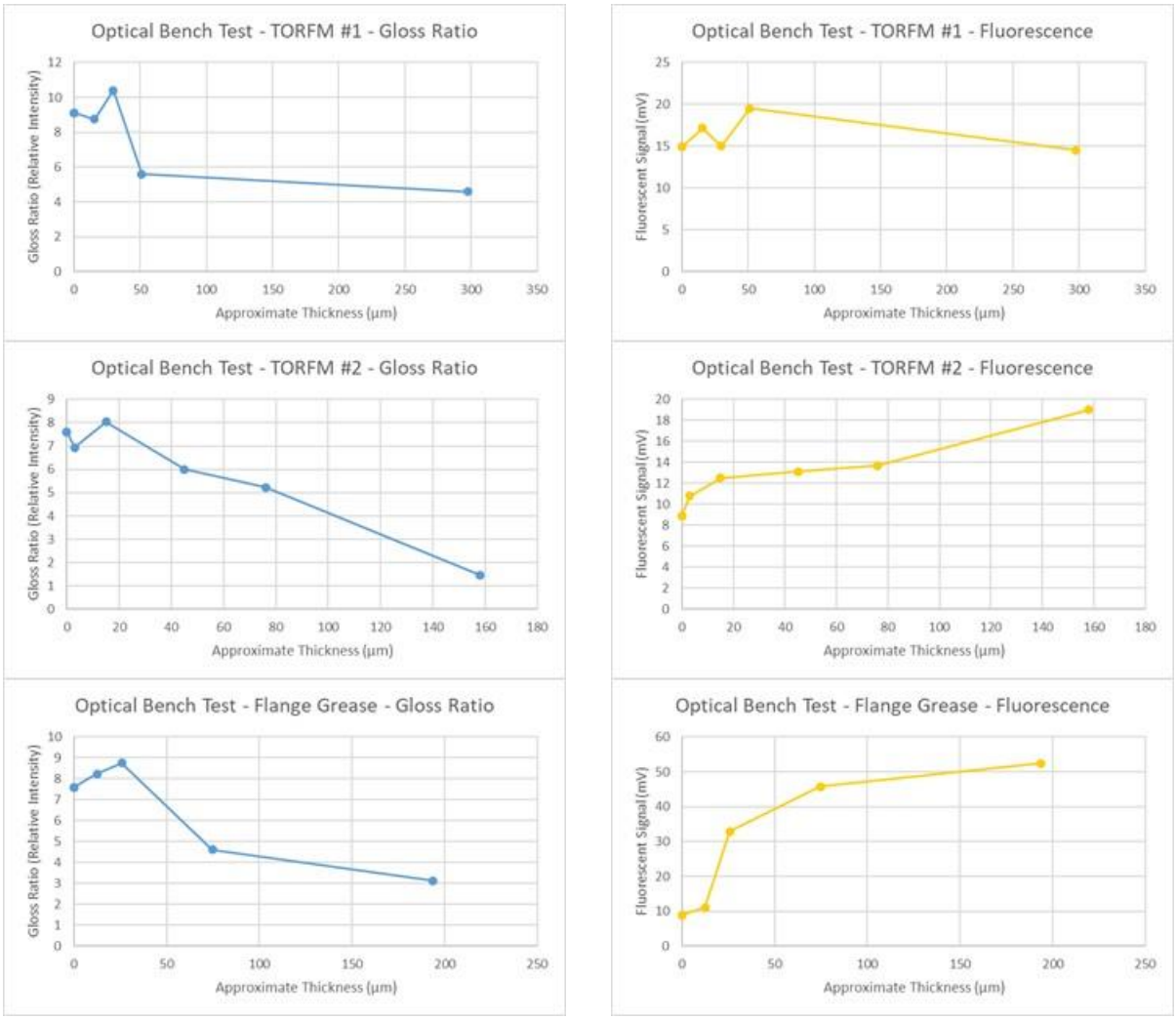

Figure 3-13: Optical bench tests for 3 different rail lubricants

Consistent with the research and testing done by previous lubricity researchers, a 3 step cleaning process was performed on the track panel at RTL to prepare it for each test. Three successive washes of isopropyl alcohol, hydrogen peroxide, and distilled, deionized water, are used to clean the rail. A scouring pad is used first each step to agitate and remove the majority of the lubricants and then a lint and bleach free Kim-Wipe is used to clean the remaining lubricant and dry the rail head before the next step. The isopropyl alcohol and hydrogen peroxide were chosen to remove positive and negative ions respectively and the distilled, deionized water is used last to remove any traces of the previous two cleaners. The Kim-Wipes are used in chemistry applications because they do not leave behind lint and do not have bleaching agents. The lint and bleaching agents can be left behind on the rail head and are detectable by the fluorescence sensor. This process is used to create a clean rail condition. Tests on the lab panel have been conducted both moving and static. A static test allows the track panel to be easily separated into different regions and different TOR conditions to be generated on each section. This allows for a faster array of different TOR conditions to be tested without demanding that the entire 40 foot track panel being cleaned every time. Because each section is compared clean to lubricated, the specific local conditions are consistent although it does mean some care should be taken in comparing different sections across one another.

The following tests show a section of track that was first cleaned, and then had heavy amount of lubricant applied to it. Every successive test, a fresh Kim-Wipe was used to incrementally clean the surface and reduce the lubricity condition. Finally, the section was once again cleaned and the next lubricant was tested on the same section of track. Clean rail measurements were observed in-between tests to verify that the underlying rail conditions were identical. This was done for two different brands of TORFM and for the sample of flange grease supplied to the lab.

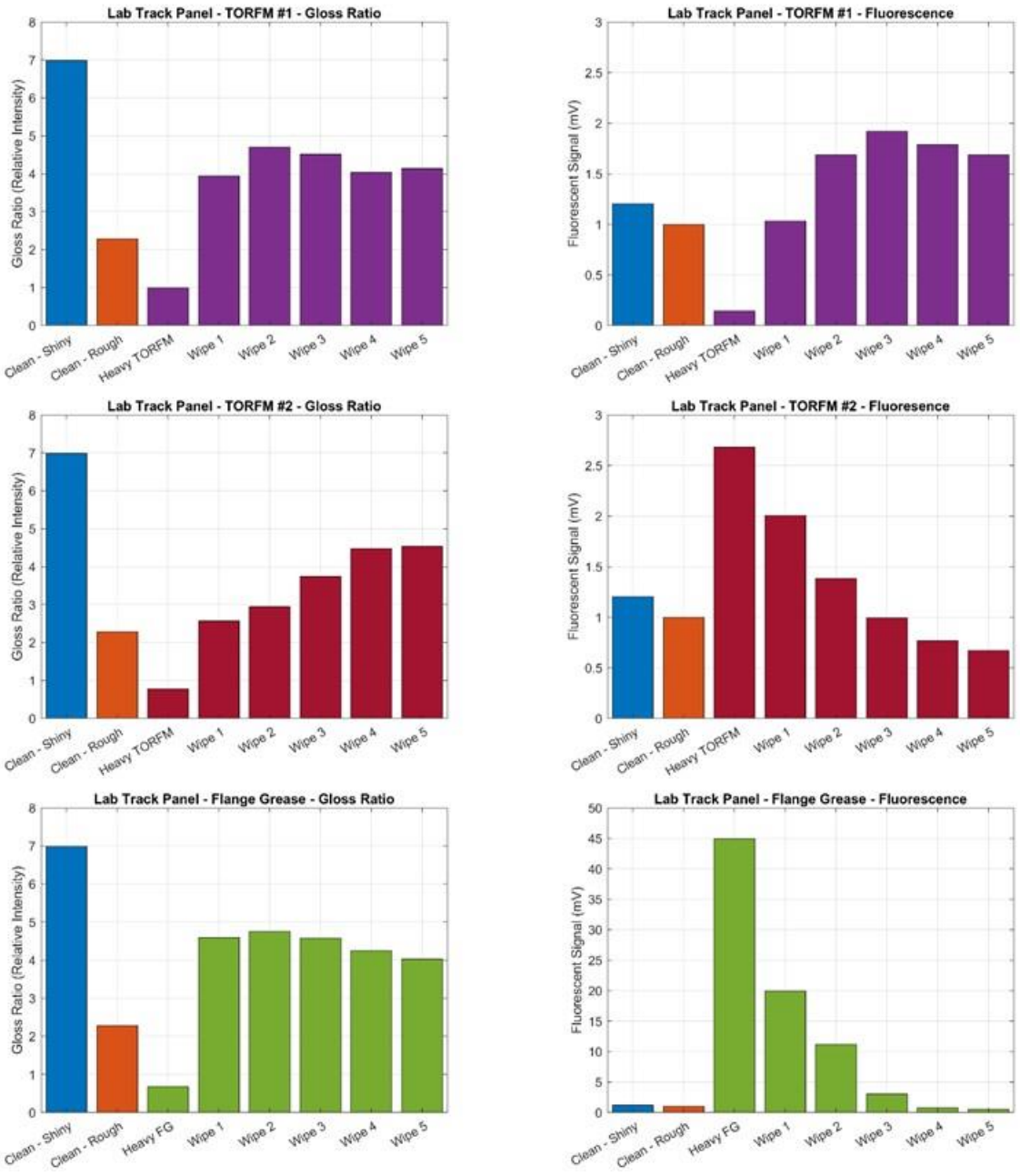

Figure 3-14: Laboratory Track Panel tests for 3 different rail lubricants

The "Clean – Shiny" condition represents a very shiny almost mirror like top-of-rail surface condition where rail wear has brought the surface to an almost mirror finish. The "Clean – Rough" condition likewise represents a clean section of rail with significant roughness from wheel/rail contact or leftover deep grooves from rail grinding. The "Clean – Rough" condition also exhibits a darker patina to the steel surface strongly limiting the surface reflections. This has larger implications for the gloss ratio measurements where the different surface conditions directly impact the scattering behavior of the steel surface but can also affect the fluorescence behavior depending on how the rail lubricants become entrained in the surface figure of the rail.

In the gloss ratio tests, these lab tests demonstrate the complexities with the measurement in terms of absolute determination of lubricant presence. A heavy application of all of the lubricants represents a suppression in gloss ratio below all of the clean rail measurements. This is a transient effect and the gloss ratio quickly rises to a value that is bracketed by the two separate clean rail signals. Near applicator sites, this dip is useful in demonstrating the lubricator performance in the optical data. In general, however, the low gloss ratio readings are less useful in determining track lubricity and convey more information about the surface roughness condition of the rail.

The wiping method of changing the lubricity condition is useful in generating lab tests easily but has significant drawbacks in representing true wheel/rail contact behavior as it relates to wearing of rail lubricants. For these tests, the final wipe leaves very little lubricant visible to the human eye but tactilely, the rail surface still has a slick surface condition which highly lubricated in terms of rail vehicle dynamics. If a more realistic method of wearing off TORFM was available in a laboratory setting, the gloss ratio condition would approach the upper "Clean – Shiny" condition as the TORFM is worn away completely. This could be the subject of a future test on a wheel/rail contact mechanics roller rig.

For TORFM #1, the fluorescence data follows a different trend than the other rail lubricants tested. It has been suggested that the thick, dark consistency of this lubricant leads to a large amount of absorption of the incident light which fundamentally changes the fluorescent behavior of the lubricant. The flange grease is also thick and dark but as a base material the grease behavior has a much higher fluorescent behavior than the TORFM #1 which is clearly demonstrated by the significant increase in fluorescent signal.

3.4 Evaluation of sensor repeatability

For test data to be useful historically and compared run-to-run, it is important that the resulting sensor be repeatable: that is, not a "random number generator." To that end, several tests were conducted on the track panel at RTL to verify consistent performance. The track panel is first cleaned and then a clean rail baseline measurement is collected of the entire length along the track. The track is scanned from a semi-permanently marked starting position so that each test should be aligned exactly in space when compiled afterwards. This is only possible for in-lab testing but allows for localized track irregularities to be compared directly against each other increasing the ability to evaluate the sensor performance independent of the track surface. After a clean rail test is collected, the track panel can be lubricated with any of the selection of sample track lubricants and a lubricated test run can be collected.

The figure below shows the test data of 8 runs: 4 runs on clean rail and 4 runs with TORFM. For each run, the cart is moved from one side of the track panel to the other. Odd numbered runs are all moving east from the start marker to the stop marker and the even numbered runs are the return trips back westbound. This shows that the data is not only consistent in a single direction but the repeatability is actually independent of the direction that the sensor is traveling. The first 2 clean trials were before applying the TORFM. The TORFM was then applied and 4 TORFM tests were conducted. Following that, the track was returned to a clean condition and the final 2 clean trials were conducted. This ensures that not only are the clean runs consistent with themselves but also

from one clean condition to the next. This shows that the cleaning process is consistent and repeatable and the sensor is likewise repeatable.

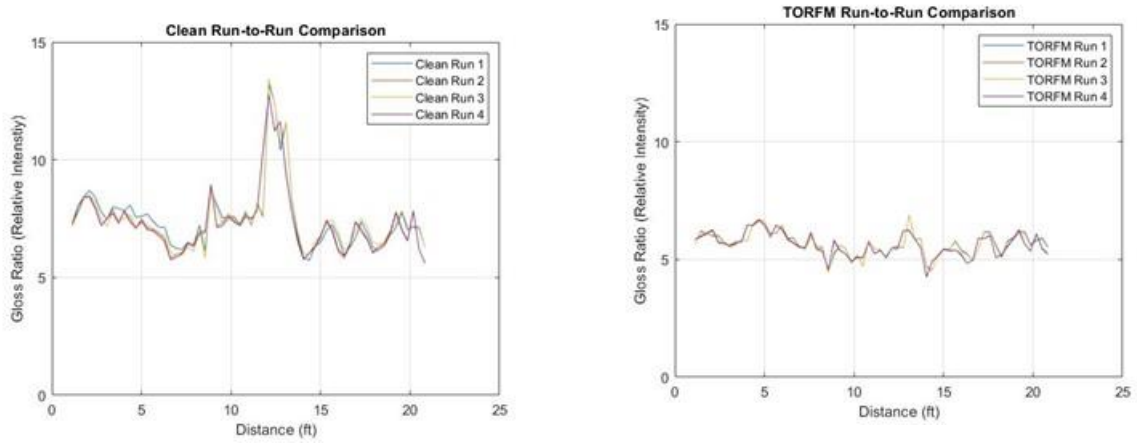

Figure 3-15: Run-to-run repeatability evaluation for clean and lubricated condition

The above two figures show all four runs of the clean and TORFM lubricated moving tests. At this short distance, the tachometer blocks are evident and the block averaging that results from converting the time series data into linear spatial data creates some small deviations on a run-to-run basis especially at extreme peaks. Regardless, the independent trials are very similar and indicate good repeatability for the device.

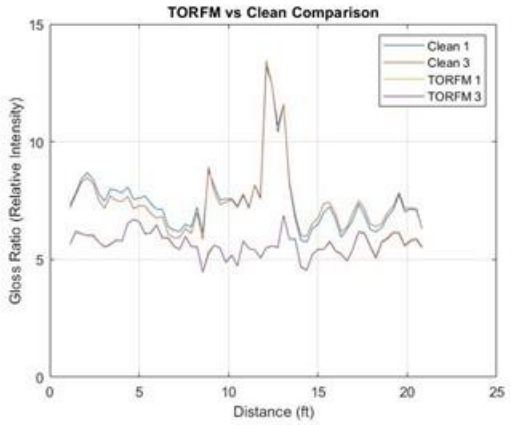

Figure 3-16: Caption

When plotted on the same set of axes, the difference in calculated gloss ratio magnitude is evident. In every case for this set of tests the shiny clean rail condition is a higher gloss ratio than the lubricated condition. In the center section of the test data, it is especially clear that the TORFM reduces the very shiny sections of the rail and provides a very even and consistent gloss ratio. It is also clear that the underlying base reflectivity condition can vary greatly and a single point measurement could be inconclusive. For example, there is sufficient margin for overlap at the 7 foot mark and between 15 and 20 feet. This is not a failing of moving testing, rather it highlights

an effect that cannot otherwise be observed with a simple spot test. Having a clean rail comparison measurement can be a potential solution to this problem but also relies on a length test procedure that is restricted to a single spot. Longer data sets can allow for more averaging which will help reduce uncertainty and better data analytics and machine learning processes will eventually be able to develop a more definitive instrument. Partnering optical measurements with other metrics such as track wear data and creating a historical log of track conditions will be even more beneficial to building tools and algorithms to more confidently predict wayside applicator performance. For this research, conclusions about lubricity data are for more dependent on analyzing lubricity trends rather than evaluating the absolute lubricity at a single point.

3.5 Shakedown run at Riverside

To further validate the sensor and RC rail cart, the Lubricity Assessment System was taken out to a passing siding parallel to the same section of track that would be used for field testing. By working with our corporate sponsor we were able to trial run the data collection and field testing process with the new test equipment and also investigate some track we assumed to be mostly clean from TORFM to provide a "field clean" baseline for our data analysis. During this testing we were able to verify that the device could function outdoors and cope with environmental conditions. We were also able to investigate a curve that had flange grease applied but not TORFM.

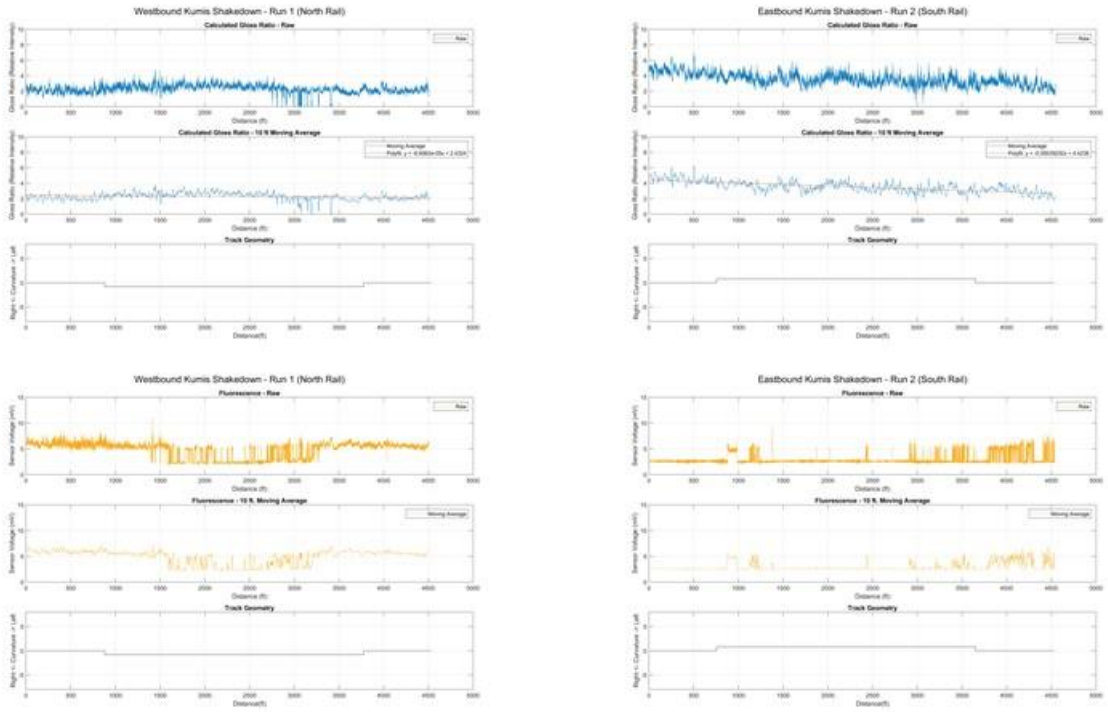

Figure 3-17: Caption

Unfortunately, this data shows that the assumption that the passing siding would be nearly clean rail was not an accurate assumption. For the first run, the gloss ratio plot has trends that would suggest that the rail is clean but the variation in the fluorescence data suggests that this is not the

case, particularly in the middle section of the run. The sensor was pointed to the opposite rail for the return trip from the stop point to the support truck at the service road. This rail shows a strong downward trend in the calculated gloss ratio and the fluorescence channel has a notable uptick in signal close to the stop point.

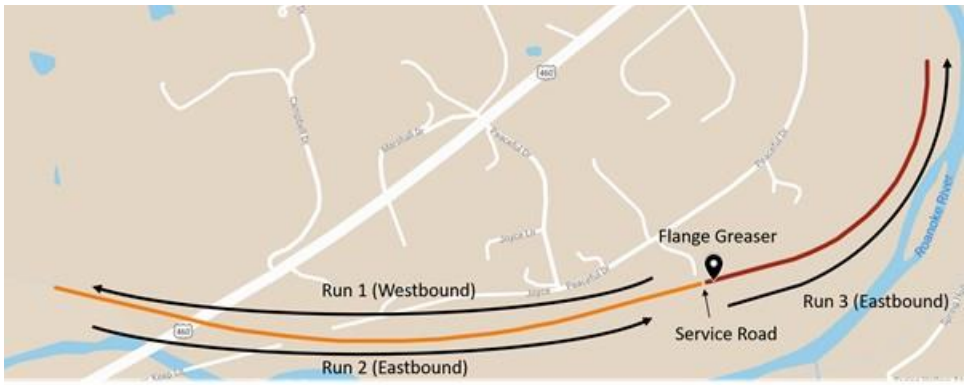

Figure 3-18: Map of shakedown tests at the passing siding at Riverside

The passing siding at Riverside has a flange greaser east of the test section. For the first run, the cart was traveling away from the flange greaser and for the second run, the cart was headed back towards it. The passing siding does not have a TOR applicator but any trains traveling eastbound on the passing siding would still be carrying TORFM from the previous applicator. According to our industry partner, a good portion of the traffic on the passing siding should be westbound traffic which is confirms that run 2 is correctly identifying flange grease from the applicator being carry westward by traffic on the passing siding.

A third test run was conducted on the opposite side of the service road in the curved section following the flange applicator. In the first few feet of the lubricity data there is a spike in the fluorescence channel as the sensor passes over the gage face applicator. There is a large amount of flange grease on the rail at this point from the application process so the fluorescence spike is expected. At about 500 feet into the curve, however, the calculated gloss ratio drops dramatically and the fluorescence signal spikes. This indicates that at this part of the curve flange grease is migrating onto the top-of-rail surface. As previously mentioned, the loss of adhesion at the top-of-rail surface is undesirable and this test demonstrates that the new third generation Rail Lubricity Sensor is able to identify this errant migration of flange grease.

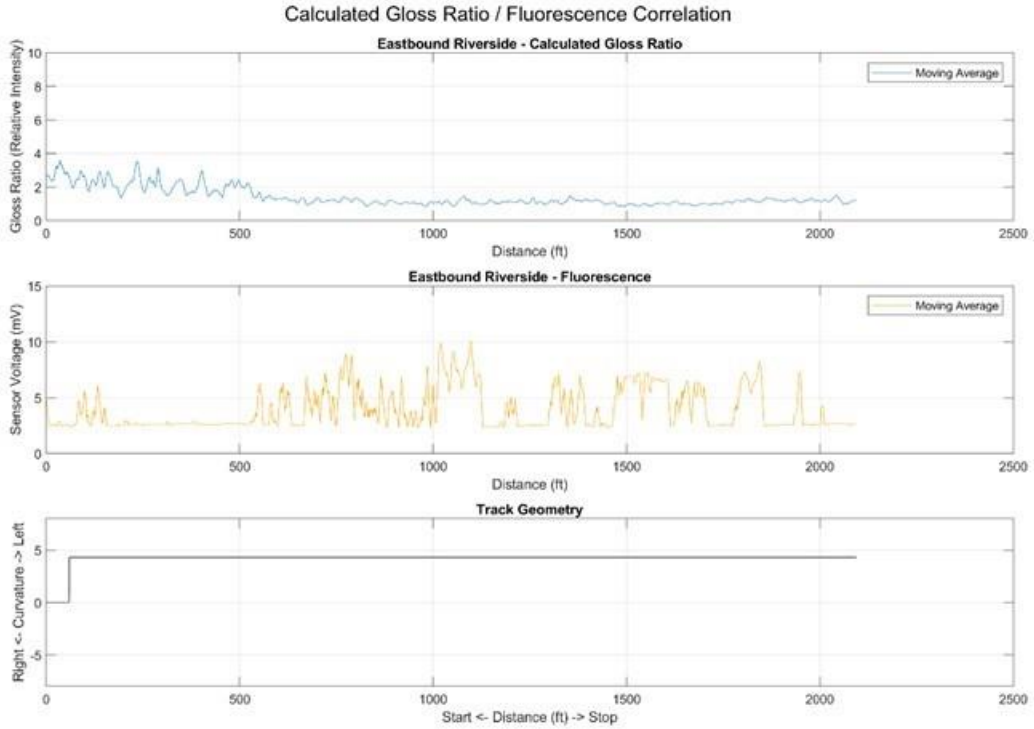

Figure 3-19: Flange Grease crossover at Riverside

For this particular trial, there is a clear crossover point where the flange grease is appearing on the top-of-rail surface and diminishing the calculated gloss ratio signal as was demonstrated in the laboratory track panel tests. This test demonstrates a key ability of the Lubricity Assessment System. Flange grease migration is a metric that railroad maintenance-of-way engineers would like to identify and mitigate either through adjusting gage face applicator performance or by modifying the physical placement of the wayside applicators. This test conclusively demonstrates that the system is capable of making these determinations of flange grease contamination and was a fortunate byproduct of the shakedown testing beyond demonstrating the satisfactory performance of the optical Rail Lubricity Sensor and remote control rail cart.

These shakedown tests proved the primary objective of testing the remote control rail cart and rail lubricity sensors performance in field testing conditions. During the shakedown testing, certain logistical challenges were noted such as the order for assembling the Lubricity Assessment System components when setting up for a test. These notes were considered when making final preparations and plans for the full field test. With the success of the shakedown test, the mainline lubricity testing could move ahead.

4. Laboratory Evaluation of Prototype Unit

Field testing is a key part of the evaluation of the Lubricity Assessment System. As previously mentioned, the actual train dynamics of revenue service freight are complicated and extreme. The spreading of TORFM and the contact pressures that affect the third body layer of these rail lubricants is not something that has been adequately researched. Because of this, rail lubricity conditions representative of actual field conditions are very difficult, if not impossible, to create in a laboratory environment. It was incredibly fortunate to have an industry partner that is willing to provide us with both access to their revenue service track and also to the experience of their maintenance-of-way personnel for guidance and insight into the work performed on wayside applicator placement and operations.

4.1 Development of Remote Controlled Rail Cart

the field testing conducted with the Second Generation Rail Lubricity Sensor and the rail pushcart, it was determined that a new platform would be needed for conducting future field testing. The pushcart served an important function in validating the ability of conducting moving rail lubricity measurements but it also highlighted the gross scale of the railroad infrastructure in the United States. The Association of American Railroads reports that the United States railroads own and operate almost 140,000 route miles according to a fact sheet published on their website [54]. The first moving test with the pushcart covered about 1 mile of revenue service track [4], an insignificantly small amount of track compared to the vast North American rail network. The goal for the next phase of testing was around 5 miles of revenue service track testing which, while still very small compared to the overall rail network, is a substantial increase to the previous testing conducted and prohibitive to the pushcart platform.

While working with the pushcart, the vision for the future of the project always included mounting the rail lubricity sensor on a Hyrail truck or track metrology car. During the design and planning phase for the intermediate range (5 to 10 route miles) testing, it was determined that the new rail sensor platform would need to be able to travel at speeds around 10 mile-per-hour. It was also decided that a separate cart would add versatility over a mounting system for a Hyrail truck. A separate program at the Railway Technologies Laboratory included testing a velocity Doppler Lidar mounted to a Hyrail truck. All the Hyrail trucks are owned by the industry partner and each one is slightly different. The Lidar system mounts required access to a specific Hyrail truck and introduced scheduling issues for conducting testing as the truck had other requirements by the host railroad personnel.

Figure 4-1: Hyrail truck during Lidar field testing

A Remote Control (RC) Rail Cart had the benefit of being independent of any specific Hyrail vehicle as its own test platform and could be controlled remotely from inside any available Hyrail. The frame of the RC Rail Cart was designed from aluminum extrusion for structural rigidity, low weight, and modularity for any sensor attachments or future modifications. The drive system draws from the enthusiast electric skateboard community where brushless motors and open source speed controllers are affordable and very capable of moving a small rail cart. The motor is a 6380 170KV Brushless Motor where the 6380 references the 63mm motor diameter and the 80mm motor length. The motor can draw a peak 4100 Watts and supply a max torque of 5.06 Nm. The maximum motor speed is derived from the peak supply voltage and the KV rating of the motor. The motor battery pack is an 8S (8 battery cells in series) configuration of Lithium Iron Phosphate (LiFePO4) cells commonly used in other applications around CVeSS). The battery supply voltage is nominally 25.6 Volts yielding a maximum motor speed of 4352 RPM. The motor runs through an Apex Dynamics AE090 10:1 gearbox and then a 2:3 final drive chain and sprocket set to connect to the drive shaft. The rail cart wheels are tapered to 7 degrees but have an approximate rolling circumference of 23.25 inches. Therefore, the resulting theoretical maximum speed of the cart is 14.373 miles per hour. This meets the top speed requirement set for the cart.

$$RPM_{Max} * Gearbox\ Reduction * Final\ Drive * Wheel\ Circumference = Velocity_{Max} \quad (9)$$

$$\frac{4352\ Revolutions}{1\ Minute} * \frac{1}{10} * \frac{3}{2} * \frac{23.25\ Inches}{1\ Revolution} = 15177.6\ \frac{Inches}{Minute} = 14.373\ MPH \quad (10)$$

The decision to design a rail cart also added the requirement of transporting the cart to and from the worksite. The Railway Technologies Laboratory has a pickup truck with an 8 foot bed that can be used for this kind of field testing. The cart needs to be wide enough to accommodate the rail wheels and the track gage. This constrains the width of the cart. The length of the cart was then decided by the overall size of the truck bed and the need of the cart to be able to fit inside. This way there is no need for a trailer and the truck can easily navigate any of the gravel or similarly

rough service roads to get to the testing site and removes the need to do any onsite assembly prior to the test. Upon arriving at the test site, the cart can be removed from the bed of the truck and set on the track immediately ready for testing.

Figure 4-2: Test fit of remote control rail cart in the bed of the lab pickup truck

Sourcing the rail wheels for the cart was one of the more challenging parts of building the cart. Flanged and tapered metal wheels would have been a custom order part out of the budget of this project. A high density polyurethane was identified as an ideal wheel material. Polyurethane is strong, dense, and smooth enough to avoid disturbing the rail surface condition unnecessarily before the sensor passes over the test site. It is also light weight and cheaper than a custom metal wheel. The polyurethane wheels came with a heavy crowned surface and required modification to be used in this rail application. The wheels were faced to a flat tread and then tapered to 7 degrees. This taper allows the wheels to steer like normal rail wheels in curves and also moves the wheel contact closer to the gage corner and away from the area of interest on the rail head. This assists in removing unnecessary contact with the point of interest on the rail head causing disturbances the rail surface before measurements can be taken. Finally, aluminum wheel flanges were cut out on a waterjet abrasive cutter and fitted to the inside of the wheels. At extreme lateral shifts, the wheel flanges keep the rail cart on the tracks and direct it through the curve.

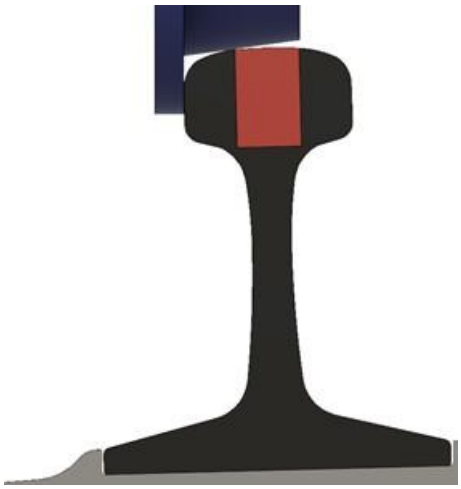

Figure 4-3: Wheel-rail contact analysis of tapered wheel. Wheel taper allows wheel to contact outside of the point of interested on the rail head shown in red

The cart is controlled by 3 different control systems. The motor is controlled by an open source Electronic Speed Controller (ESC). The ESC has a built in connector for traditional PWM remote control throttles. When connected, the cart can easily be controlled in an open loop velocity control with a simple handheld remote. For more precise control, the ESC has a built in closed loop PID velocity controller. The ESC can be communicated with via serial communication from a vehicle controller board mounted on the cart. The vehicle controller system was developed by Cameron Earle, a summer intern at RTL from Blacksburg High School. It uses an Arduino based microcontroller to send and receive commands from a WIFI enabled Arduino tablet and communicate velocity set points to the ESC. This vehicle controller can allow the user to operate the cart in a constant velocity, cruise control mode.

All of these systems allow the cart to being moving but for safety reasons, the cart needed to have a failsafe or emergency stop controller. During his internship at CVeSS, Cameron also worked on the safety controller for the cart. The safety controller is paired with several handheld emergency stop pendants. The pendants pair with the safety controller with a unique ID every time they controller and emergency stop pendants are powered on. When the emergency stop button on the pendant is pressed, the safety controller removes power from the drive motor and applies the pneumatic emergency brake on the cart. The safety controller also monitors multiple different communication systems and resolves to an emergency stop condition should any of them fail. Disrupted communication from the ESC, dropped communication between the vehicle controller and the user tablet, or dropped communication from the emergency stop pendant and the safety controller all result in a faulted state that triggers an emergency stop event. Safety is very important for the railroads. This safety system has multiple points of redundancy and ensures that the testing can be conducted safely.

The final design of the cart includes two water resistant cases for housing the different control systems, some warning and indicator lights, sensor mounting posts, and an air reservoir and brake system. There are two amber strobes mounted to the top of the cart structure. As the cart is capable of moving at relatively high speeds on its own, the amber strobes serve as warning beacons and

increase the visibility of the cart. This has an added benefit of alerting bystanders to the cart as it approaches railroad crossings. In-between the amber strobes is a red emergency stop light. The emergency stop light turns on when the cart is in an emergency stop state. This state disconnects the motor from power and applies the brake. This alert light lets the operator confirm that the cart has come to a safe stop and also alerts the driver of the chase Hyrail truck that the cart is no longer moving and to bring the Hyrail truck to a stop a safe distance behind the cart.

There are sensor mounting posts on either side of the cart allowing the Rail Lubricity Sensor to be mounted on both sides to scan either rail. The air reservoir and brake cylinder provide emergency braking to prevent the cart from free-wheeling downgrade and bringing the cart to a stop during an emergency stop event. The brake system requires air pressure to release the brake and is passively spring actuated to an applied position so that the brake fails to the applied position if air pressure is lost. When the Rail Lubricity Sensor is combined with the remote control rail cart they form a complete Lubricity Assessment System that is capable of conducting optical measurements of the top-of-rail surface for evaluating track lubricity conditions.

4.2 Field Testing Plan and Objectives

The goal for this field test was to cover about 5 miles of revenue service track where wayside TORFM applicators were present. Previous Rail Lubricity field tests were conducted on a set of curves in Riverside, Virginia. It was decided to include this set of curves in the test set to be able to compare results from previous field testing and begin to catalog historical data for the rail lines tested.

Specifically, the goals of the test were to measure several miles of track with top-of-rail lubrication. The test would need to measure both the left and right rail. Multiple wayside TORFM applicators should be covered in this testing to help identify and discard and location specific signals that could influence the lubricity readings. To accommodate the chase Hyrail truck, start and stop points would need to be accessible to a Hyrail truck and ideally also accessible to the lab support truck so that the cart can be delivered and collected from the tracks at the beginning and end of each test.

Considering this, a start point was selected near Ironto as it had easy access from the highway and had a siding ideal for setting the Hyrail truck on the rail. All of the tests would be conducted eastbound following the direction of the majority of traffic on this section of track. There is a flange grease applicator shortly before the start point but the first TOR applicator is just a short distance east. This is the first TOR applicator for a series of applicators on this rail line. In a 2014 AREMA paper, researchers found that placing two applicators close to each other would help condition or “kick start” the top-of-rail lubricity and increase the carry distance [32]. This scheme is implemented on this section of rail and a second TORFM applicator is located a short distance from the first one.

The test region extends just over 5 miles from the start point. This includes the set of curves previously tested near Riverside. The stop point was set at a road crossing about 5.2 miles from the start point allowing for the Hyrail truck to set off on the track and the cart to be removed and placed in the back of the RTL support truck.

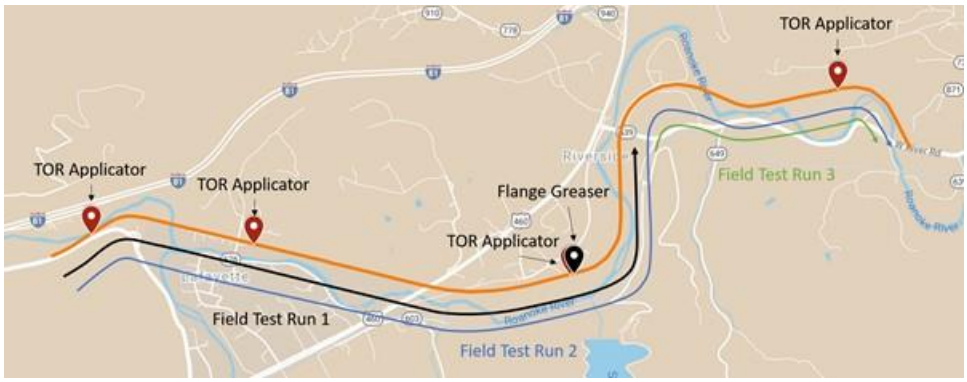

Figure 4-4: Map of mainline lubricity field testing at Riverside

From experience, requesting track authority windows of about 1 hour tends to be the most successful. The ideal travel speed of the cart would be around 10 mph which would cover the about 5 miles of track in only half an hour. This approximation, however, does not take into account any set up or clean up time. Additionally, the field-testing plan calls for the operator to get out of the Hyrail truck and escort the cart across railroad crossings. The cart is rather small compared to cars and rail vehicles and several of the smaller crossings do not have crossing gates. It was decided that having test personnel monitor grade crossings was prudent from a safety perspective to protect the test equipment supplement the traditional grade protection equipment. This also provided a convenient break point where the data logger could be stopped and started to create a new data file. Creating a new logger file serves to protect against data loss should a file become corrupted. All of these tasks impose additional time requirements with the net result being that a 5 mile test ended up requiring about an hour to safely complete.

4.3 Field Testing on Revenue Service Track

Revenue service field testing began November 14th at 8 am. With heavy revenue traffic the first day of testing, it was not until after 1 pm that a track authority was available for the lubricity test. This first test run began at Ironto following an eastbound track geometry train. The Hyrail truck set on and the RC rail cart was unloaded from the back of the truck and set on the rail. The Rail Lubricity Sensor was mounted facing the right hand (south) rail when facing east. Once a system check was performed the data acquisition unit was started and the Hyrail crew boarded the Hyrail truck and began the testing eastbound. The support crew took the RTL truck and proceeded to the next level crossing to assist with traffic. A new data file was started every crossing to both serve as a location reference for aligning the data was well as to protect data integrity in case of a corrupted file.

During the test at around the halfway point, the drive chain between the gearbox sprocket and the drive axle sprocket broke. This issue had not been present in any of the previous testing opportunities but evidently during the tuning of the speed controller the chain had been compromised and wore out sooner than anticipated. Fortunately, the failed chain now meant that the motor was completely disconnected from the drive wheels allowing the cart to coast if the brake was released. As a result, the test was able to partially continue as the cart was pushed by hand until the next road crossing. With the chain broken and the end of the shift for the

maintenance-of-way crew, the test was concluded for the day with the plan to continue the next day.

The drive chain was replaced by the next morning and a motorcycle chain lubricated had been procured to protect the chain during the coming day of testing. The November 15th tests began at the start location near Ironto with the Rail Lubricity Sensor head now mounted on the left hand (north) rail while facing east. Once a passing loaded coal train cleared the mainline, the track authority was issued for the second run of the lubricity field test. This time, in addition to restarting the data logger at every crossing, the motorcycle chain grease was sprayed on the drive chain to ensure that it would not fail. The second run was able to cover the entire 5.2 mile test section of track uninterrupted.

Following the completion of the second test run, the support truck and Hyrail truck deadheaded back to the road crossing where the previous days test had stopped. With the remaining time available in the day, it was possible to pick up from where the right hand (south) rail test had been interrupted the previous day and complete the run to the planned stop point. Once a grain train stopped at the signal at the end of the Riverside passing siding had cleared the mainline, the Rail Lubricity Sensor was again mounted on the right hand side of the cart and the final test run collected the missing data from the first day. During the second day of testing there were no other issues with the cart and the drive chain survived throughout both tests without any issues.

4.4 Testing Outcomes

As a result of the November 14th and 15th revenue service field tests, over 10 miles of field test data was gathered representing about 5.2 route miles of mainline track. This region covered 4 TORFM wayside applicators and 1 Flange Grease wayside applicator. This data will serve as the basis for determining the suitability of the Third Generation Rail Lubricity Sensor for use in medium to high speed testing over intermediate to long distance field testing. In the future, a new drive chain will be procured that is rated for higher forces to avoid similar equipment failure in the future.

The three separate test runs were conducted over two days and had different trains preceding them. The right hand rail was tested immediately after a track geometry train passed by headed eastbound. The track geometry trains are typically pulled by a single locomotive and consist of as research vehicle equipped with various track sensors and a research passenger car which carries the research engineers and computer equipment. This train would have less than 20 axles, far shorter and lower weight than the coal train represented on the left rail test. This first part of the right hand rail test was conducted on the first test day, November 14th, and was interrupted midway through by equipment failure on the RC rail cart.

Figure 4-5: An example of a track geometry train operated by Norfolk Southern. Photo taken with permission.

On the second day of testing, the first test began back at the start point at Ironto and tested the left hand rail. For the left hand rail, the train directly before lubricity testing was an eastbound loaded coal train. The coal train had multiple engines on the head end and a single helper locomotive on the rear end of the train. Typically, coal cars will have 36 inch diameter railroad wheels although the locomotive wheels will be larger. These types of coal trains can be around 100 cars long so 400 axles would be an appropriate approximation for the train length. The left hand rail test was the second test run and was able to run continuously from the start point to the stop point approximately 5.2 miles east.

The third test run was also conducted on November 15th, the second test day. It started mid-way through the test section as shown in Figure *4-4* above. Prior to this test, an eastbound grain train was stopped at the signal near Riverside, VA. Once the train was given a signal indication, it preceded forward and, once clear, the test was allowed to continue. Unique to this test, the train had come to a stop in the middle of the test section with the middle of the train on top of a gage face and TOR applicator. From consulting with industry experts, it is expected that the contact of the brake shoes on the wheel tread will strip much of the TORFM from the wheel surface. In this case, the front half of the train should have minimal TORFM on the wheels and will not have any applied since the wheels are already passed the wayside applicator. For the rear half of the train, TORFM and flange grease will be applied when moving past the applicator but if the lubricity on the wheels has been mostly removed, the conditioning or kick starting behavior will no longer be present [32]. This creates a unique test condition that is different than both of the other preceding trains.

The resulting data contains sensor readings from both the normal diffuse and off angle diffuse scattering sensors as well as the signal from the fluorescence sensor. The sensor control box calculates a form of the gloss ratio in the field termed “Field Gloss Ratio,” or FGR, that is used for a quick reference during the testing. This value is also stored by the data acquisition unit. Some additional cart dynamics measurements are also captured for reference like sensor tilt and roll angle as well as cart vertical acceleration and pitch. The tachometer signal from the Hall Effect sensor is also stored as is a relative time vector. Finally, the data acquisition system logs environmental conditions through humidity and temperature sensors and its own condition through two battery voltage measurements. The environmental sensors will become increasingly important when future measurements need to be correlated with the measurements taken during this late fall 2019 testing series.

4.5 Raw Lubricity Data

The actual process of data processing will be discussed in detail in chapter 5. For reference, the first step was to delineate all of the time series data into spatial data compartmentalized by individual tachometer pulses. The tachometer pulses represent the spatial resolution of the data, however, it is important to verify that the tachometer frequency does not violate the Nyquist sampling rate for the time domain sampling rate of the data acquisition unit. Multiple time samples during a single tachometer pulse are averaged together to create a spatial data set in units of tachometer pulses down track. The raw data for both the numerically calculated gloss ratio, called "Calculated Gloss Ratio" or "CGR," and the fluorescence signal is presented below.

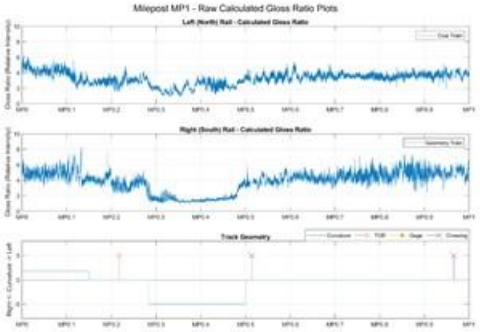

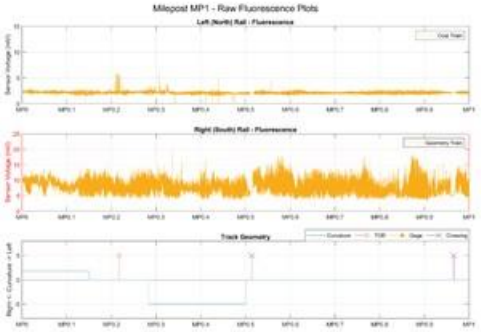

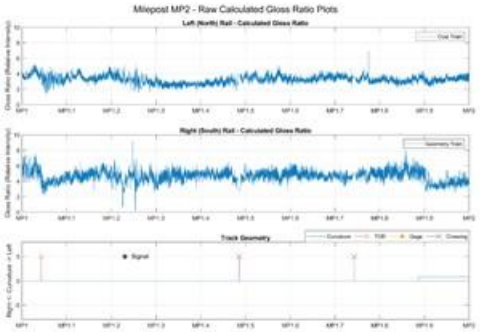

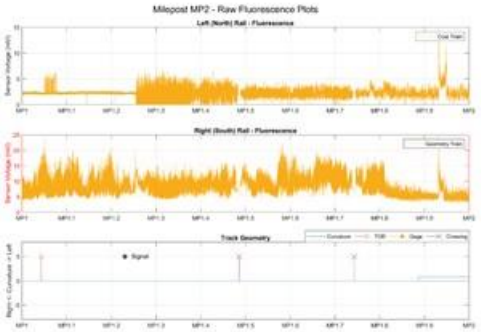

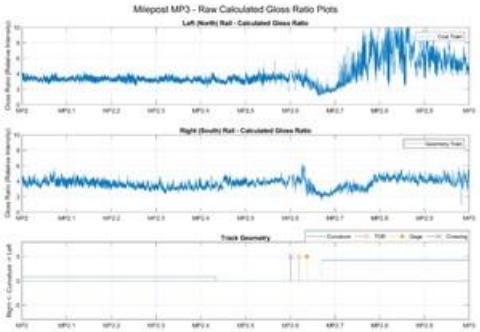

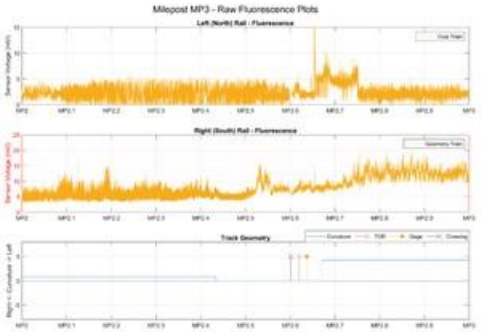

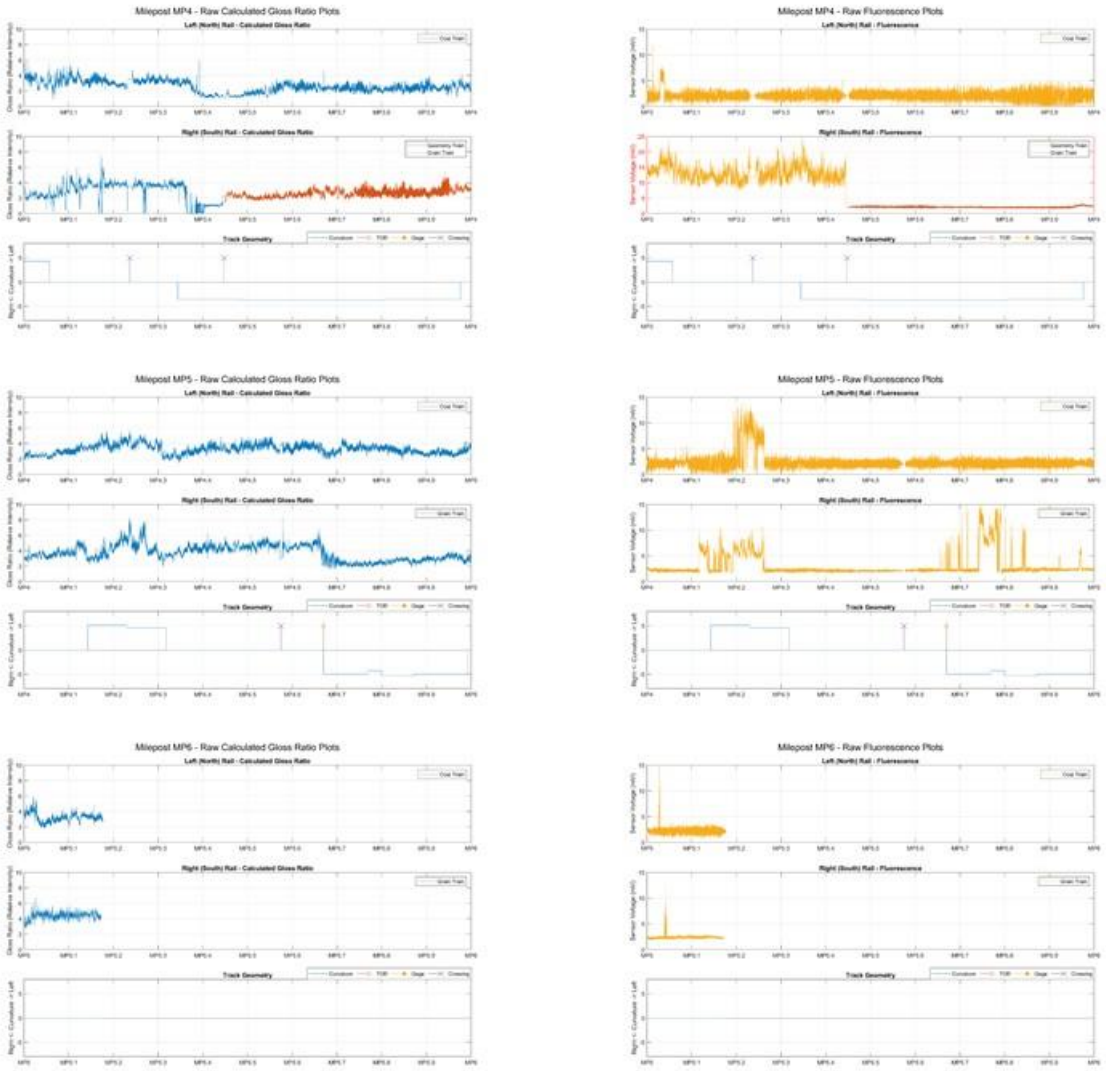

Figure 4-6: Raw Mainline Field Test Data

5. Signal Processing and Data Analysis

This chapter provides an overview of the signal processing techniques used to evaluate the track lubricity conditions. Some conclusions can be drawn from the raw data collected during field test but some simple signal processing steps can be applied to improve the ability of the sensor to provide conclusive lubricity assessment and can also greatly increase the readability of the data. All of the testing conducted for this research was conducted on a new sensor. As a result, there is a large opportunity for deeper study of the collected data through more complex signal processing techniques. This learning will continue with future data sets and in the long term may provide for an excellent opportunity for machine learning to analyze the data. As the knowledge and expertise with the sensor increase, this signal processing and data analysis step will become more developed and more essential to making conclusive lubricity assessments.

5.1 Tachometer Delineation and Data Signal Overview

The first step in processing the test data is to convert time based signals into distance based signals. Using the tachometer mounted to the wheels on the cart, time stamps where there is a rising edge for the tachometer can be identified and recorded. This creates an array of time stamps for each tachometer pulse with the first entry being defined as 0 by default of the start of the test. The start point near Ironto was designated as the zero point for the distance and the forward eastbound testing direction of the cart was defined as positive distance. The array of tachometer pulse time stamps is used to construct an array of distances where each consecutive index is on tachometer distance further than the last. In this case, the wheel circumference is 23.25 inches and the tachometer has 6 teeth. That results in an increment of 3.875 inches for every tachometer pulse. Each consecutive data file was given an offset starting position corresponding to the distance from the beginning of the test section of track.

At this point, it is important to once again discuss Nyquist-Shannon sampling theorem. According to the theorem, in order to accurately reproduce a signal, the sampling rate must be twice that of the highest frequency content [55]. If the frequency of the tachometer exceeds this Nyquist criterion, the tachometer signal will become aliased and the apparent tachometer frequency will be incorrectly reconstructed. The data acquisition system is set to poll at 200 Hz. That means that the tachometer pulse frequency can be no higher than 100 pulses per second. The tachometer has 6 pulses per revolution and travels a distance of 23.25 inches per revolution. As such, the fastest the cart can travel without aliasing is 22 miles per hour.

$$\frac{100\ Samples}{1\ Second} * \frac{1\ Revolution}{6\ Samples} * \frac{23.25\ inches}{1\ Revolution} = 387.5 \frac{inches}{second} = 22.017\ mph \qquad (11)$$

As this exceeds the top speed of the cart, there is confidence that the tachometer signal is accurate and correctly represents the distance travelled by the cart.

Once the individual time stamps are identified, a second algorithm takes the individual time blocks and averages all of the optical data from each block into a single value and appends that value to an array. This becomes the tach delineated raw data set which is used for all analysis. This applies

to all of the optical channels which include diffuse scattering, normal scattering, fluorescence, and field gloss ratio.

The Rail Lubricity Sensor has an analog divider inside the control unit that calculates a version of the gloss ratio for reference in the field. This allows for the operator to check and verify the operation of the instrument from a front panel readout while testing out in the field. The metric, termed "Field Gloss Ratio" or FGR, is also logged into the data acquisition system. There are some drawbacks to the Field Gloss Ratio. The voltages from the optical detectors are very small and close to zero and the analog divider, as with any division operation, cannot divide by zero. To ensure that this does not happen, a small DC offset is injected into the normal channel to protect against a divide by zero condition. This means that the Field Gloss Ratio is not a true representation of the gloss ratio. Additionally, the division occurs before the Field Gloss Ratio is sampled by the analog to digital converter (ADC). The DATAQ unit has a 14 bit ADC so by logging the value after the field division some precision is lost. The formula for the Field Gloss Ratio is presented below.

$$Field\ Gloss\ Ratio = \frac{Diffuse\ Scattering}{Normal\ Scattering + DC\ Reference\ Offset} \tag{12}$$

By recording the raw 14 bit signals and post processing them in MATLAB it is possible to take full advantage of modern computer processing to increase the precision of the measurement. MATLAB by default uses 16 digits of precision which far exceeds the 14 bit values logged by the DATAQ unit [56] so no precision is lost during this MATLAB processing step. This is increase in precision is valuable because the actual lubricity signals are very small. Any errors in calculating the glass ratio dramatically reduce the detectivity of the sensor. This MATLAB processed gloss ratio is what is used for all analysis and is referred to as "Calculated Gloss Ratio" or CGR. Calculated Gloss Ratio is the ratio of the off angle diffuse scattering over the normal scattering and the equation is shown below.

$$Calculated\ Gloss\ Ratio = \frac{Diffuse\ Scattering}{Normal\ Scattering} \tag{13}$$

The Fluorescence channel is the final optical channel analyzed for its ability to detect TORFM. The Fluorescence channel, like the other channels, has a very small voltage coming out of the photovoltaic detector. To compensate for DC voltage offset from the photodetector in the Rail Lubricity Sensor during logging, a second DC offset is applied during post processing to correct this and to make the data more presentable. The formula for this processed Fluorescence value is shown below.

$$Processed\ Fluorescence = Raw\ Fluorescence + Fluorescence\ DC\ Offset \tag{14}$$

To plot the data, the tach delineated data was split into mile increments by milepost. The left rail and right rail are from different trial runs and were preceded by different revenue trains, however, they represent the same physical location down track and are therefore plotted together. The resulting plots have the left and right rail in separate subplots with a third subplot on the bottom displaying the track layout including curvature, railroad crossings, and TOR (Top-of-Rail) and

Gage face applicators. This template is used across most of the different data processing steps. The plots for the raw, tach delineated data are presented in section 4.5 as a conclusion to the section on field testing. For this shorter section of testing, rigid adherence to a template for plots like this one is less necessary. As the data set for this sensor grows, having a common way of reporting the test data will be important for comparing data from different tests. Further, if mounted to a high speed test platform like a track metrology car it will be essential for large amounts of data to be processed quickly with a consistent format.

5.2 Moving Average Filter

The raw data as presented has a high degree of noise in the system even after the block averaging step that occurs during the tachometer delineation from time to displacement. Rail lubricity condition is going to be largely dependent on long term trends in the data so it is necessary to average the data to emphasize the low frequency content. Averaging is a very simple and intuitive tool to apply smoothing to raw test data to make it more readable. A block average is easy to apply but would result in a stair step effect between blocks so a moving average filter was applied to the data instead. The moving average applies a moving window of a user specified length to the test data and averages all of the data in the window. This allows the data to have remain smooth between each averaging step and removes the undesired stair step effect from a block average. The moving average filter can apply different amounts of smoothing based on the filters construction and create the desired effect of making the legible without removing too much of the signal dynamics.

5.2.1 Moving Average Filter Method

A moving average filter is by definition a form of low pass filter but for this level of signal processing it is more convenient to treat it as a simple average. Designing a better low pass filter may become a task for future work on the project. Nevertheless, it is prudent to investigate the filter performance of the moving average filter to understand the effect processing the data in this way has on the frequency domain of the signal.

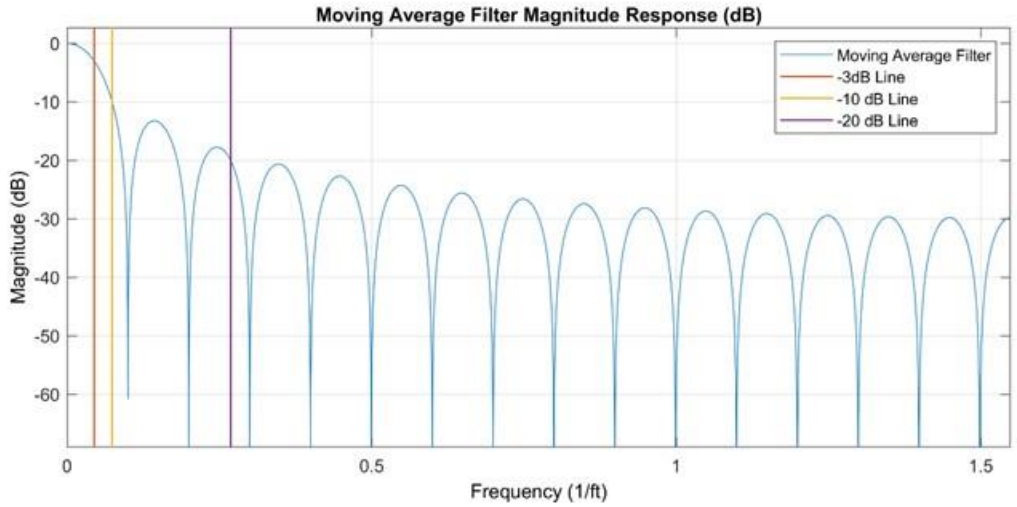

Figure 5-1: Moving Average Filter Response Plot

The above figure shows the filter visualization for a 31 tach sample moving average filter. By multiplying the number of tachometer pulses in the moving average window by the distance per tachometer pulse, the 31 sample moving average is equivalent to a 10 foot moving average window.

$$31\ Tachometer\ Pulses * \frac{3.875\ inches}{1\ Tachometer\ Pulse} * \frac{1\ foot}{12\ inches} = 10.010\ ft \qquad (15)$$

The cutoff frequency is typically represented at the -3 decibel point which is also referred to as the half power point [57]. Because the index for the data is represented by distance and not time, the frequency is in units of inverse feet (ft^{-1}) instead of Hertz. For this moving average filter, the cutoff frequency is at 0.04423 1/ft which corresponds to a spatial period of 22.61 feet. For sufficient attenuation -20 decibels is often used as the suggested practice but -10 decibels can also be used if less separation is needed. A 10 decibel reduction is equivalent to dividing the signal magnitude by 3.16 and a 20 decibel reduction is equivalent to reducing the signal to a tenth of its unfiltered value. For this filter, the -10 dB point is at 0.0737 ft^{-1} which equates to a period of 13.57 feet. The -20 dB point is more complicated since the filter ripple fluctuates above and below -20 dB until 0.2684 ft^{-1}. Any signals with a period shorter than 3.73 feet will be well attenuated.

Small localized spikes in the optical channels are prevalent as the rail surface is not a uniform, smooth surface. The rail surface is very stochastic with a high amount of surface imperfections. Different angled cracks in the rail surface can sharply change the scattered power for a single sample and surface glints are common during measurements on rail surfaces. Some of these surface features can be easily visible by the human eye and some of the cracks and facets will require a microscopic view of the specimen. Because all of these features are far below the -20 dB cutoff period of 3.73 feet, the majority of the effects of these high frequency, low period effects should be strongly attenuated by the moving average filter.

Figure 5-2: Top-of-Rail Surface roughness of RTL track panel

Once the raw data is averaged, the long term trends become more visible and local phenomenon are averaged out. The decision to choose a 10 foot (31 tach) rolling average window was somewhat arbitrary. Several different rolling window lengths were plotted and compared visually for their ability to recreate specific spikes in the lubricity data while still significantly reducing the variance found in the raw data file. A short sample from a fluorescence plot is shown in the figure below. Note that the green 40-foot window fails to accurately represent the peak at the end while the purple 10 foot window removes a significant amount of variance while accurately capturing unique signals in the raw data.

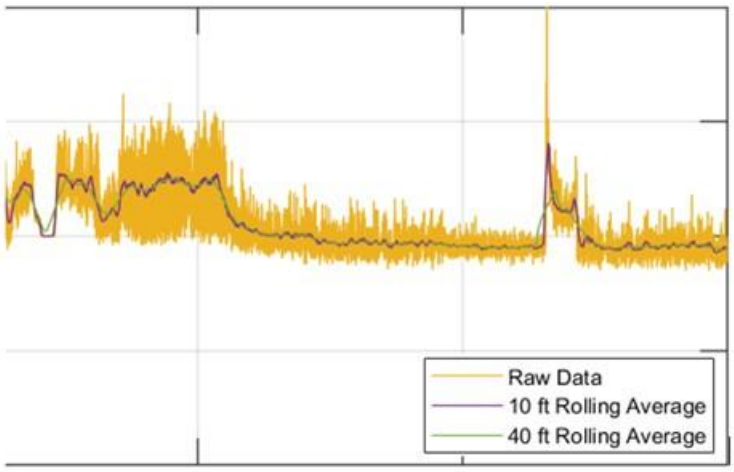

Figure 5-3: Section of Fluorescence data with 2 different length moving average windows applied

Using the same template developed for presenting the raw lubricity data, the raw data was fed into the moving average algorithm and plotted.

5.2.2 Moving Average Results and Analysis

The beginning of the test section is designated as Milepost 0 (MP 0) and is located near Ironto, Virginia. There is a flange greaser approximately 0.8 miles prior to the start of this test section but otherwise, the TOR applicator in the first mile of testing is the first TOR applicator in over 8 miles of track. Traffic on this line is mostly eastbound but occasionally there will be a westbound train and helper locomotives will also return west after assisting a train up the hill. This means that although the majority of the rail lubricants should be propagating eastbound, some westbound traffic may move TORFM and flange grease the opposite direction. Specifically, this was found to be the case on the passing siding at Riverside during the shakedown testing.

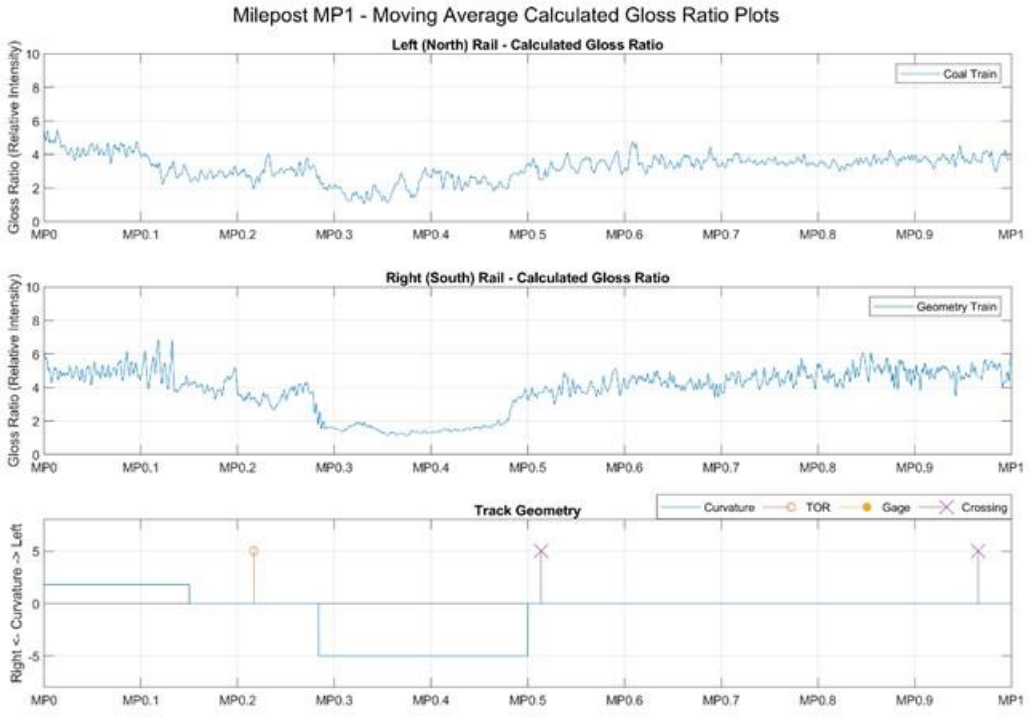

Figure 5-4: Moving Average Filtered Calculated Gloss Ratio Data from Milepost 1

Prior to the TOR applicator, the right hand rail has a high gloss ratio indicating that there is very clean and shiny rail. Near the applicator, this signal drops to a gloss ratio of around 4 which is representative of lubricated rail. This is to be expected close to the applicator. In the curve, the gloss ratio drops to a value around 2. An inspection of the rail shows that there are heavy grooves from rail grinding on the gage side of the rail with heavy TORFM on the outside of the rail. This indicates that there is plenty of TORFM on the rail at this spot. A gloss ratio of around 2 was found to be representative of a rough rail condition like the condition found on the passing siding at

Riverside and the same is true here. This indicates that the cart had slid laterally towards the left hand rail driving the sensor spot to the gage side of the rail and away from the heavy TORFM built up on the outside of the rail.

Figure 5-5: Picture from field survey of the right hand rail near MP 0.4. Heavy TORFM can be seen on the field (outside) side of the rail. Heavy grinding marks can be seen on the gage (inside) side of the rail.

The left hand rail shows a similar trend although in this case the sensor spot is shifted towards the TORFM on the outside of the rail. The higher gloss ratio tends to indicate that the sensor is identifying heavy TORFM rather than rough rail steel.

The fluorescence data shows that the signal trailing the track geometry train on the right hand rail is significantly different than the signal following the coal train on the left hand rail. With fewer axles and lower loads, it is expected that more of the TORFM would be worn off with the coal train than the geometry train. This is reflected in the fluorescence signal where the signal magnitude is significantly higher for the right hand rail compared to the left hand rail.

The fluorescence signal is already elevated for the right hand rail prior to the TOR applicator. Flange grease has been demonstrated to be highly fluorescent and as a result, the flange greaser is imparting a significant lubricity signal for the geometry train even before it arrives at the TOR applicator. For the left hand rail, it appears as though much less flange grease is migrating to the top-of-rail surface. At the TOR applicator, there is a small bump in fluorescent signal indicating that the sensor has correctly identified the presence of the TOR applicator. There are a few other small jumps directly at the entrance of the curve.

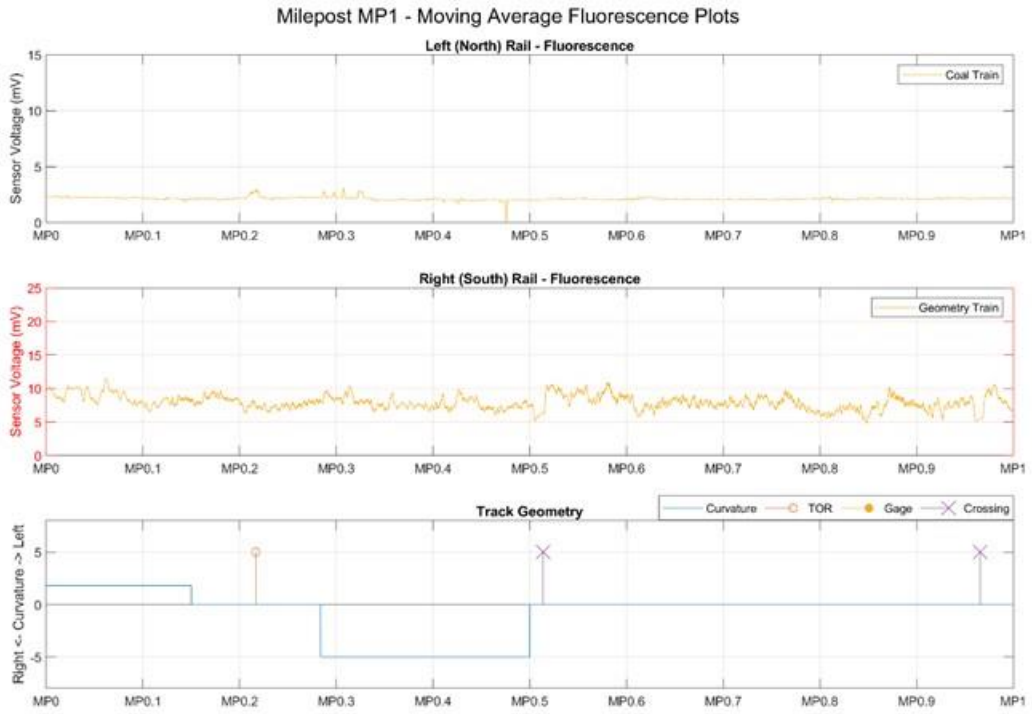

Figure 5-6: Moving Average Filtered Fluorescence Data from Milepost 1

After the right hand curve, the gloss ratio trends differently for the left and right rail. The left rail shows a shallower trend to the gloss ratio data indicating that the rail condition is more uniform after the coal train. The overall gloss ratio value is indicative of lubricated rail but the fluorescence sensor and overall trend of the data suggest that the lubricity is much lower. The right hand rail trend shows a significant positive trend in the lubricity data. This would suggest that the lubricity condition is trending towards clean and the dynamics of the signal are more prevalent. This will be revisited during the curve fitting section of the analysis.

The next TOR applicator is very close to MP 1. This time the dip in CGR is prominent on both the left and right handrails as heavy TORFM is present at the wayside applicator. The CGR quickly rebounds from a heavy TORFM condition to a gloss ratio of around 4-5 which is more typical of lubricated rail. Again, the right hand rail shows a higher lubricated condition than the left hand rail from the preceding traffic. This section of rail is straight for almost a mile and after passing over the second applicator, the conditioned wheels tend to maintain their lubricity longer.

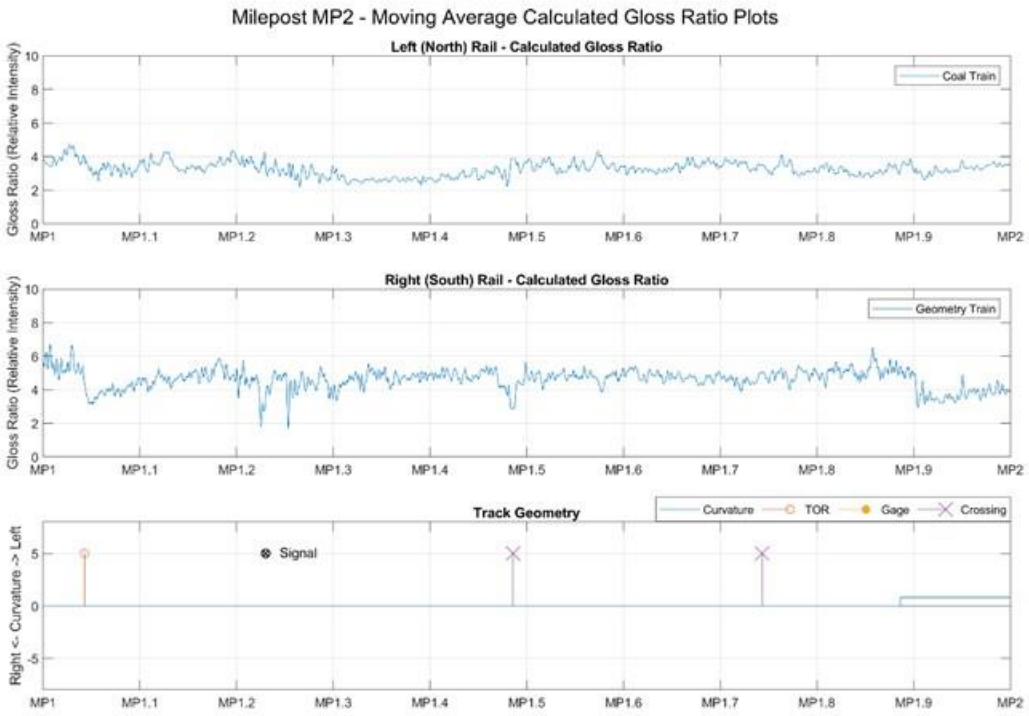

Figure 5-7: Moving Average Filtered Calculated Gloss Ratio Data from Milepost 2

Near MP 1.2, there are a few dips in the gloss ratio on the right hand rail. At this spot there is a signal and a switch to the passing siding at Riverside. The right hand rail passes through a switch frog which allows for the diverging rails to cross and the trains to navigate from one track to the other. When the sensor goes over the switch frog, it is exposed to the rough oxidized steel surface of the frog and the gloss ratio drops for a short distance. With access to track data, it is easy to identify these anomalies and disregard the local effects caused by them.

Figure 5-8: Example of a switch frog

At MP 1.9, there is a sudden dip in the gloss ratio for the right hand rail. The shape of this signal is almost identical to the shape of the gloss ratio right at the TOR applicator. It has been suggested that at the entrance and exits of curves, the lateral shift of the wheelsets introduces fresh TORFM that has been lying dormant on the wheels to come into contact with the rail. This acts as a sort of "phantom applicator" in that additional TORFM is introduced in a spot far from any physical wayside applicator. This phenomenon has been observed other places in the lubricity data as well.

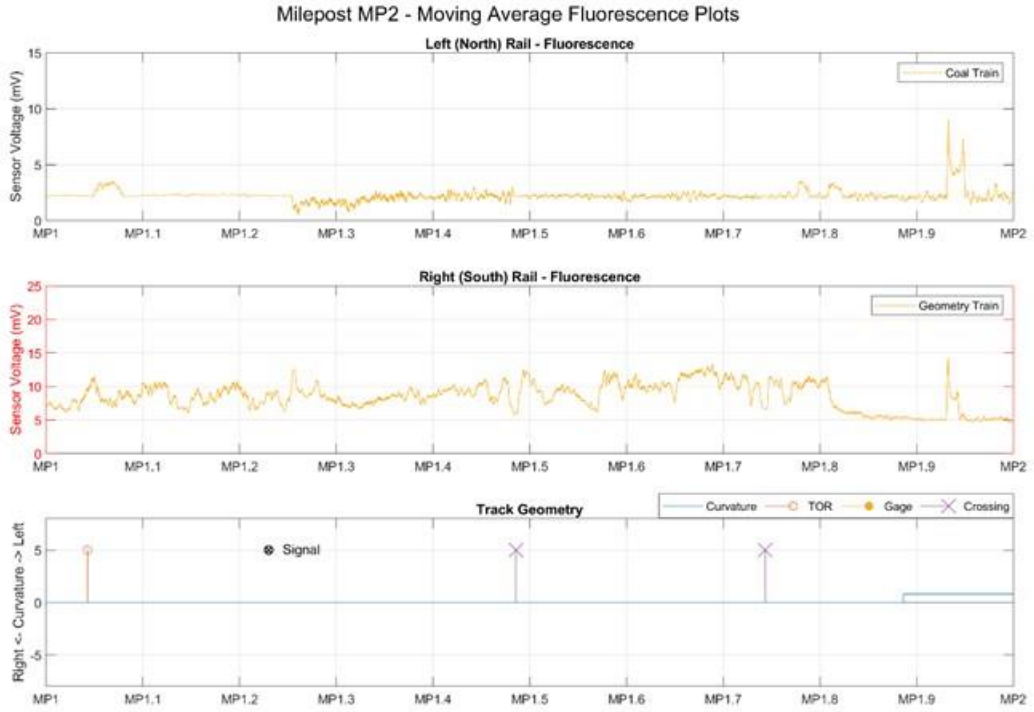

Figure 5-9: Moving Average Filtered Fluorescence Data from Milepost 2

The fluorescence data shows a spike in fluorescence for the left hand rail directly at the TOR applicator. A similar spike can also be seen for the right hand rail although it is less prominent to the overall signal. At MP 1.25, the left hand rail fluorescence data changes and significant more activity can be seen in the signal. This corresponds directly to the signal at this spot. There are two theories to explain this behavior. The first is that the engineer applied the airbrakes while approaching the signal and released them the train had passed the signal. This section of track is slightly downgrade and the engineer could be braking the train either in preparation for an approach or stop signal or to help control the descent. With the airbrakes applied, the brake shoes contacting the wheel tread would have a negative effect on the propagation of TORFM down track [32]. Once released the lubricity condition would begin to rise and this point represents the start of that rise.

The other theory suggests that this is demonstrating the conditioning effect covered in a 2014 AREMA paper [32]. Researchers from Whitmore Rail and Norfolk Southern found that placing two lubricators in close proximity served to condition the wheels to dramatically increase the carry distance of the TORFM. This second applicator is within a mile of the first applicator to generate this conditioning effect and the rise in lubricity condition would suggest that shortly after the second applicator, the rail wheels are conditioned and more TORFM is left on the track after a passing train. From this point onward the left hand rail shows more signs of higher lubricity levels which correlates the findings in the AREMA paper.

At MP 1.8, the fluorescent signal for the right hand rail drops off dramatically. The higher fluorescent level seen prior to this point is higher than the fluorescence seen from typical TORFM

suggesting that the fluorescent sensor was detecting flange grease. The signal drops to around 5 mV which is still twice the signal found on the right hand rail. This shows that the lubricity level is still higher following the track geometry train than it is following that coal train but that the flange grease has been worn off the top-of-rail surface at this point. A field survey of the track found evidence of flange grease further down track than this point but to a lesser degree than points further west supporting this theory. The two fluorescent peaks at MP 1.95 are directly under a highway overpass. During a field survey, nothing was found on the rail to correlate directly with the fluorescent spike but it is suggested that this is an effect of oil and other contaminants dripping off either side of the highway overpass.

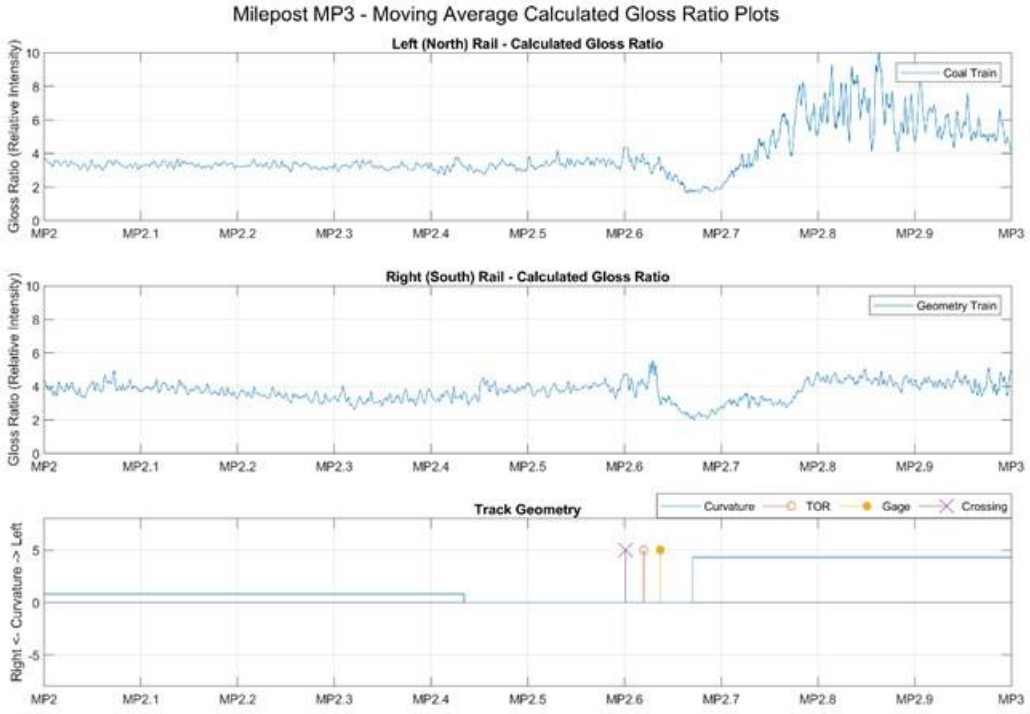

Figure 5-10: Moving Average Filtered Calculated Gloss Ratio Data from Milepost 3

The third milepost starts off with a gentle curve before crossing over a gage face and TOR applicator and then turning into a sharp left hand curve. The passing siding that parallels the mainline here is the passing siding that was used for the shakedown run. Both the left hand rail and right hand rail gloss ratios are very consistent and stable through the first section of track in this milepost. This suggests that the conditioning effect is working and that the lubricity condition of the wheels is consistent. The gloss ratio value of around 4 suggests that TORFM is present although it is important to note that absolute gloss ratio magnitude can be a poor indicator of lubricity condition depending on the underlying rail surface condition. A field survey of the track here shows that there are signs of TORFM remaining on the field side of the rail. This section of rail is less than 2 miles from the previous applicator so it is expected that the TORFM would carry this far. This also suggests that eastbound traffic on the passing siding would be likely to carry TORFM this far confirming that the passing siding tests were not a good example of clean rail.

Figure 5-11: A field survey of the mainline track shows evidence of TORFM on the outside of the rail.

When passing the wayside applicators, both rails show characteristic signals of the presence of the applicator. For the left hand rail, the gloss ratio in the curve is very erratic but overall shows a very high gloss ratio value. This would be indicative of very shiny, highly polished rail which would be expected in a tight, high wear curve. Because of the proximity to the wayside applicator, it is expected that the TORFM is protecting this curve but that the majority of the TORFM is being worn off quickly in the curve. A field survey of the track reveals that the valleys of the signal are patches of TORFM on the rail head. This suggests that there is a large amount of lateral sliding and stick-slip behavior of the wheels in this curve. Under these conditions, TORFM is especially effective and protecting this curve is very important.

Figure 5-12: Patchy TORFM condition in a sharp left hand curve

These conditions also demonstrate a failing of spot measurements. A single spot measurement could easily test only a lubricated patch or an unlubricated patch and present a misleading conclusion to the test engineer. Moving testing, however, revealed the patchy nature of the lubricity condition and allowed for a more accurate evaluation of the lubricity condition.

For this curve, some of the patchy TORFM is inherent to the lateral sliding of the train through the curve and cannot be avoided. Moving the TOR applicator farther back from the curve and using a longer applicator bar could assist with creating a more uniform application of TORFM onto the train wheels and having less phase coherence with the application spot further down track.

The fluorescent data corroborates the conclusions drawn from the gloss ratio data. For the left hand rail, the lubricity condition rises very quickly near the applicator sites before dropping down to low values throughout the rest of the curve. The activity in the left hand rail signal is an indication that there is lubrication on the track rather than the entire curve being worn clean.

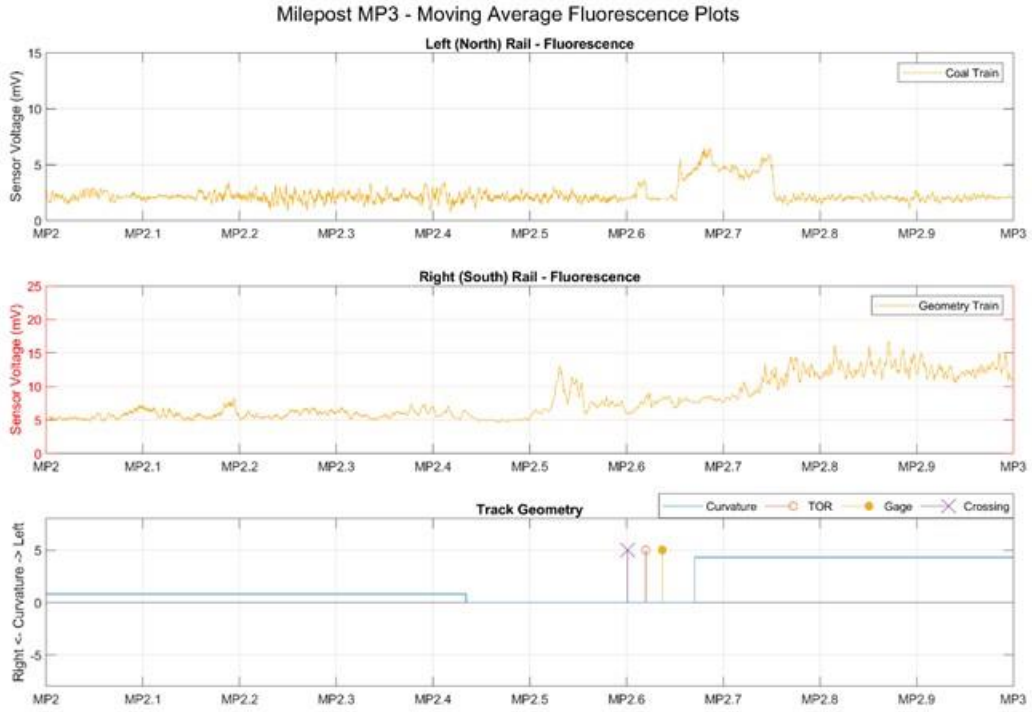

Figure 5-13: Moving Average Filtered Fluorescence Data from Milepost 3

For the right hand rail, the lubricity condition rises at the applicator and then continues to rise through the curve. The right hand rail is the high rail through the curve and will have heavy flange contact. This pushes the flange grease from the wayside applicator onto the top-of-rail surface and contributes to the elevated fluorescence signal. This reading can be used to inform the maintenance-of-way engineers to errant flange grease migration but in a curve this sharp there may be very little that can be done to avoid this. The gloss ratio for the right hand rail here is around a value of 4 which indicates that this section of the curve remains well lubricated.

At the end of MP 3, the gloss ratio of the left hand rail was around a value of 6 or higher and the right hand rail had a gloss ratio of around 4. The left hand curve ends at MP 3.05 and the phantom applicator effect can be seen in both rails. The left hand rail drops to a value of 4 and the fluorescence signal also shows a sudden spike near this location. The right hand rail drops all the way to a value of 2 which based on the trends and the high fluorescence signal is likely indicative of heavy lubricity and not a rough surface figure. The right hand rail quickly rebounds to a gloss ratio of around 4 and a field survey of the track shows signs of rail lubricants all the way up to the crossing.

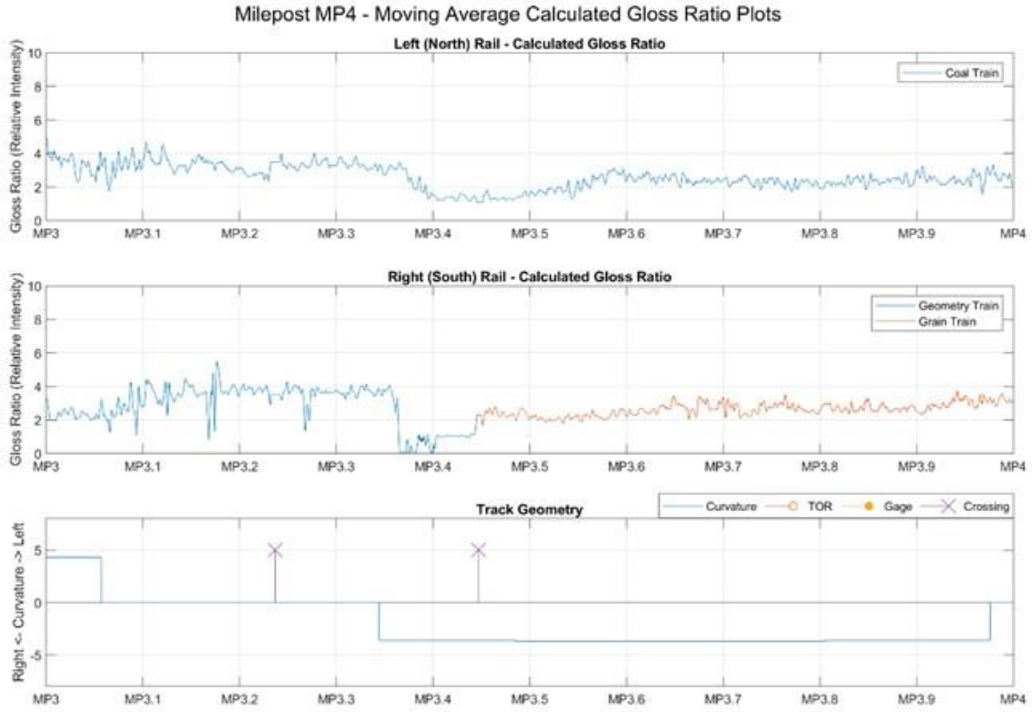

Figure 5-14: Moving Average Filtered Calculated Gloss Ratio Data from Milepost 4

The gloss ratio of the right hand rail shows an anomaly near MP 3.4. This location was tested in 2018 with the second generation rail lubricity sensor and the push cart and a similar signature was observed then too [4]. This was inspected during the field survey but no culprit could be identified. The splice between the track geometry train test and the grain train test occurs at this crossing. The two trains are given different colored lines and are identified with different legend entries on the right hand rail.

Here, the fluorescence data is able to give a clear indication to the drastic difference in signal levels between the revenue service trains such as the coal train and grain train and the track geometry train. When account for the difference in y axis scale, the grain train and the coal train both have fluorescent signals of around 2.5 mV which is significantly lower than the 10 to 15 mV readings of the track geometry train. This further supports that more lubricity is left on the tracks after the track geometry train has passed than after typical freight trains. In 2000, an FRA study on TORFM found that the track was clean after a passing train [6]. It was later found in 2004 that unlubricated trains following lubricated trains still saw the advantage of TORFM suggesting that not all of the TORFM was consumed by the passing train [7]. These fluorescent readings corroborate the 2004 study but show that the amount of lubricant left depends on the train traffic.

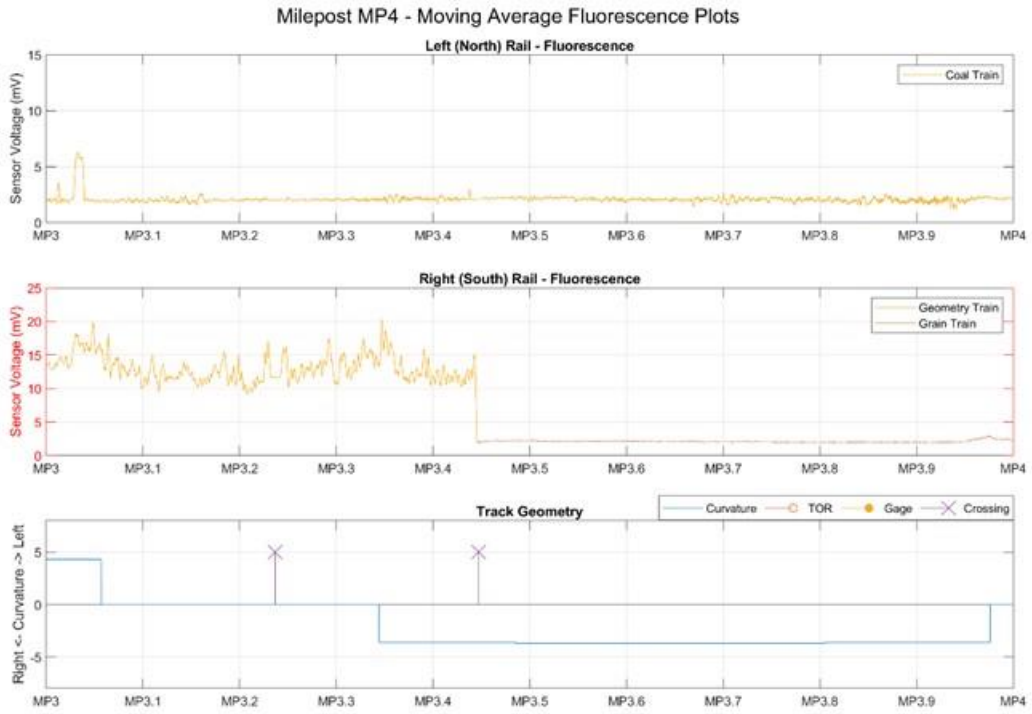

Figure 5-15: Moving Average Filtered Fluorescence Data from Milepost 4

The low fluorescent signals and gloss ratio values from MP 3.5 to MP 4 suggest that both rails are relatively unlubricated at this point. This indicates that the sharp left hand curve has a much more aggressive rate of consumption of the TORFM than other sections of track. A field survey of this section of track revealed some signs of lubricity but that the overall lubricity condition of this rail was overall lower. The marginal nature of the lubricity on this curve is challenging for this sensor with only a limited amount of historical data. This would be an ideal section of track to install a strain gage site to better understand the lateral forces and lubricity condition at this spot.

Figure 5-16: A field survey of the track near MP 3.7 shows limited signs of TORFM

The coal train on the left hand rail shows a slight rebound going into the sharp left hand curve in milepost 5 and a phantom applicator effect at the end of the curve as well. The gloss ratio never rises much above a value of 4 so it is not expected that the rail is brightly polished from high wear here. Small drips of heavily compacted TORFM could be found at various spots in this section further suggesting TORFM is propagating this far down track. This section of track is approximately 2 miles from the previous applicator so it would be expected for TORFM to carry this far although clearly the sharp curves in this region have restricted the carry distance somewhat. The right hand rail shows higher gloss ratio values corresponding to shiny clean rail in the sharp left hand curve.

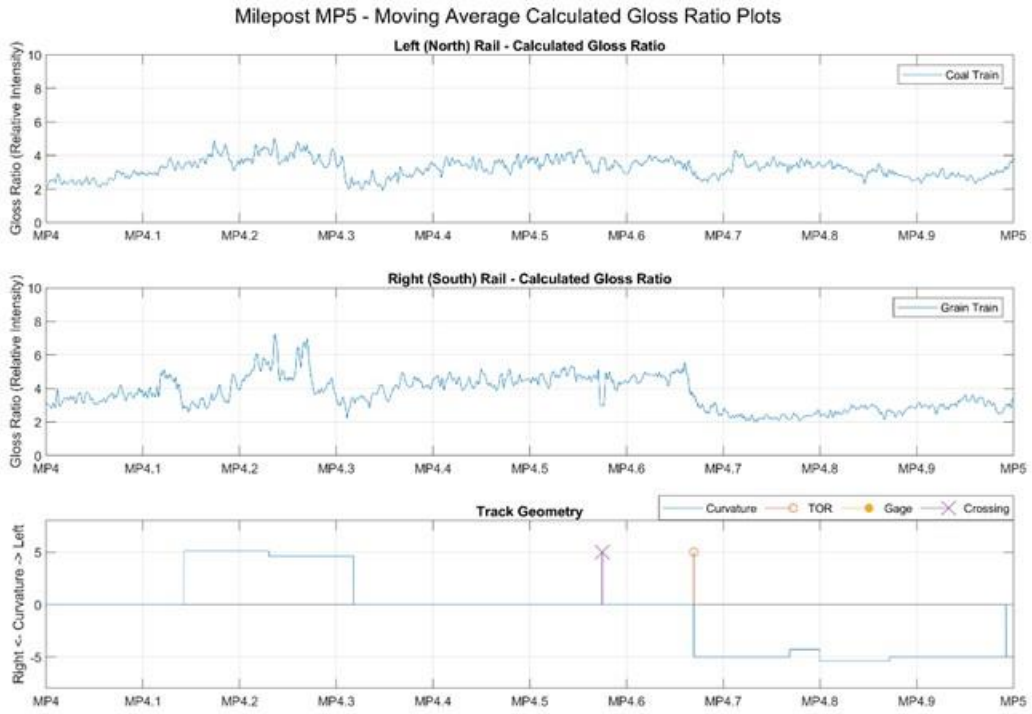

Figure 5-17: Moving Average Filtered Calculated Gloss Ratio Data from Milepost 5

A field survey of this section of track showed that the rail was overall very clean around MP 4.5 but signs of TORFM and flange grease could be found in the curve at MP 4.2. In the curve, the gage corner of the right handrail was very shiny as seen in Figure *5-18* from a high amount of flange contact in the sharp curve. This section of track is also in a forested section and a number of crushed leaves could be found on the surface. Past research has indicated that the lignin in leaves can be detected with fluorescent sensors [31].

Figure 5-18: A patch of dried TORFM can be seen on the field side of the rail.

Figure 5-19: A crushed leaf can be seen packed onto the surface of the rail

The fluorescent signal shows a high amount of fluorescent content in the sharp curve at MP 4.2. This sudden increase in fluorescence helps demonstrate the phantom applicator effect as rail lubricants not previously in contact with the rail are brought into contact during the lateral shifting of the wheelsets while entering and exiting curves.

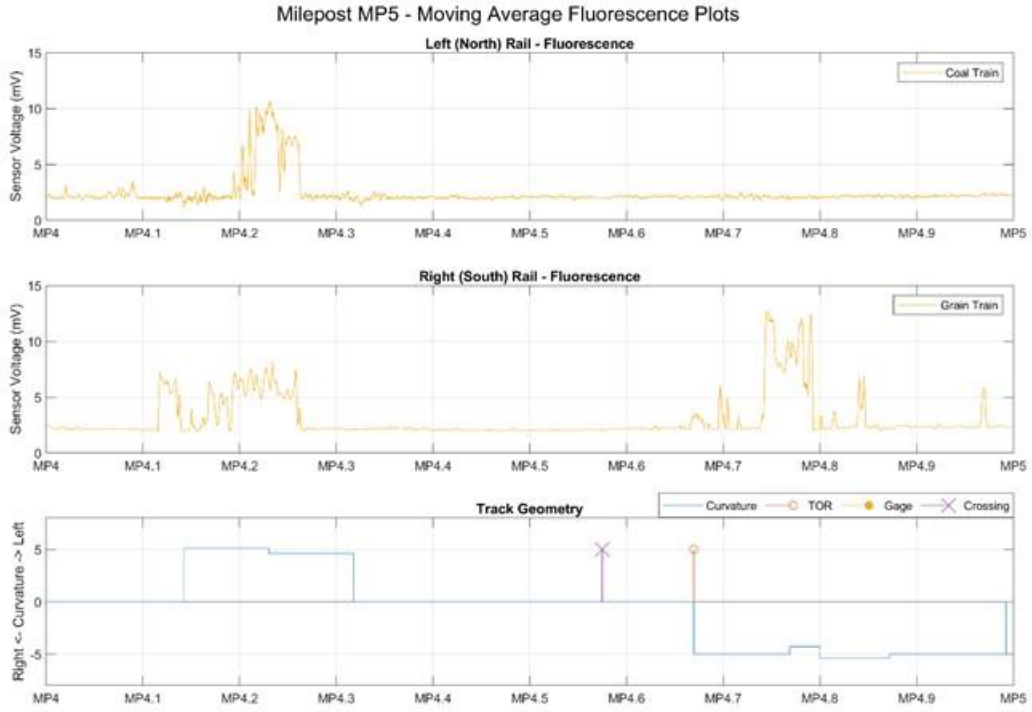

Figure 5-20: Moving Average Filtered Fluorescence Data from Milepost 5

The right hand rail has a very typical set of lubricity signals right at the TOR applicator at MP 4.7. There are several strong spikes in the fluorescent data and a strong dip from heavy TORFM in the gloss ratio. The same, however, is not true for the left hand rail. Neither the gloss ratio data nor the fluorescent data show any strong indication as to the presence of a TOR applicator. One of the failure modes of a TOR applicator is a clogged nozzle.

During the field survey, the TOR applicator was checked and verified to be operating correctly. Some time had passed between the field test and the field survey. If the nozzle had been clogged temporarily, the pressure from the wayside applicator pump could have eventually cleared the line resolving the issue. Figure *5-21* below from the field survey clearly shows the large amount of TORFM at the applicator site that can clearly be identified by the sensor.

Figure 5-21: TOR wayside applicator functioning correctly in the field with TORFM applied to the rail surface.

It is possible that there was an issue with only the left hand nozzle at this site on the day of the test. It is also possible that because the TOR applicator is so close to a sharp curve, the TORFM signal on the high rail, in this case the left hand rail, is obfuscated when the wheels shift laterally. Looking farther down track to the next milepost block there is a phantom applicator curve and a spike in the fluorescence data shortly past the curve at MP 5 for the left hand rail.

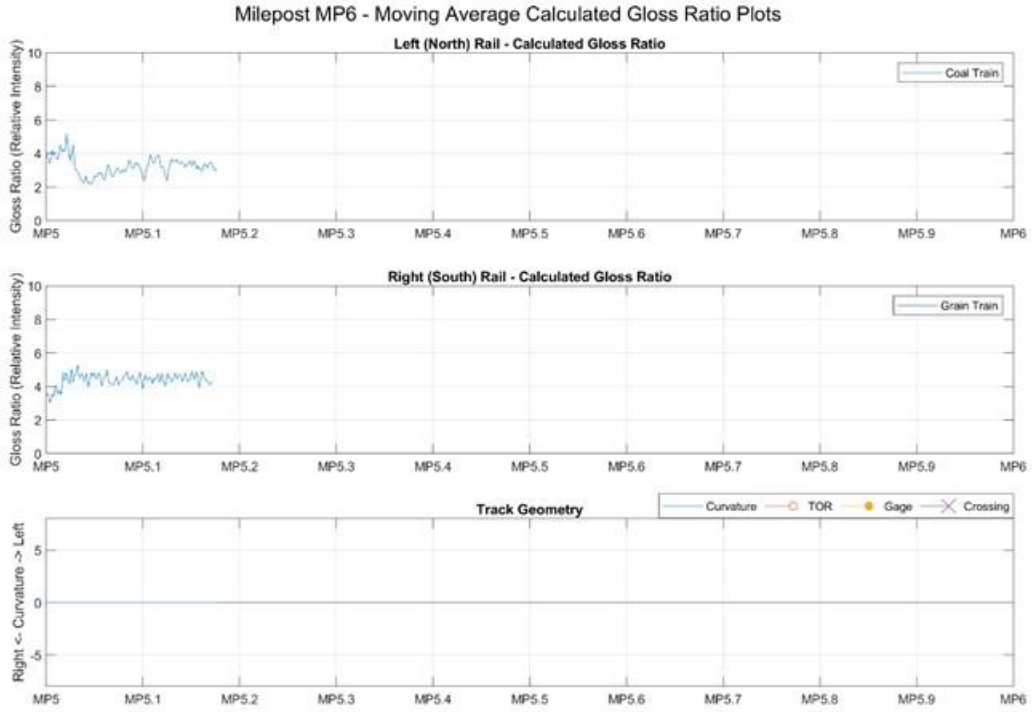

Figure 5-22: Moving Average Filtered Calculated Gloss Ratio Data from Milepost 6

Right at MP 5, there is a small dip and quick rise in the gloss ratio for the right hand rail which is part of the phantom applicator effect when exiting the curve. The end of the test was within 0.2 miles of the end of the final curve and about 0.5 miles from the last TOR applicator. This limits the conclusions that can be drawn about the effects of the final applicator but every test must come to an end and the crossing at this site was ideal for terminating the test section.

For the fluorescence data, there are two particular peaks in similar spots in the last milepost block. These are very short peaks indicating some sort of spot anomaly. This was investigated during the field survey but not specific culprit could be identified. In this section of track during milepost block 5 and 6 there are several spots where crushed leaves are compacted onto the top-of-rail surface. It is suggested that these peaks are from the lignin from leaf fall and no significant lubricity implications could be found from the presence of these peaks.

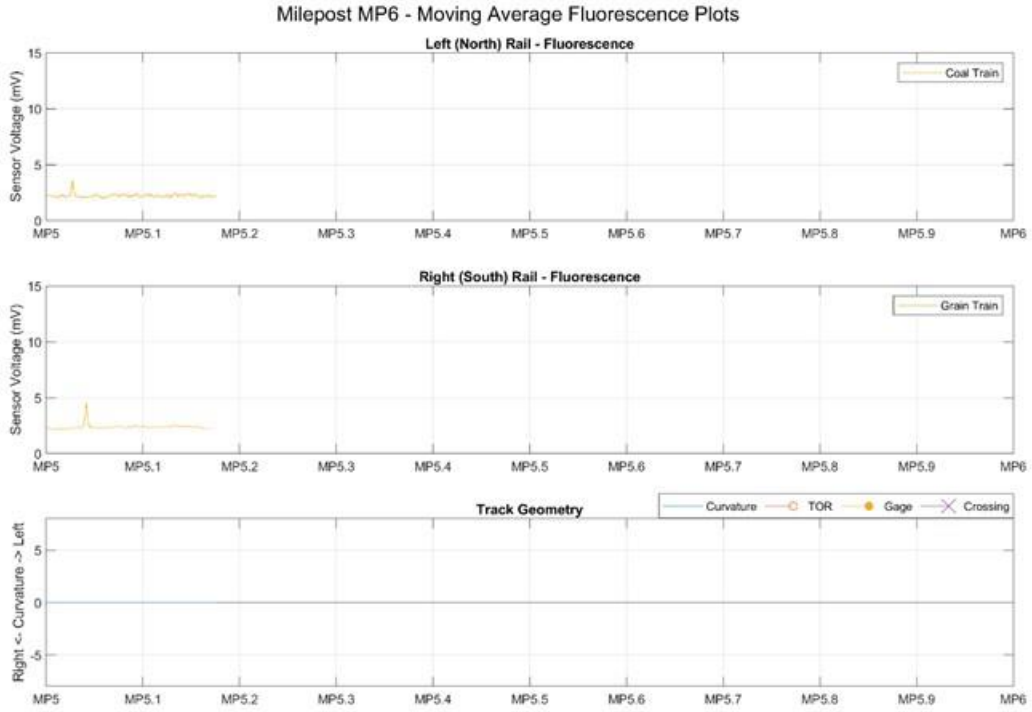

Figure 5-23: Moving Average Filtered Fluorescence Data from Milepost 6

5.3 Linear Curve Fitting

The next step in the data analysis was to begin numerically characterizing the performance and trends of the gloss ratio. Analysis of the fluorescence plots shows that the fluorescent signal does not have strong trends and tends to resolve to a more binary representation of lubricity. The gloss ratio plots have several regions that appear to have significant linear trends and other non-linear dynamics are also present. For this reason, curve fits will only be applied to the calculated gloss ratio data.

Curve fits, if predictive of actual track lubricity conditions, can be used to extend the understanding of test data beyond the scope of the data captured. This will allow for extrapolation beyond the actual test data and, with enough validation, could result in a predictive model that could be applied to section of track that have never been tested. Such a model could also be applied parametrically to entire rail systems to test and evaluate a wide array of candidates for wayside applicator placement and evaluate the effectiveness and return on investment for any proposed lubricator deployment.

5.3.1 Linear Curve Fitting Method

To accomplish this, a simple linear regression was applied to select sections of the test data. This type of curve fitting can be accomplished with many different statistical tools including Microsoft Excel and MATLAB. Both Excel and MATLAB are capable of generating different types of curve

fits beyond a simple linear regression; however, while observing the CGR plots, it is apparent that the gloss ratio signal has significant regions that have strong linear correlations. It is posited that at the extinction points of TOR lubricity may be strongly nonlinear, but the current data set does not offer a clean demonstration of any extinction effects. This presents an opportunity for further research in the future.

To apply a curve fit, a linear region of lubricity data was first identified and then isolated as a separate data set to be fed into the curve fit tool. In MATLAB, the "polyfit" function generates a linear curve fit if the polynomial degree parameter is set to a value of "1." The resulting curve fit parameters are fed to the "polyval" function and an array of values is returned for plotting. The resulting array is plotted on top of an existing moving average plot and a legend entry is added with the polynomial equation. A sample for milepost MP 1 is shown below. The equation is written with the y intercept set at the start of the curve fit and the slope is change in gloss ratio per mile.

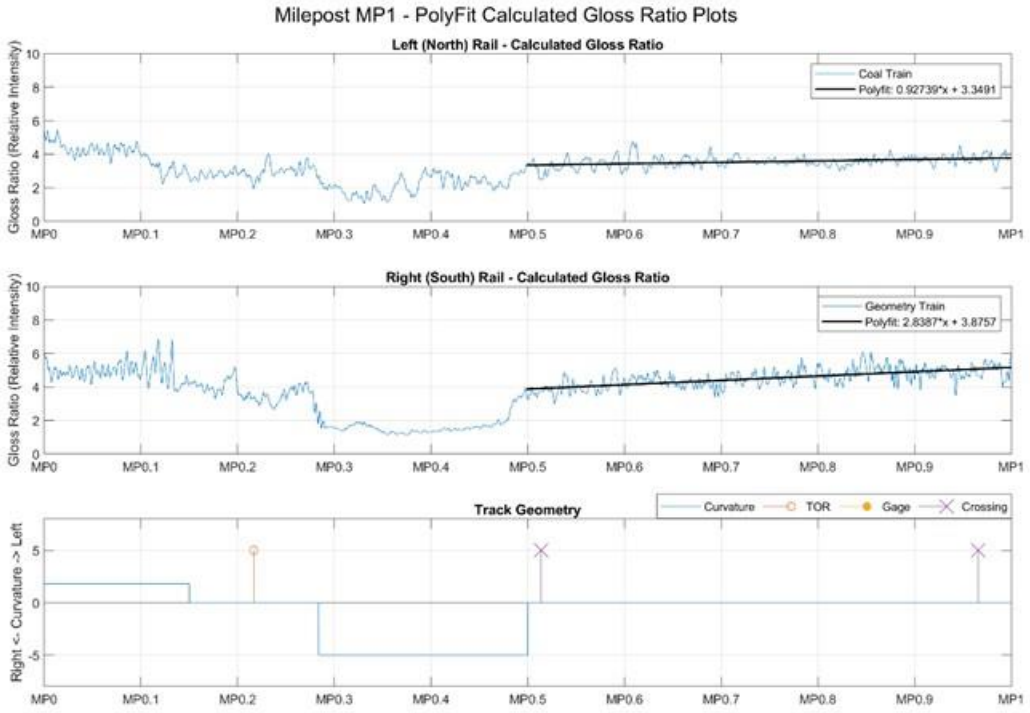

Figure 5-24: Example Linear Curve fit of Moving Average Filtered Calculated Gloss Ratio Data

Typically linear regression analysis is paired with the coefficient of determination, commonly called R^2 or "R Squared." This is calculated by the equation below where R^2 is the coefficient of determination, SS_{res} is the sum of squares of the residuals, and SS_{tot} is the total sum of squares.

$$R^2 \equiv 1 - \frac{SS_{res}}{SS_{tot}} \tag{16}$$

In this case, the R^2 value for the left hand curve is 0.1345 and the R^2 value for the right hand rail is 0.4509. These are R^2 values are not the approximately 0.9 values typically indicative of a good curve fit, however this does not mean that the curve fit is not representative of the trend of the data. By visual inspection, it is clear that the trend lines track the trend of the data but is also clear that there is significant variance of the gloss ratio about the trend line.

For this phase of the research project, there is insufficient information to define a statistical confidence interval necessary to determine if a linear fit is appropriate or not to characterize the lubricity data. To produce a final, production-ready version of a rail lubricity sensor, a statistical threshold for lubricated versus clean condition will need to be determined from a larger data set of track lubricity measurements. For now, the curve fit will be assumed to be predictive and used to roughly approximate the wear off rate and carry distance of the friction modifiers. For that reason, R^2 values will be omitted from the linear curve fitting results and any conclusions on carry distance will be understood to be rough approximations made from a limited data set.

5.3.2 Linear Curve Fitting Results and Analysis

The linear curve fits for the first mile of data were fit to the tangent section of track following the TOR applicator and the right hand curve. The tangent section of track should have more linear effects as the wheel sets have less incentive to shift laterally and should provide more uniform results. As has been pointed out in the previous section with the results of the moving average analysis, the gloss ratio behavior near the entrances and exits of curves and near the wayside applicators has transient nonlinear behavior. At this point in the modeling and analysis of optical lubricity measurements, signal processing effort was focused on the more steady-state trends beyond these transient, step input style disturbances.

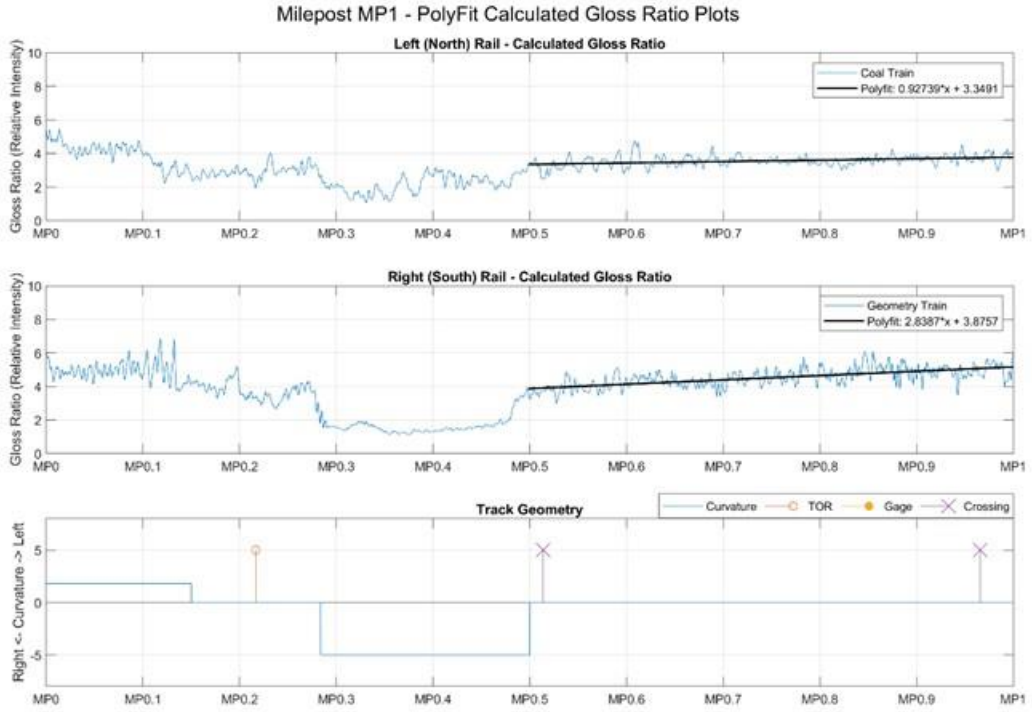

Figure 5-25: Linear Curve fit of Moving Average Filtered Calculated Gloss Ratio Data from Milepost 1

Although the track geometry train appeared to be leaving behind much higher levels of track lubricity due to the fewer number of axles, it also appears that the shorter train may have a decreased ability to carry as much TORFM down track. As a result, the slope of the gloss ratio curve fit for the right hand rail is significantly steeper than the slope for the left hand rail. In fact, the slope of the linear curve fit for the geometry train is almost three times as large as the slope for the coal train. This may also suggest that the higher number of axles on the coal train leaves a very stable lubricity condition while the shorter geometry train has a transient trend when the train has passed. The trace of the geometry train gloss ratio quickly approaches a shiny clean rail condition which is was also represented in the fall off of fluorescence data as shown in the moving average plots shown in the previous section.

Using the curve fit equation as a guide, the right hand rail reaches a clean rail gloss ratio of around 7 in approximately 1.1 miles.

$$2.8387 * x + 3.8757 = 7 \; when \; x \; is \; equal \; to \; 1.101 \; miles \tag{17}$$

After adding the 0.28 miles offset between the TOR applicator and the start of the trend line, this would be an estimated carry distance of 1.4 miles, roughly the expected carry distance for a single applicator and an unconditioned wheelset [32]. This does not hold for the left hand rail where the expected carry distance would be 4.2 miles according the curve fit equation with the 0.28 mile offset added.

$$0.92739 * x + 3.3491 = 7 \; when \; x \; is \; equal \; to \; 3.937 \; miles \tag{18}$$

The curve fits in the next mile segment again starts a short distance after the TOR applicator and is plotted along tangent track to take advantage of the tangent track measurements wherever possible. This section of track has a significantly longer straightaway allowing for a longer curve fit to be applied and a longer section of track to be evaluated for trends in lubricity data. The linear regression is stopped short of the curve at the end of the milepost to avoid any transient effects of lateral wheel shift while entering a curve.

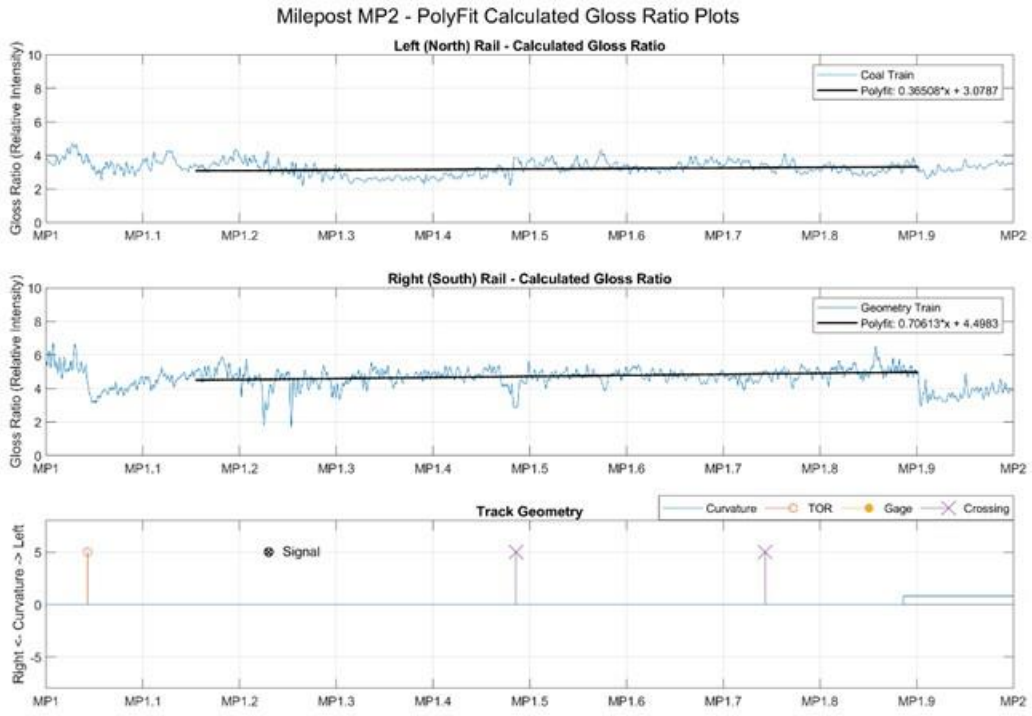

Figure 5-26: Linear Curve fit of Moving Average Filtered Calculated Gloss Ratio Data from Milepost 2

In this milepost, the slopes of the trend lines are drastically reduced. This would serve to confirm the conditioning, or "kick starting," effect as the wear off rate, the slope of the line, is notably reduced directly following the second applicator within a one-mile stretch. The right hand rail trend line slope decreases from 2.8387 to 0.70613 and the left hand trend line slope drops from 0.92739 to 0.36508. This represents a 4 times reduction in slope for the right hand rail and a 2.54 times reduction for the left hand rail.

Table 5-1: Gloss Ratio Slope comparison between MP 1 and MP 2

	Left Rail (Coal Train)	Right Rail (Geometry Train)
MP 1 Slope	0.92739 Gloss Ratio Index / Mile	2.8387 Gloss Ratio Index / Mile
MP 2 Slope	0.36508 Gloss Ratio Index / Mile	0.70613 Gloss Ratio Index / Mile
Reduction Factor	2.54x	4.02x

Using the trend lines as rough estimates for carry distance again, the right hand rail now extends to about 3.6 miles after the last (second) applicator which is again consistent with estimates published in the AREMA paper by Whitmore and Norfolk Southern [32]. The trend line equation gives a carry distance of 3.5 miles as shown below and there is a 0.1 mile offset between the start of the trend line and the TOR applicator.

$$0.70613 * x + 4.4983 = 7 \; when \; x \; is \; equal \; to \; 3.543 \; miles \tag{19}$$

Unfortunately, the trend line for the left hand rail is not predictive of a likely TORFM carry distance. The equation yields an estimated carry distance of more than 10 miles which is not consistent with any existing measurements of TORFM carry distance, even in best case scenarios. This suggests two conclusions. The first is that although the gloss ratio data may appear to be piecewise linear, the overall trend of the data is significantly nonlinear. When the lubricity is in a condition where the slope of the line is very small and the trend is almost horizontal, the slope of the trend line is not predictive of the carry distance. Because the coal train data on the left hand rail is very stable, there is insufficient dynamics to create a predictive curve fit model in this short section. This leads to the second conclusion which suggests that the different spreading dynamics inherent to the track geometry train may result in a curve fit that is predictive of the overall carry distance. If this is true, then mounting a rail lubricity sensor on a track geometry car would be very useful since the data following a track geometry train is uniquely predictive of carry distance. With only a single test, there is insufficient data to determine if this is a coincidence or actually predictive. This should certainly be the topic of future study.

Table 5-2: Comparison of estimated carry distances between two trains and assessment of the accuracy of the prediction

	Left Rail (Coal Train)		Right Rail (Geometry Train)	
	Estimated Carry Distance	Realistic Prediction?	Estimated Carry Distance	Realistic Prediction?
MP 1	4.2 Miles	No	1.4 Miles	Yes
MP 2	>10 Miles	No	3.6 Miles	Yes

Into the next milepost, the slopes of the trend lines remain very low, almost horizontal. After positioning two TOR applicators close to each other to facilitate the conditioning effect, the benefit is that subsequent lubricators can be spaced farther out as the carry distance is increased. This

appears to hold true and even a mile away from the previous applicator the gloss ratio signal remains very constant. In the previous section it was reported that a field survey of this section of track confirmed signs of TORFM. The trend lines end at the wayside applicators as the region following in the sharp curve is far to stochastic and nonlinear to attempt a curve fit model at this stage in the research.

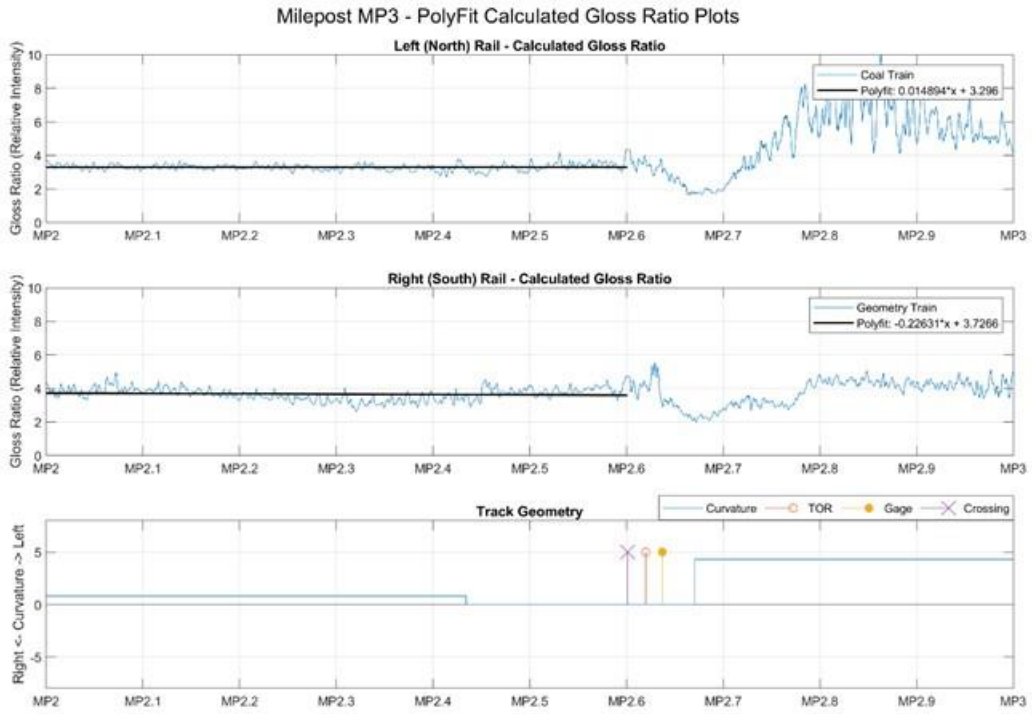

Figure 5-27: Linear Curve fit of Moving Average Filtered Calculated Gloss Ratio Data from Milepost 3

For this set of trend lines, there is really no benefit to calculating a predicted carry distance. The trend line generated of the right hand rail actually has a negative slope which cannot algebraically estimate an intercept with a clean rail condition. Similarly, the left hand rail has a very small, near zero slope. Any approximation of carry distance becomes unrepresentative as the slope approaches zero. This demonstrates that the assumption of truly linear relation between gloss ratio and lubricity condition is not accurate and a piecewise or nonlinear function is needed to predict the carry distance of TORFM in this section.

Milepost block 4 has several nonlinear regions while exiting the sharp left hand curve and entering a moderate right hand curve. This also extends across the division between the geometry train test data and the grain train test data as annotated on the plot. A relatively linear section of test data was found starting at MP 3.6 and continuing to MP 4.

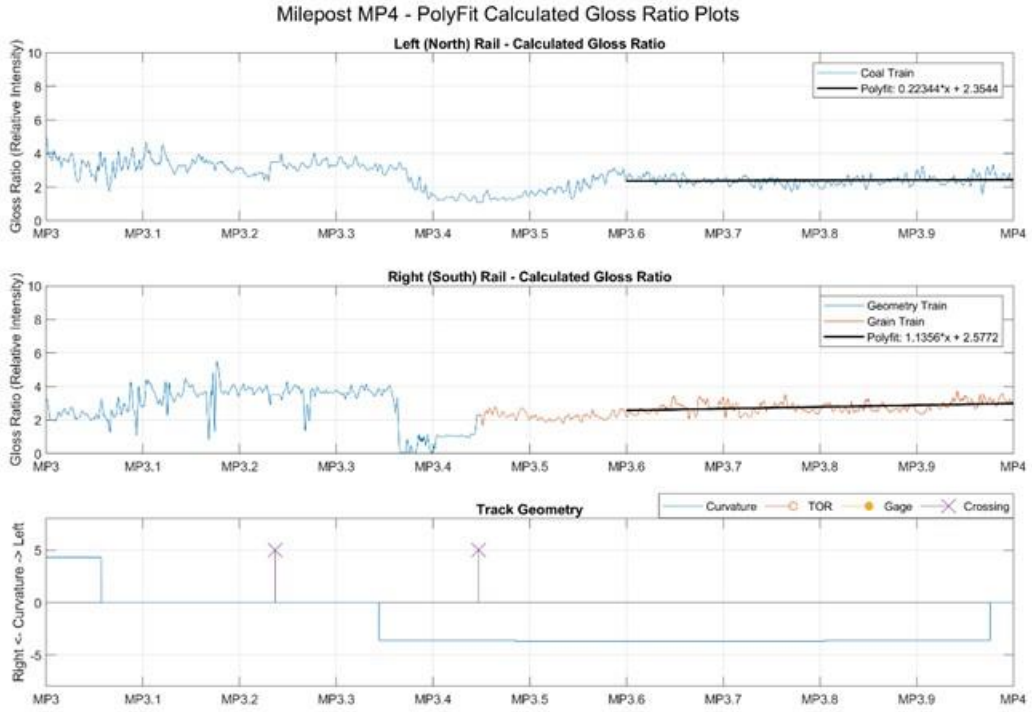

Figure 5-28: Linear Curve fit of Moving Average Filtered Calculated Gloss Ratio Data from Milepost 4

The values of the slopes indicate that on this section of track, the conditioning effect is less than it was on the previous sections of track. The left hand rail trend line slope has risen from 0.015 to 0.223 suggesting that the elevated curving forces in the previous section of track have had resulted in an increase wear rate for the TORFM. As a result, some of the conditioning effect appears to be gone. This 0.223 value is still less than the unconditioned gloss ratio slope of 0.927 on milepost MP 1 so the conditioning effect does not appear to be completely lost, just reduced.

For the right hand rail, the preceding traffic had come to a complete stop across the previous applicator. Under the assumption that the contact of the brake shoes on the wheel tread surface wore off the majority of the TORFM, the grain train wheelsets were effectively unconditioned by the train coming to a stop for the signal. This is represented by a high gloss ratio slope of 1.136, a value that is significantly lower than the 2.839 gloss ratio slope at MP 1 for the geometry train but higher than the 0.927 gloss ratio slope for the coal train at MP 1.

Applying a carry distance approximation from the trend line equation for the grain train appears to be unrealistic and **not** predictive. From the start of the trend line, the previous wayside applicator is almost exactly 1 mile away. The trend line equation predicts another 3.9 miles of carry distance which would far exceed the expected carry distance at almost 5 predicted miles of carry after coming to a stop on top of the previous wayside applicator and removing some of the conditioning effect of the wheels. At this point, the only two predictive carry distances have come from the curve fits following the geometry train. This again shows that a linear approximation is not accurate over long distances for revenue service trains like the coal train and the grain train.

$$1.1356 * x + 2.5772 = 7 \; when \; x \; is \; equal \; to \; 3.895 \; miles \tag{20}$$

The milepost block MP 5 linear fit plots continue from where the previous trend lines ended at MP 4 and continue up to the TOR applicator at MP 4.7. Although there is some significant nonlinear variance in the sharp left hand curve at MP 4.2, the linear fit lined up well with the linear segments on both sides of the curve for both rails so the decision was made to include the curve as part of the linear regression.

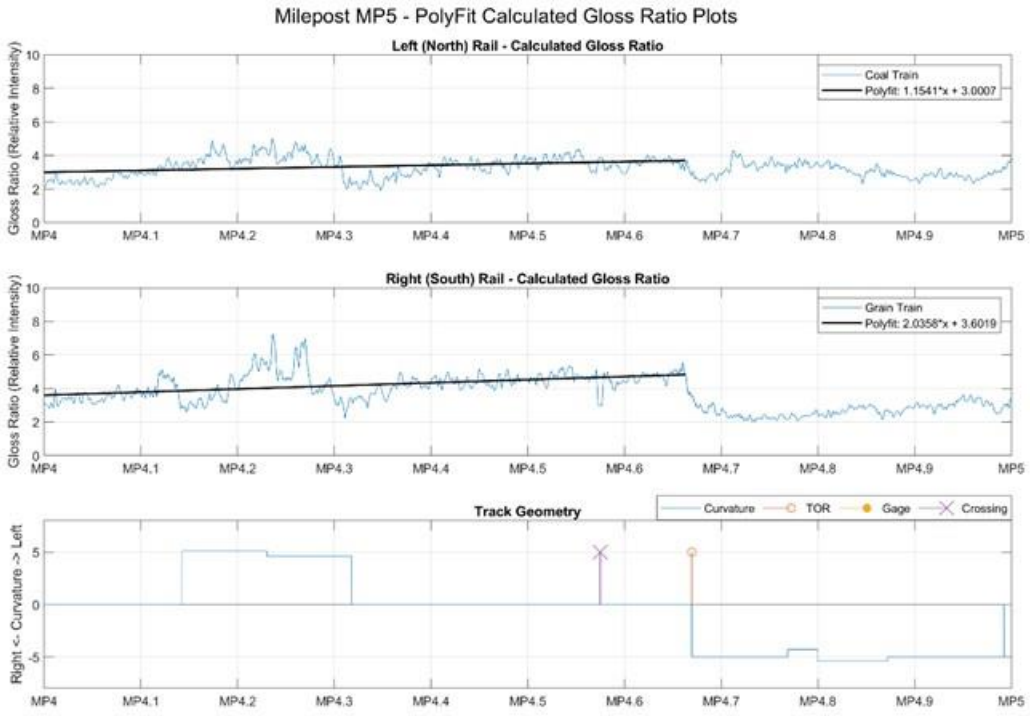

Figure 5-29: Linear Curve fit of Moving Average Filtered Calculated Gloss Ratio Data from Milepost 5

slopes of the two trend lines are notably higher than the slopes of the trend lines in the previous milepost. This further serves to reject assumption of linear behavior for the gloss ratio trend. With small changes over long x axis distances, the nonlinear effects of the gloss ratio become harder to perceive as the actual curve appears piecewise linear or linear within a limited range of operation / observation. For the left hand rail, the previous trend line had a slope of 0.223 which subsequently increases to 1.154 in this milepost. Likewise, the trend line for the right hand rail increases from 1.136 in the previous trend line to 2.036 for this trend line.

Table 5-3: Gloss Ratio Slope comparison between MP 4 and MP 5

	Left Rail (Coal Train)	Right Rail (Grain Train)
MP 4	0.223 Gloss Ratio Index / Mile	1.136 Gloss Ratio Index / Mile
MP 5	1.154 Gloss Ratio Index / Mile	2.036 Gloss Ratio Index / Mile

Based on the underlying physics and typical behavior in wear systems, it is in fact logical to assume that the lubricity trends would be non-linear especially during the transient section near the applicator and far down track at the extinction point of the TORFM third body layer. This extinction behavior will need to be studied in more detail both from both an optical perspective of the scattering behavior was the TORFM fades away completely and also from a contact and wear mechanics perspective to gain an understanding of the exact wheel/rail contact physics that cause the third body layer to wear away.

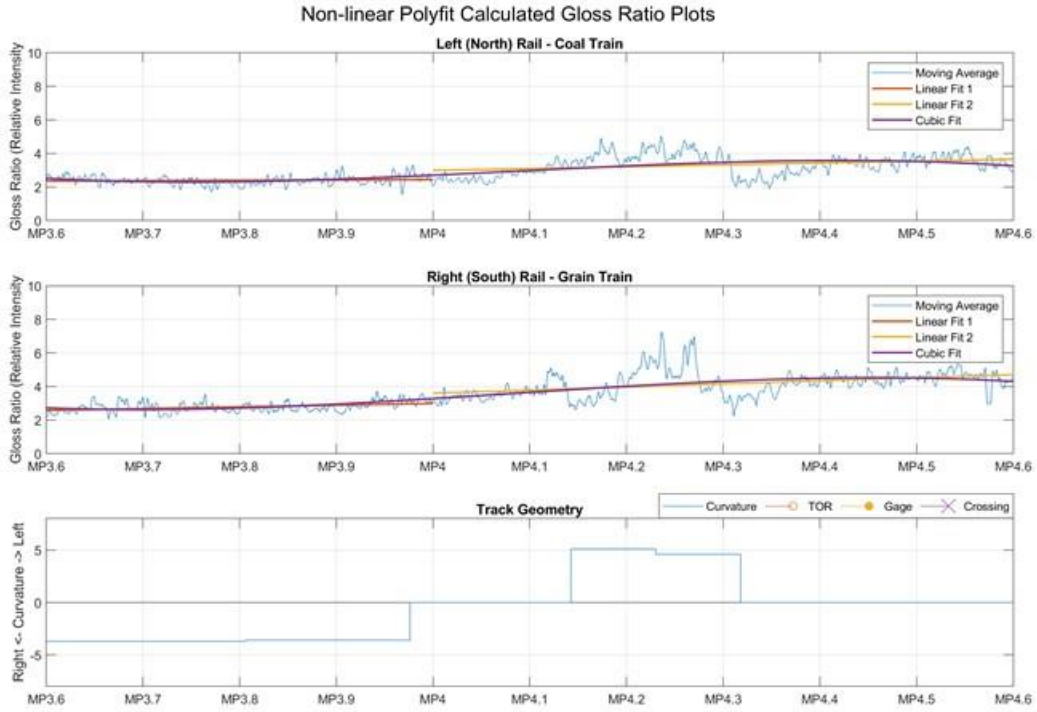

Figure 5-30: Nonlinear curve fit of Moving Average Filtered Calculated Gloss Ratio data in Mileposts 3 and 4

Figure *5-30* shows both linear curve-fits from milepost 3 and milepost 4 as well as the non-linear cubic fit that was attempted. In the body of the curve fit, the cubic fit looks to match the data well. At the ends, the fit becomes less good as the final inflection point causes the cubic function to approach a vertical asymptote on both sides, not a horizontal asymptote. The equations for the two cubic curve fits are shown below where d is the distance in miles and $d = 0$ at the origin located at MP3.6.

$$Left\ Rail: CGR(d) = -8.4296d^3 + 12.2629d^2 - 3.0873d + 2.5143 \qquad (21)$$

$$Right\ Rail: CGR(d) = -8.7163d^3 + 12.5287d^2 - 2.2422d + 2.7311 \quad (22)$$

Higher order polynomials will add more degrees of freedom to create a better match but it is important to note that the goal is to model the behavior, not construct an arbitrary curve that happens to fit this particular set of test data.

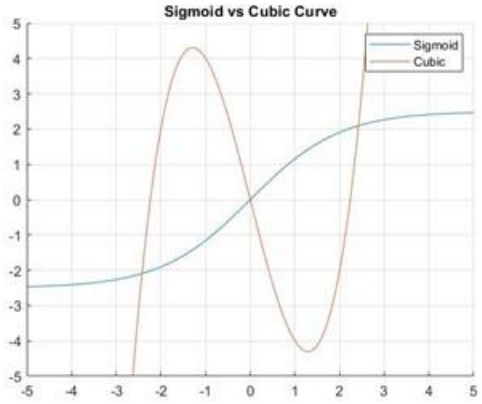

Figure 5-31: Comparison of Sigmoid and Cubic curves for fitting to lubricity data

A sigmoid curve would be a better for the carry behavior of this section of TORFM. Aside from some transience at the TOR applicator, it is expected that the TORFM condition will rise from a baseline value and eventually experience a horizontal asymptote at a clean rail condition. Creating an experimental sigmoid fit requires advanced knowledge of the extinction behavior of the rail lubricity which will need to be the focus of future studies to create a predictive model of TORFM carry distance.

5.4 High Pass Filter and Moving Variance

In addition to overall signal magnitude for both the fluorescence and gloss ratio, the dynamics of each signal also have potential implications on the rail lubricity condition. For example, it is suggested that rail with a large amount of surface roughness will exhibit higher amounts of variance as the signal spikes from highly reflective glints off the surface. In the moving laboratory tests, it was shown the TORFM produced a very even signal response where the clean rail condition showed significant spikes and variations off the shiny steel surface. Longer periods of variance could also suggest inconsistent or "patchy" rail lubrication conditions where short sections of rail are lubricated while adjacent sections are clean. The TORFM and flange grease are applied to single spots or short sections of the passing wheels so as the lubricant is applied there is a spatial coherence where the wheels align with the same contact patch. The wheels will remain in phase until the rail vehicle dynamics and slight differences in wheel circumferences cause them to fall out of phase and the mechanics of applying the TORFM to the rail spread the lubricant to the rest of the wheel.

5.4.1 High Pass Filter Design and Moving Variance Method

The variance of the optical signals is caused by high frequency oscillations so the baseband, near DC content of the signal can be filtered out to target the signals that directly generate the variance. The High Pass and Moving Variance plots are primarily targeting signal performance that is caused by surface roughness on the rail.

The tachometer increments in 3.875" steps. This results in a spatial frequency of 3.097 ft^{-1}. After applying the Nyquist-Shannon sampling theorem, the highest possible measureable frequency is half the sampling frequency which is 1.548 ft^{-1} [55]. Converted back into a spatial period, this means the smallest period, based on the highest frequency, that can be accurately reconstructed is 7.75 inches. This is much larger than the surface roughness and other imperfections on the rail head surface as can be seen in Figure *5-2*. This instrument is designed to investigate long term data trends, not local surface roughness so this is to be expected. There is still variance in the test data so although this will not be entirely representative of the optical performance on a micro or local scale, it still serves to characterize the trends of the lubricity data at the higher frequencies captured.

$$f_{Spatial} = \frac{1}{T_{Spatial}} = \frac{1}{3.875\ inches} * \frac{12\ inches}{1\ foot} = \frac{1}{0.3229\ feet} = 3.097\ ft^{-1} \qquad (23)$$

Choosing a cutoff frequency at this juncture is somewhat arbitrary. There is insufficient test data to draw any specific conclusions about individual component frequencies. This will certainly be a focus for future research with this instrument. Some notable frequencies are laid out below. Knowledge of these frequencies can help make an informed decision on selecting a cutoff frequency. The cart wheels have 23.25 inch diameter wheels so a spatial frequency of 0.5161 ft^{-1} will be directly linked to cart vibrations. Railroad car wheels tend to have 36-inch diameter freights wheels and mainline locomotives typically have either 40 or 42 inch wheels. Rail wheels have FRA standards the dictate the shape and profile of the wheel which allow for significant tread where before the wheel must be completely replaced. This will cause some variation in the exact spatial frequency so minor variations in the location of this frequency peak are expected. This will be covered further in the frequency domain evaluation section.

Table 5-4: Comparison of Spatial Periods, Frequency, and corresponding wheel diameters

Wheel Diameter (in)	**Circumference (in)**	**Period (ft)**	**Frequency (ft^{-1})**
---	18	1.5	0.6667
7.4	23.25	1.9375	0.5161
---	48	4	0.25
36	113.10	9.4248	0.1061
40	125.66	10.472	0.0955
42	131.95	10.996	0.0909

Once the cutoff frequency is determined, a 6th order Butterworth filter is designed and applied to the raw test data. The 6th order magnitude was chosen as a balance between strong filter roll off while limiting the computational requirements. Higher or lower filter orders can be adopted as they prove necessary. The filter is applied to the raw test data after it has been delineated into spatial data, not the data that was passed through the moving average filter. A moving average filter is a type of low pass filter so once the data is passed through the moving average filter, much of the

high frequency data is filtered out. The results of two cutoff frequencies are shown below for comparison.

$f_{Cutoff} = 0.25\ ft^{-1}$ $f_{Cutoff} = 0.6667\ ft^{-1}$

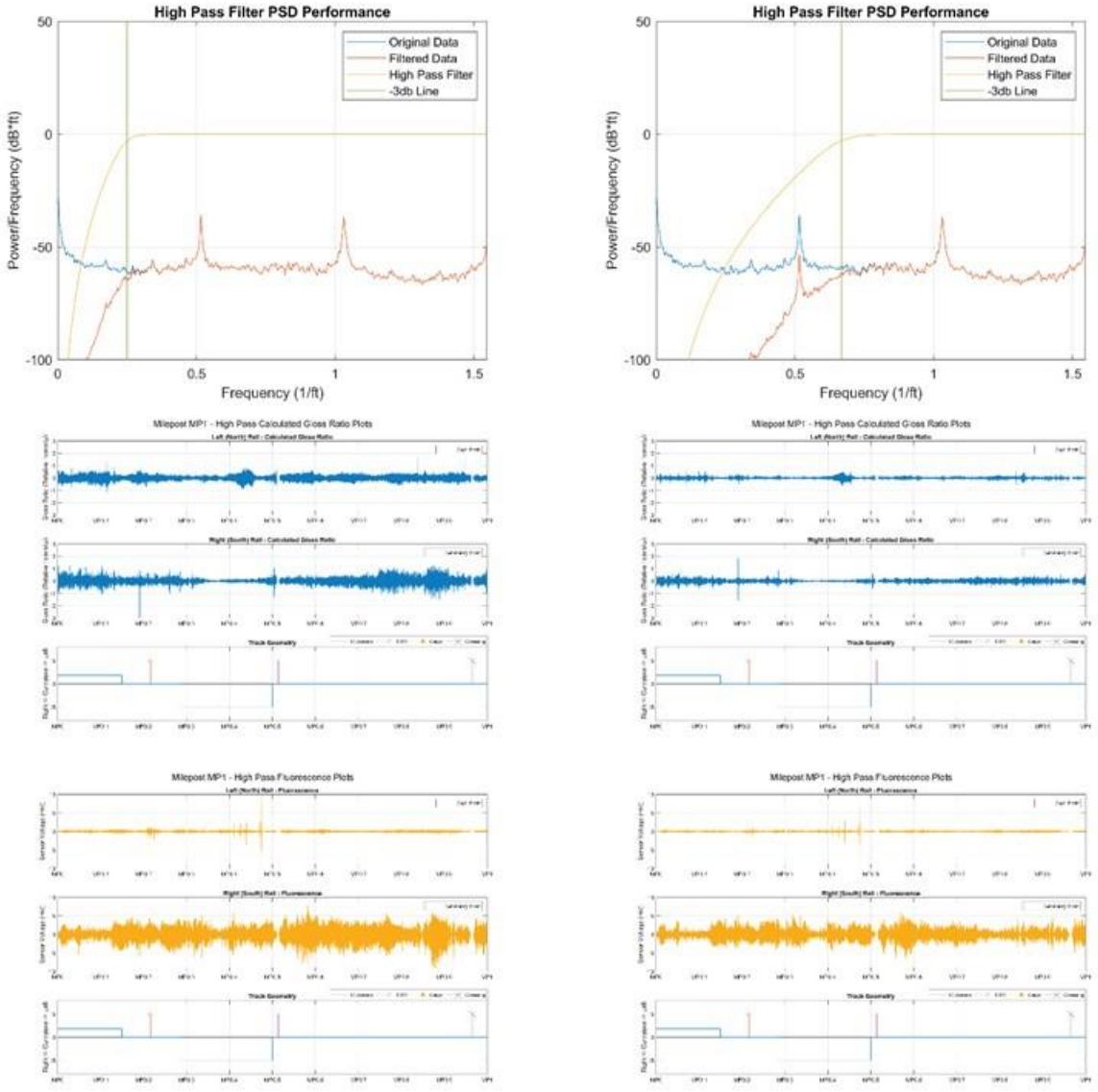

Figure 5-32: Comparison of effects from high pass filter for different cutoff frequencies

Choosing a higher cutoff frequency removes a larger percentage of the signal which limits the available data that can be analyzed. For this research, a cutoff frequency of 0.6667 ft^{-1} was selected. By choosing a cutoff frequency above the peak related to cart vibrations, the high pass filtered data can identify traits less than 1.5 feet or 18 inches long that are related to the rail surface. A cutoff frequency of 0.6667 ft^{-1} represents a spatial period of 18 inches which still represents a fairly long period when compared to the micro surface imperfections. This does, however, strongly filter out any signals with longer spatial periods. As more is learned about the propagation behavior of TORFM, this decision of a cutoff frequency should be revisited in the future. For now, the

decision to use 0.6667 ft^{-1} removes the cart dynamics from the high pass filtered data and allows the filtered data to be used for analysis of the rail surface without the interference of the cart vibrations.

The high pass filtered data in its raw form can illustrate the areas with more or less variance qualitatively. Visually, it is possible to see the areas with more or less variance but quantifying the magnitude of variance will make the information more usable when making direct comparisons. To do this, the variance of the high pass filtered data is calculated. Much like the with the moving average filter, a moving variance window is more representative to the local track condition. MATLAB has a built in function for creating a window of test data and taking the variance of that block. This function is called "movvar" and is applied using the same 10 foot, 31 sample window used for the moving average data. The "movvar" function is applied to the data after it has been processed through the high pass Butterworth filter. This allows the variance to only characterize the high frequency changes in lubricity data independent of any long term trends, particularly in the gloss ratio. This variance calculation helps to quantify the variance for direct comparison rather than a visual, qualitative assessment of variance from the raw or even moving average filtered data.

5.4.2 High Pass Filtered Data and Moving Variance Results and Analysis

In milepost block 1, the left hand rail shows the variance of the data is higher before the TOR applicator than it is afterwards. During the previous sections, it was noted that the overall signal dynamics for the left hand rail were lower. Based on previous TORFM testing, this variance data suggests that the left hand rail has lower variance both due to the more uniform nature of the lubricity condition after a larger number of wheels have passed over and also due to the lower levels of signal in the raw data. The larger number of wheels will have an averaging effect where any stochastic effects become more uniform as several random applications average out to a more uniform value.

In both the gloss ratio data for the right hand rail, the variance shows the lubricity condition becoming very uniform with low variance immediately after the TOR applicator. This is more likely to indicate a heavy lubricated condition where any surface glints for the steel rail are covered in dark, less reflective TORFM. This suppresses any of the very random and high gloss ratio spikes caused by surface glints.

In both the fluorescent data and the gloss ratio data, the variance increases dramatically towards the end of the milepost. In terms of general trends, this can suggest that the rail underneath the track has a higher degree of surface roughness than other more uniform sections of rail. Specific to this run, this would tend to indicate that the lubricity condition is very low and approaching clean for this section of track. The significant difference between the two rails would tend to suggest that the track geometry train leaves more TORFM behind on the rail but also has less capacity to carry TORFM as far down the rail too due to the lower number of wheels.

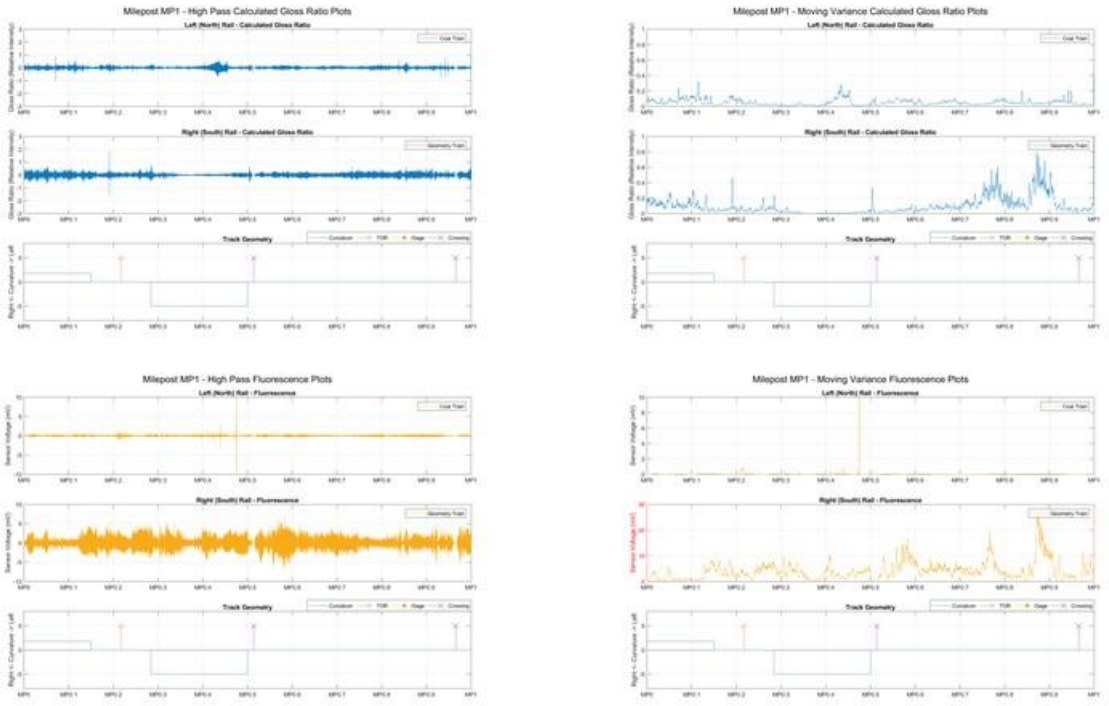

Figure 5-33: High Pass Filtered and Moving Variance Plots for Milepost 1

In the second milepost block, the gloss ratio for the right hand rail has a much lower amount of variance than in the previous milepost block. There is a noticeable spike right at the signal at MP 1.2 where the sensor has a discontinuity over the rail frog. This anomaly can be disregarded. This drop in variance indicates that the overall condition of the rail is much more uniform suggesting that the rail is also better lubricated in this section. This is additional evidence towards proving the conditioning effect of a second TOR applicator in quick succession with the first one.

The left hand rail has even less variance than the right hand rail. A failing of the raw variance calculations is that it is not normalized with overall signal magnitude. In this case, the overall signal left behind by the track geometry car is much more dynamic than the signal left behind by the coal train. There are some important conclusions about the train dynamics of the two inherently disparate trains that need to be accounted for. These differences do, unfortunately, cause some ambiguity when attempting to directly correlate the performance between the two test runs. There would be a benefit in conducting lubricity tests following the same train every time. For this reason, mounting the rail lubricity sensor on a track geometry train would have the additional benefit of identical preceding train traffic every time.

As previously noted, the fluorescence behavior right after the signal results in a large change in the variance of the fluorescent signal on the left hand rail. Nothing was explicitly noted about this location during the field survey but this would be an interesting phenomenon to investigate during future tests with different preceding trains. For the fluorescent signal, the overall signal to noise ratio of the sensor is very low. In increase in the variance is often interpreted as an increase in overall lubricity unless the fluorescent signal becomes large. Under low lubricity conditions with

small fluorescent signals, the sensor tends to have “pops" when it is only detecting fluorescence intermittently.

Figure 5-34: High Pass Filtered and Moving Variance Plots for Milepost 2

Both rails have very similar signal variances in the first part of milepost MP 3 for both the calculated gloss ratio and the fluorescence signal. The high pass data shows overall higher levels of signal dynamics for the fluorescence sensor on the right hand rail further supporting that higher variance of the fluorescent signal can be an indication of higher lubricity conditions.

The calculated gloss ratio for the left hand rail has a very high degree of variance in the sharp left hand curve at the end of MP 3. It was previously shown that the rail condition here was also highly variable and inconsistent due to the patchy nature of the remaining TORFM on the rail in the curve. The variance data would serve to indicate that condition if a field survey was not possible. A look at the actual frequency content of the signal can help identify if the variance is caused by very high frequency glints and grooves in the top-of-rail surface or longer period surface condition effects like those observed in the TORFM in Figure *5-12*. The variance also drops significantly towards the end of the turn which confirms the phantom applicator effect and return of consistent TOR lubrication at the exit of the sharp curve at MP 3.

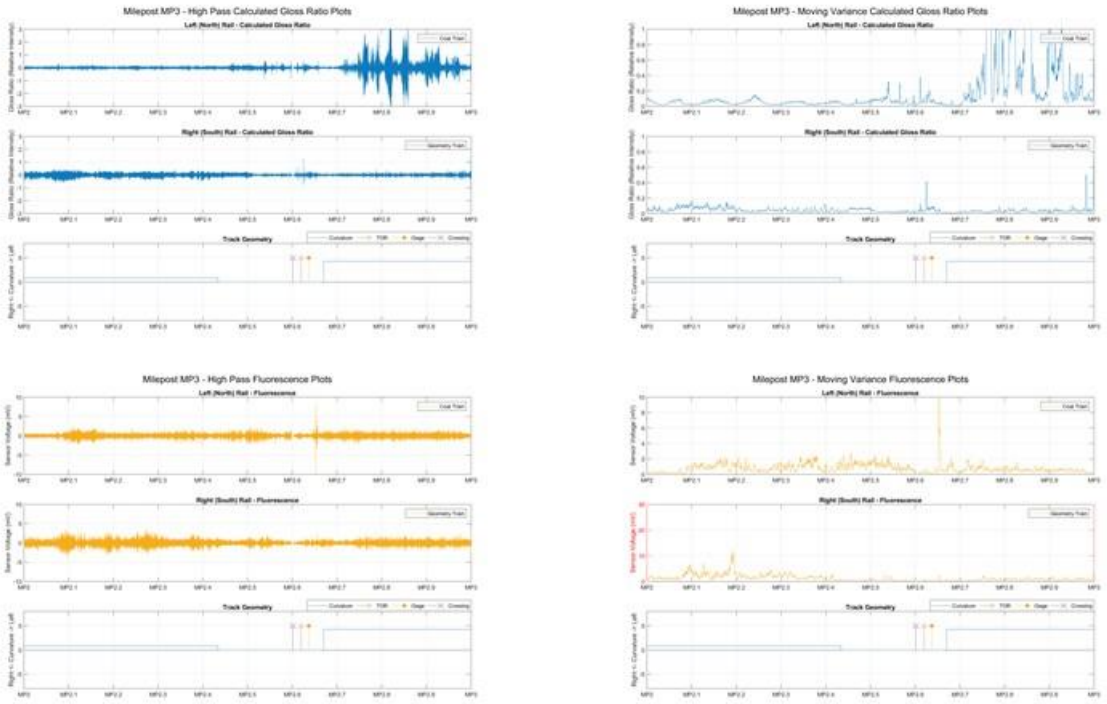

Figure 5-35: High Pass Filtered and Moving Variance Plots for Milepost 3

In milepost block 4, the gloss ratio variance of the left hand rail continues to look like the lower variance trends found in MP 2 and MP 3. This lower amount of variance indicates that the rail is better lubricated and that the conditioning effect is serving to extend the TORFM carry distance down track. The right hand rail changes test runs at MP 3.45 from the track geometry train to the grain train. Because the grain train had come to a stop over the previous TOR applicator, it was suggested that the conditioning effect was partially lost. The gloss ratio variance increases around MP 3.7 to MP 4 in a similar manner to how the gloss ratio increased for the right hand rail at the end of milepost block 1 for the unconditioned wheels on the geometry train. This suggests that it is accurate to assume that air brake applications can remove the conditioning effect from the wheels if the train comes to a stop at a signal like it did at the signal at MP 3.

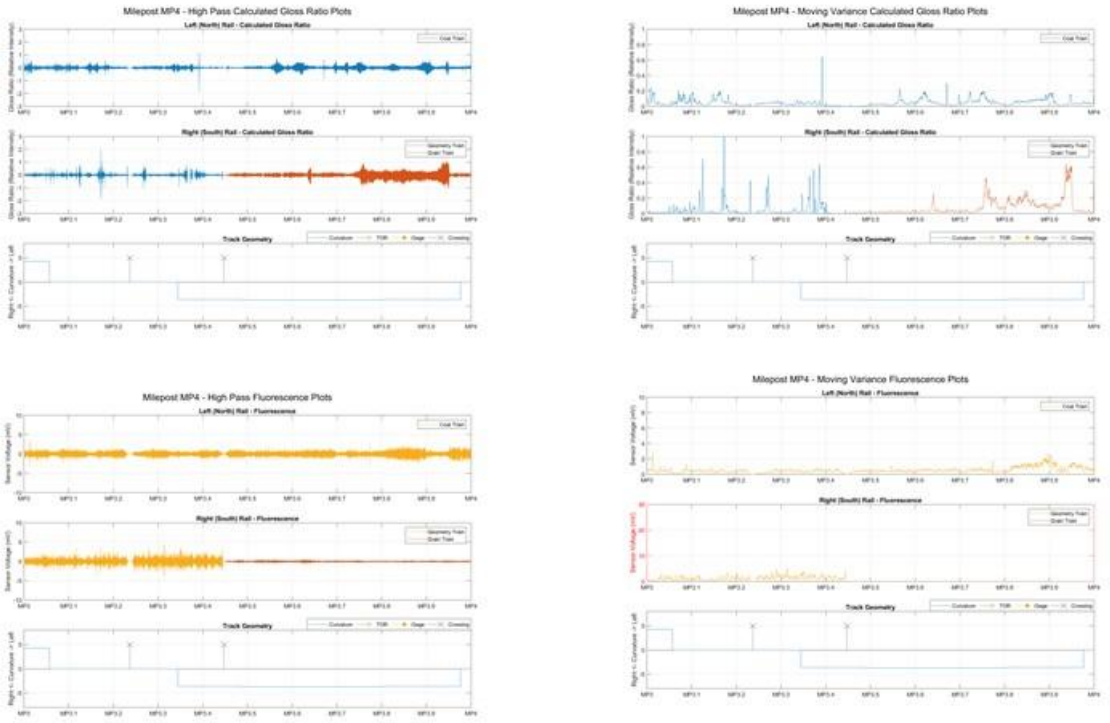

Figure 5-36: High Pass Filtered and Moving Variance Plots for Milepost 4

In milepost block 5, several spikes in fluorescent variance can be found in the sharp left hand curve at MP 4.2. The field survey found that the sharp curve and high curving forces left behind larger clumps of flange grease and drops of TORFM which is represented by the spikes in the variance data here. Like in the sharp curve at MP 2.7, this suggests that the lubricity condition is inconsistent and patchy at this location but that some lubricity is making it to this point. Based on the signal magnitudes in previous sections, it can be determined that the overall lubricity condition on this section is far lower and that these spikes are less representative of the overall track lubricity condition even if some lubricity is making it this far.

Finally, several spikes in the fluorescent signal can be seen on the right hand rail directly at the TOR applicator. Close to the applicator, the TORFM condition is strongly coherent and in phase as the lubricant is only applied to one spot on the wheel. This spreads out farther from the applicator and this frequency effect is covered in greater detail in the next section on frequency analysis. The left hand rail does not have a similar increase in variance at this section which further suggests a malfunction of the lubricator although this could not be confirmed during a field survey.

Figure 5-37: High Pass Filtered and Moving Variance Plots for Milepost 5

5.5 Frequency Domain Analysis

In signal processing, the use of the Fourier transform allows engineers to investigate signals in the frequency domain instead of only in the time domain. The frequency domain can provide a look at the component frequencies that are making up the time domain signals. Different frequencies in the signal can be representative of different physical effects on the dynamic system. For example, the remote control rail cart has a wheel with a circumference of 23.25 inches. If this is treated as a period, the resulting frequency would be 0.5161 ft^{-1} as mentioned in the previous section. A frequency domain peak at that frequency would indicate that a component of the signal is directly related to the movement of the remote control rail cart. Similarly a 36 inch diameter rail wheel, the normal diameter for a freight car wheel, has a spatial period of 113.10 and a spatial frequency of 0.1061. If this frequency appears in a frequency domain analysis then a portion of the signal content can be directly related to the freight car wheels effect on the top-of-rail surface. Several of these frequencies are listed in

.

5.5.1 Frequency Domain Analysis Methods

There are a number of different frequency domain analysis methods. The four Fourier Transform methods are the Fourier Transform, Fourier Series, Discrete Time Fourier Transform, and the Discrete Fourier Transform. The most common digital signal processing is the Discrete Fourier Transform which takes discrete and periodic signals and converts them to a finite set of discrete

frequencies [58]. The Fast Fourier Transform, or FFT, is a common modified version of the Discrete Fourier Transform, or DFT, used in many numerical computer applications like MATLAB. MATLAB also has a powerful Power Spectral Density (PSD) tool that uses Welch's method for calculating the power spectrum of a signal instead of the magnitude calculated with the FFT. The power spectral density is related to the DFT by the equation below where $P_{xx}[f]$ is the PSD of the discrete time domain signal and $X[f]$ is the DFT of the discrete time domain signal [59].

$$P_{xx}[f] \propto |X[f]|^2 \tag{24}$$

Welch's method and the PSD in general contains no phase information about the frequency domain by the way that it is calculated and Welch's method introduces windowing and overlap terms as inputs to allow for smoothing of the output spectrum compared to a raw FFT which is noisy. This makes the Welch's method PSD more ideal for presenting spectrum information and the "pwelch" function in MATLAB is also very powerful and easy to use.

The frequency domain of the Calculated Gloss Ratio and Fluorescence data were computed in two different sections. The PSD was first calculated for each milepost resulting in a mile-long section of test data for each PSD. This provides more general frequency information about the test data but does not directly correlate frequency content with precise locations down track. The test data was then split into tenth of a mile increments and run through Welch's method PSD again to create frequency power spectrums in intervals down track. This helps to identify the rise and fall of prominent frequencies in test data as the window moves down track.

5.5.2 Mile by Mile Power Spectral Density Results and Analysis

The PSD plots tend to have a few dominant frequencies. There is a peak near 0.5161 ft^{-1} that is coupled with vibrations caused by the 23.25 inch circumference remote control rail cart wheels. The second peak at 1.032 ft^{-1} is a harmonic multiple of the 0.5161 ft^{-1} peak. This strong peak indicates that future work on the remote control rail cart should add some vibration damping to remove these vibration effects. The more interesting peak, however is at 0.1061 ft^{-1} which is directly correlated to the circumference of a 36 inch freight car wheel. Strong frequency content of this particular frequency can prove that there is a connection between the collected lubricity data and the presence of TORFM on the rail surface. This is especially true of the Fluorescence data since mechanical surface features which could show up in the calculated gloss ratio should not have an effect on the fluorescent properties, or lack thereof, of rail steel.

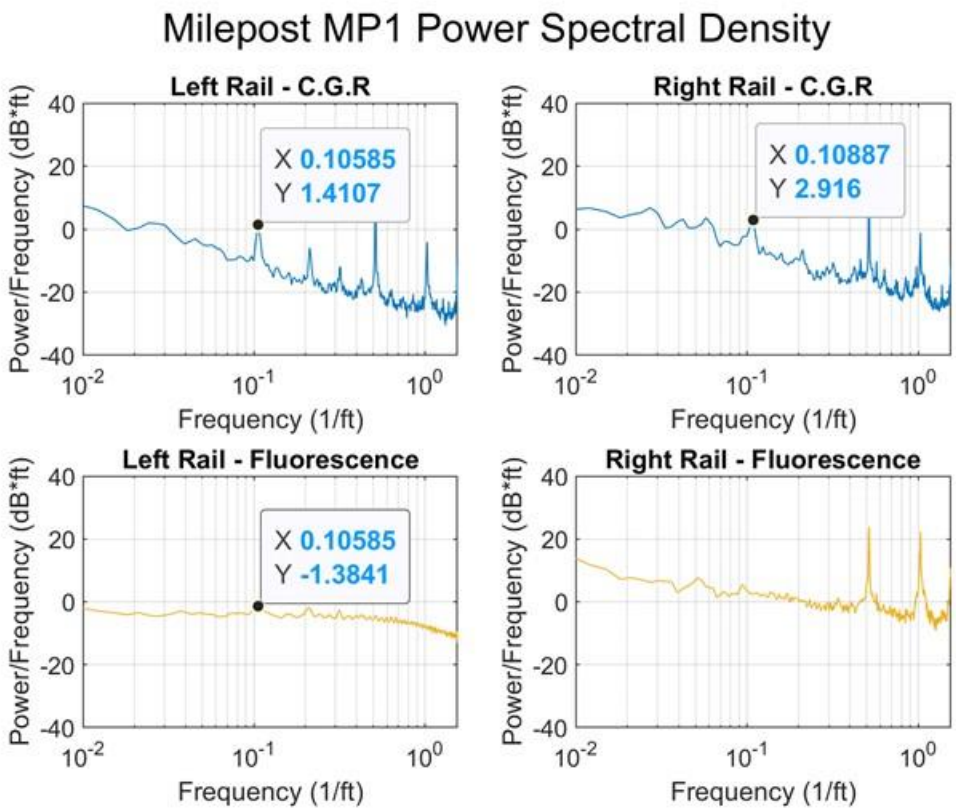

Figure 5-38: Mile long PSD plots for Milepost Block 1

For the first mile of test data, three out of the 4 PSD plots have a peak near the 36-inch freight wheel frequency. The right hand rail has a less prominent peak than the left hand rail for the gloss ratio and the fluorescence data has no significant peak relating to the freight wheel frequency at all. Because the track geometry train has less wheels than the coal train, it is suggested that there will be less frequency content near the freight car wheel frequency. This is shown more strongly in future sections.

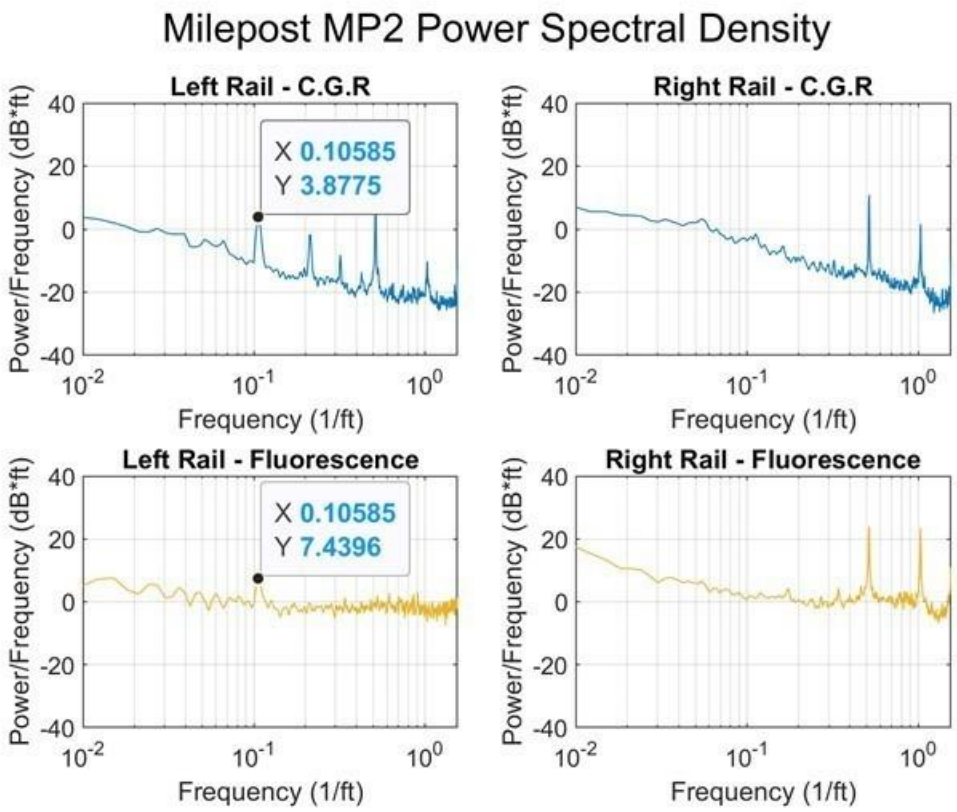

Figure 5-39: Mile long PSD plots for Milepost Block 2

In the second milepost block, there is no frequency peak associated with the freight car wheel frequency for the right hand rail while there are strong peaks for both the fluorescence data and the gloss ratio data on the left hand rail. Compared to milepost block 1, this strongly demonstrates that the increased number of wheels in coal train consist has a stronger ability to inject frequency content into the lubricity signal. More importantly, because the right hand rail lacks both significant frequency excitation near the freight car wheel frequency and also does not have a peak at this location, this demonstrates that the presence of the peak in the optical signals is caused by frequency content in the lubricity layer and not physical corrugations in the steel track surface.

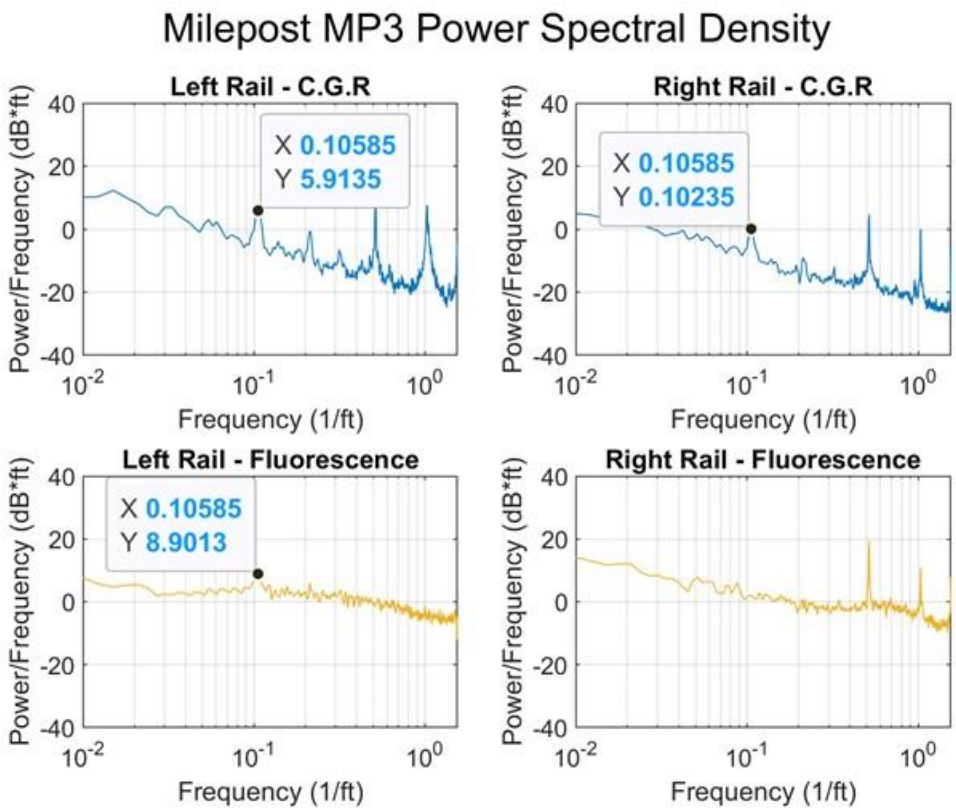

Figure 5-40: Mile long PSD plots for Milepost Block 3

The 0.1059 ft^{-1} frequency is once again present in both the left hand rail and right hand rail gloss ratios. The geometry train does have wheels with a 0.1059 ft^{-1} frequency in the train so it is not unsurprising to see this as a dominant frequency even if it is less powerful peak than the peak for the left hand rail. Further, the fluorescence data for the right hand rail has now twice failed to have the freight car wheel frequency peak when the gloss ratio has. The overall signal content of the fluorescence data is significantly lower on the left hand rail than it is on the right hand rail so this lack of frequency peak is not due to insufficient signal. This instead demonstrates that the fluorescent channel is less sensitive to frequency content from the freight car wheels than the gloss ratio is. This will become more apparent in the $1/10^{th}$ mile PSD blocks in the next section.

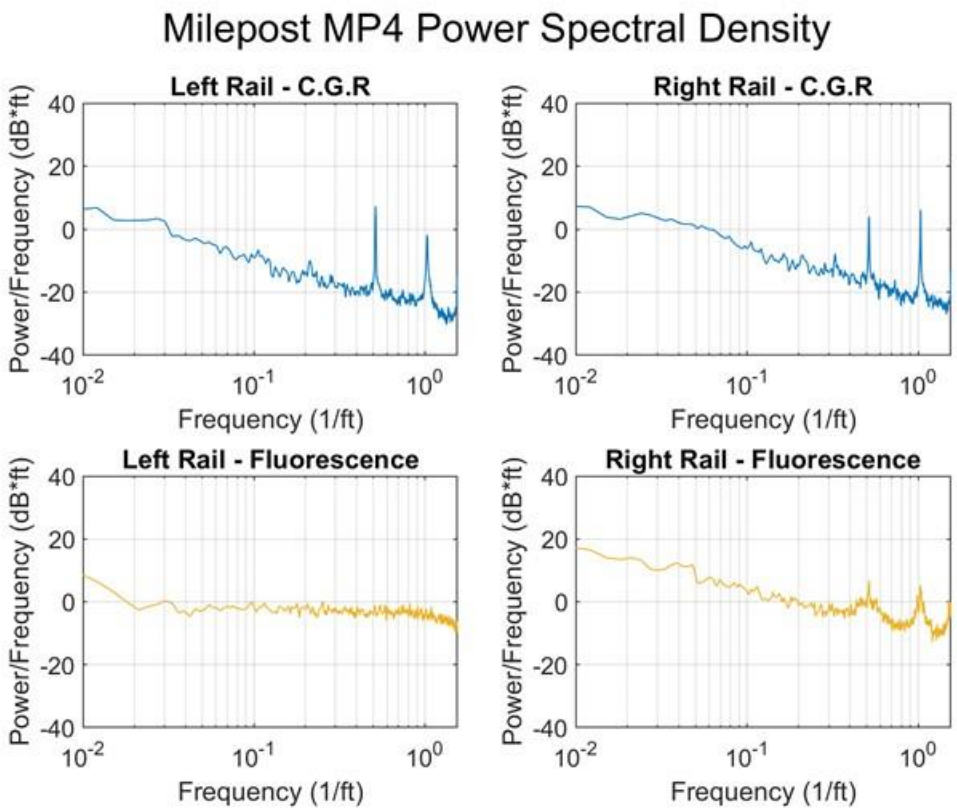

Figure 5-41: Mile long PSD plots for Milepost Block 4

Milepost block 4 comes after the TOR applicator, gage face applicator and sharp left hand curve at MP 2.7. In this mile block PSD, there is not significant frequency content associated with the freight car wheel in any of the four PSD plots. After the lubricators in the previous milepost block, there is significant distance and curvature to drive the wheels out of phase with each other. Further, with 2 previous TOR applicators to the third applicator at MP 2.7, there has now been significant opportunity for the TORFM to be spread onto different parts of the wheel tread. The lack of a precise explanation for this behavior only serves to demonstrate the need to better understand the mechanisms by which TORFM is spread down track.

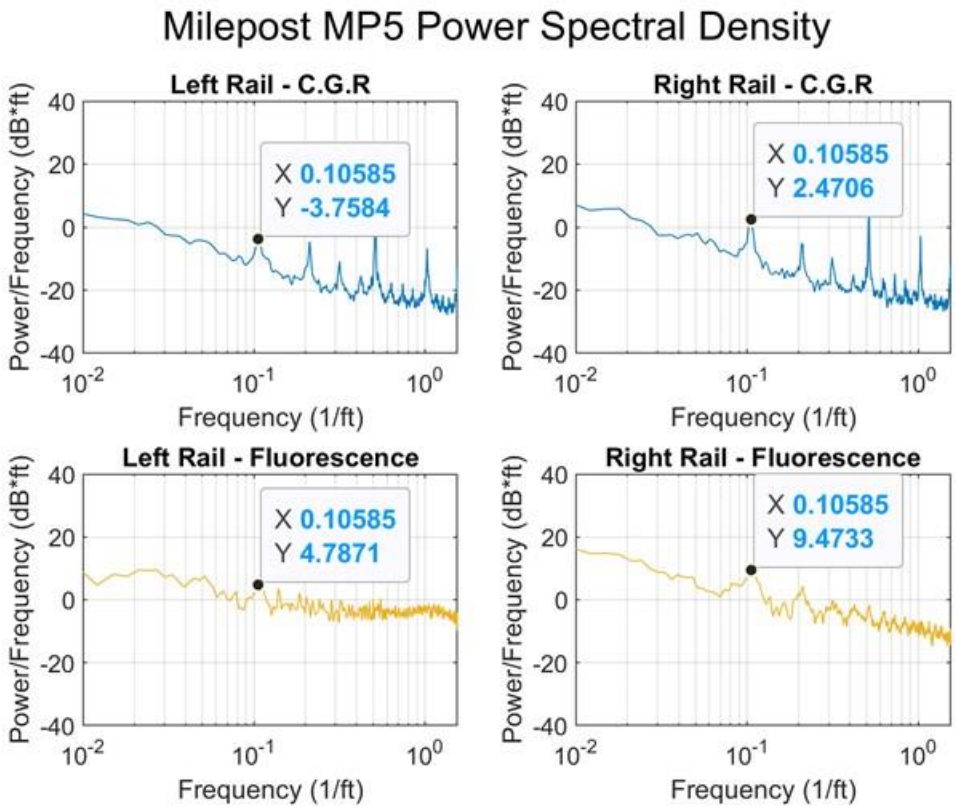

Figure 5-42: Mile long PSD plots for Milepost Block 5

The last mile long PSD block shows 0.1059 ft^{-1} frequency peaks in all four PSD plots. After seeing no freight car wheel peaks in the previous block the sudden resurgence in the frequency content is slightly surprising. While conducting the field survey on this section of track, several large blobs of dried TORFM were found on the rail head. Some combination of the multiple reverse curves between the previous applicator and this section could be incurring the phantom applicator effect and drawing extra TORFM down. It is suggested that TORFM is stored in a small reservoir blob on the spot of the wheel were it contacts the applicator. As the TORFM is spread to the rest of the wheel, this concentration becomes less defined. However, as the TORFM condition begins to wear off, it is suggested that the TORFM wears off completely on the spots it migrated too while some still remains in the reservoir from the applicator spot. The peaks are wider in this section of data suggesting some frequency bleed which would be caused by the application spot becoming less of a single point source generating an impulse response during the contact with the rail.

5.5.3 Block Power Spectral Density Results and Analysis

To better visualize how the frequency performance changes as a function of distance down track, the milepost test data was further subdivided into tenth of a mile blocks and passed through the "pwelch" function. This yields block power spectrums that can be used to identify the rise and fall of prominent frequency peaks in $1/10^{th}$ mile increments down track.

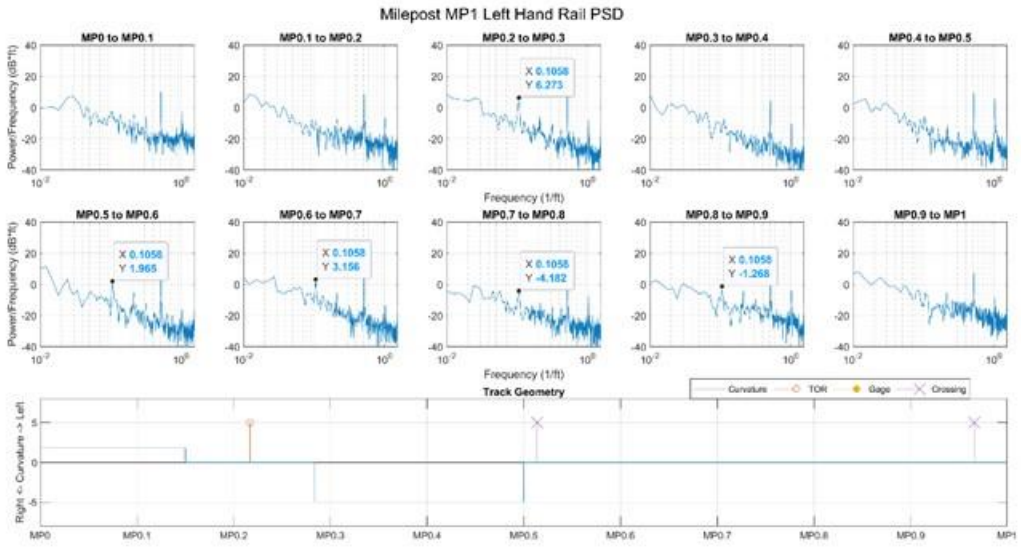

Figure 5-43: Calculated Gloss Ratio Block PSD Plots for the Coal Train on the Left hand rail on Milepost Block 1

For the first milepost block of the left hand rail power spectrum plots, the rail wheel frequency shows up directly at the applicator site as expected. The frequency peak disappears through the sharp right hand curve but reappears in the tangent section that follows. The frequency peak is once again not present in the final 1/10th of a mile from MP 0.9 to MP 1. Figure *5-44* below shows an applicator site from the field survey. In the picture, there are repeating darker patches of TORFM from the in-phase wheels only spreading TORFM in intervals corresponding to the circumference of the rail wheel. This phenomenon is what causes the beat frequency seen in the PSD plots. As the wheels become less coherent, the magnitude of the rail wheel frequency peak will diminish until the TORFM is applied to the rail evenly.

Figure 5-44: TORFM patches moving down track from a TOR applicator caused by the coherent phase of the train wheels

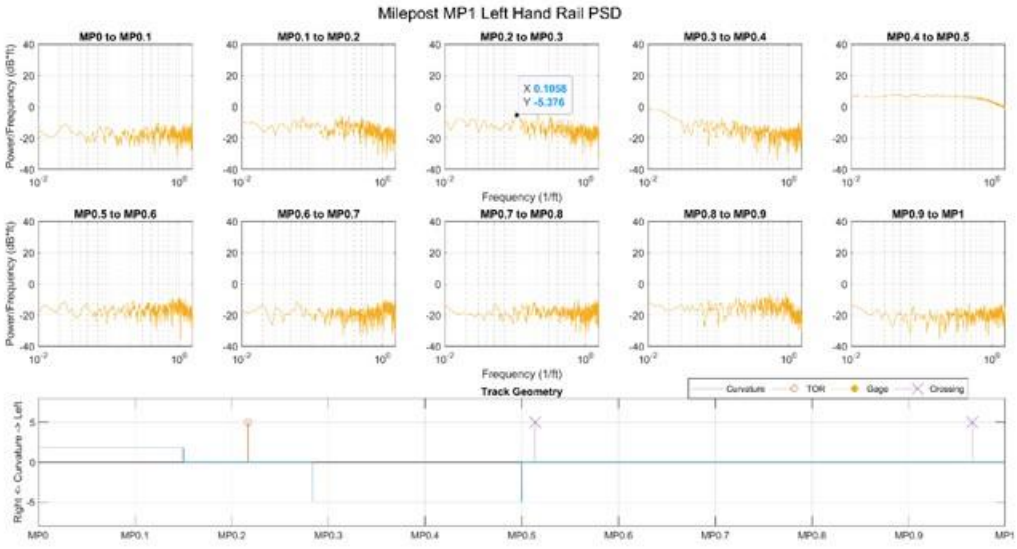

Figure 5-45 Fluorescence Block PSD Plots for the Coal Train on the Left hand rail on Milepost Block 1

In previous sections it was shown that the fluorescence signal is much lower than the gloss ratio signal both in terms of overall signal magnitude and also the optical power that is received by the photodetector. This also has an effect on the ability of the fluorescence signal to convey frequency data. The fluorescence signal has the rail wheel frequency directly at the applicator site where the

beat frequency is the strongest. Elsewhere, the beat frequency is not present even in places where it was present in the gloss ratio power spectrum.

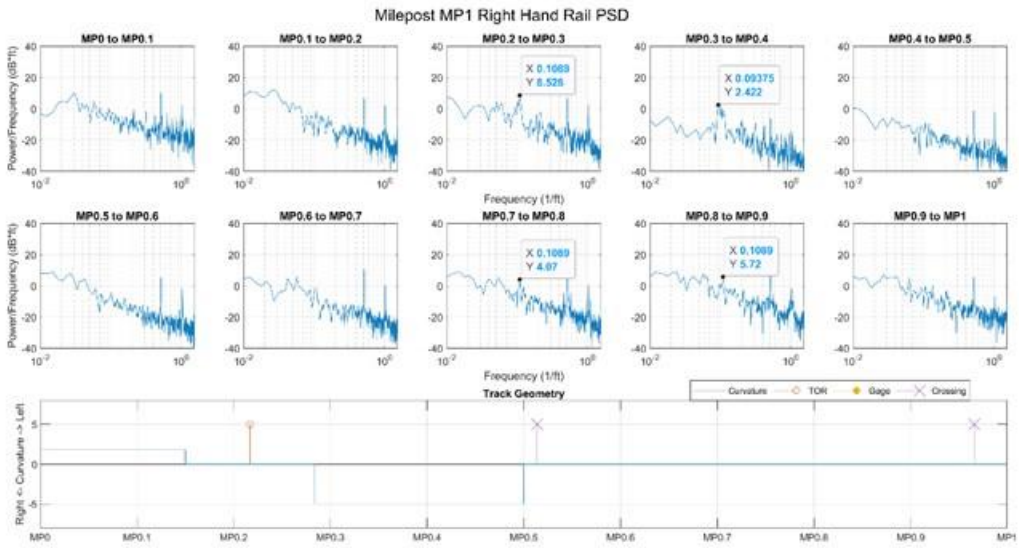

Figure 5-46 Calculated Gloss Ratio Block PSD Plots for the Geometry Train on the Right hand rail on Milepost Block 1

In the full mile PSD plot, the right hand rail did have the rail wheel frequency in the gloss ratio data. Here, the rail wheel frequency can be clearly seen at the applicator site but once past the applicator, the beat frequency is both less prevalent compared the surrounding frequencies and also not found in as many $1/10^{th}$ mile PSD blocks. This demonstrates that the lower axle count of the shorter track geometry train is less capable of exciting the frequency response in the third body TORFM layer.

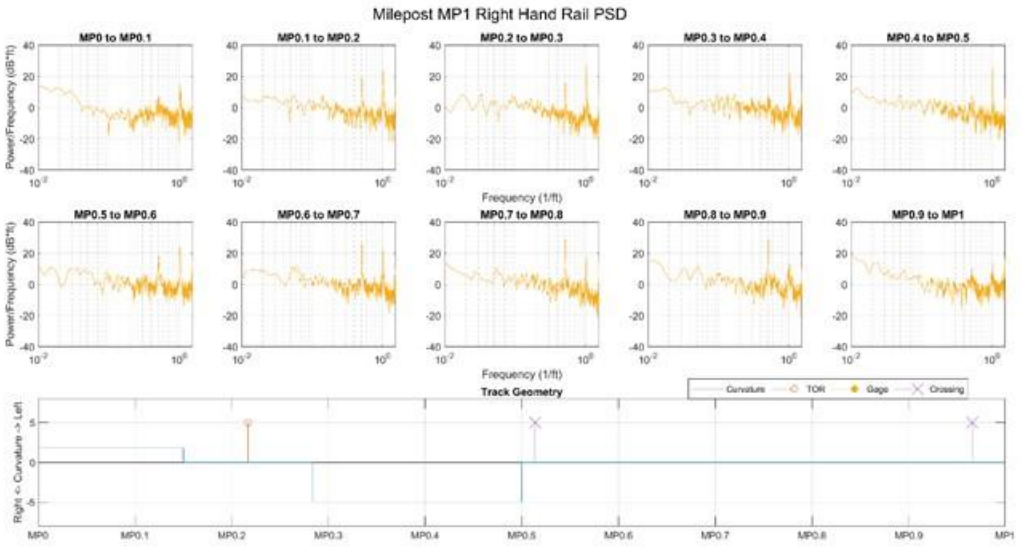

Figure 5-47 Fluorescence Block PSD Plots for the Geometry Train on the Right hand rail on Milepost Block 1

In the second milepost block, the TOR applicator is in the first 1/10th mile PSD block and once again the rail wheel frequency is immediately prevalent. Here, the rail wheel frequency peak is very prominent with regard to the surrounding peaks suggesting that the rail wheels are strongly coherent on this section of track. As the lubricity condition gets stronger from the conditioning effect, the beat frequency is prevalent for 0.7 miles before disappearing in the last two PSD blocks. Much of this track is tangent so there is less opportunity for curving behavior to drive the wheels out of phase.

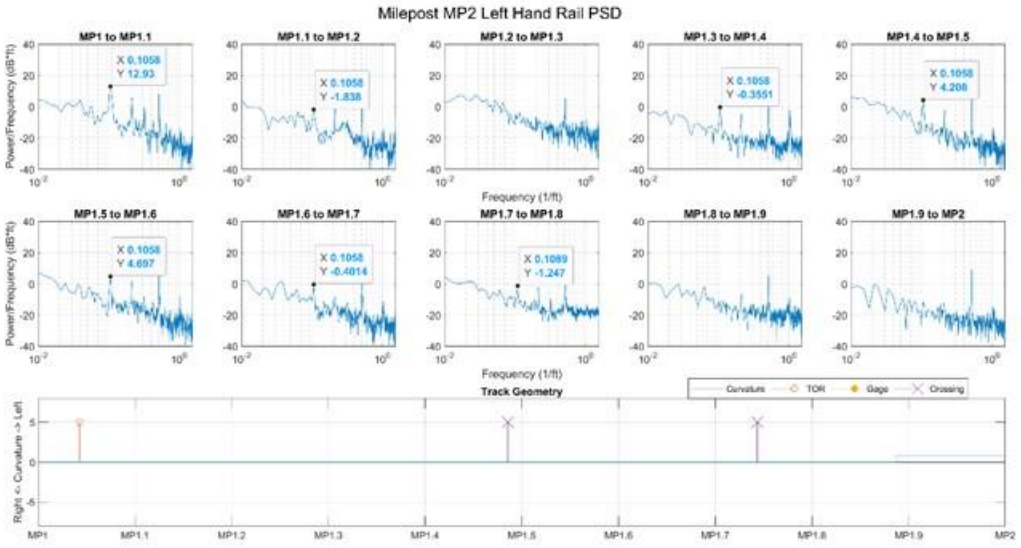

Figure 5-48: Calculated Gloss Ratio Block PSD Plots for the Coal Train on the Left hand rail on Milepost Block 2

The fluorescence block PSD is once again less sensitive to frequency content from the rail wheels. As a result, the rail wheel frequency peak is only visible in the first 1/10th mile block where the TOR applicator is located.

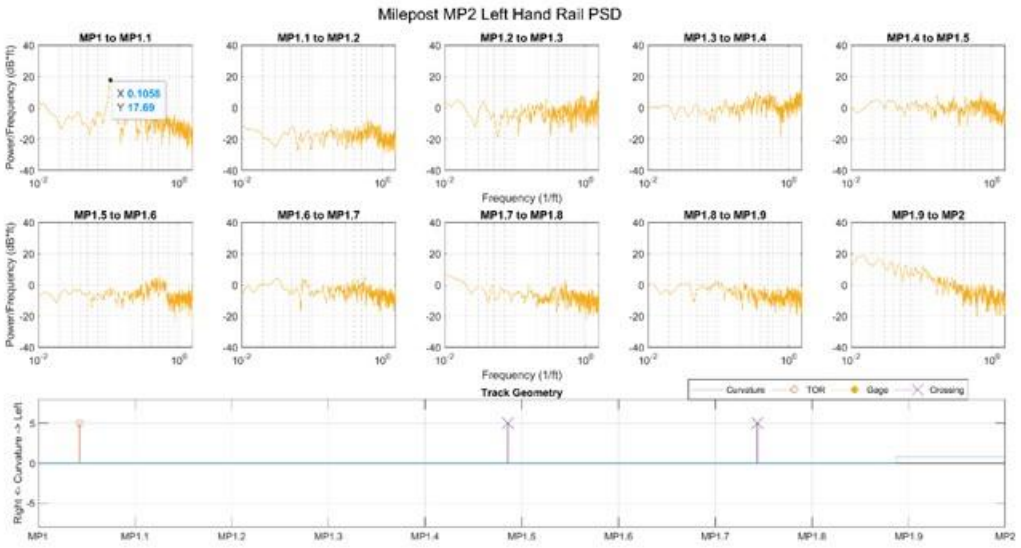

Figure 5-49: Fluorescence Block PSD Plots for the Coal Train on the Left hand rail on Milepost Block 2

In milepost block 2, the geometry train has very little frequency content from the rail wheel frequency. The beat frequency is only seen in the first 1/10th mile PSD block at the applicator site and the frequency is not prevalent for the rest of the milepost block. As shown in the full milepost block PSD, this clearly demonstrates that the geometry train has insufficient wheels to pump the rail wheel beat frequency into the lubricity condition of the rail. These PSD plots are a positive indication of both the instrument and the railroad. For the instrument, this helps conclusively prove that the beat frequency is directly correlated to the top-or-rail lubricity condition and not to some mechanical corrugations of the rail steel. For the railroads, this milepost block PSD plot show that the rail condition can have a uniform TORFM condition which is the goal of the wayside applicator.

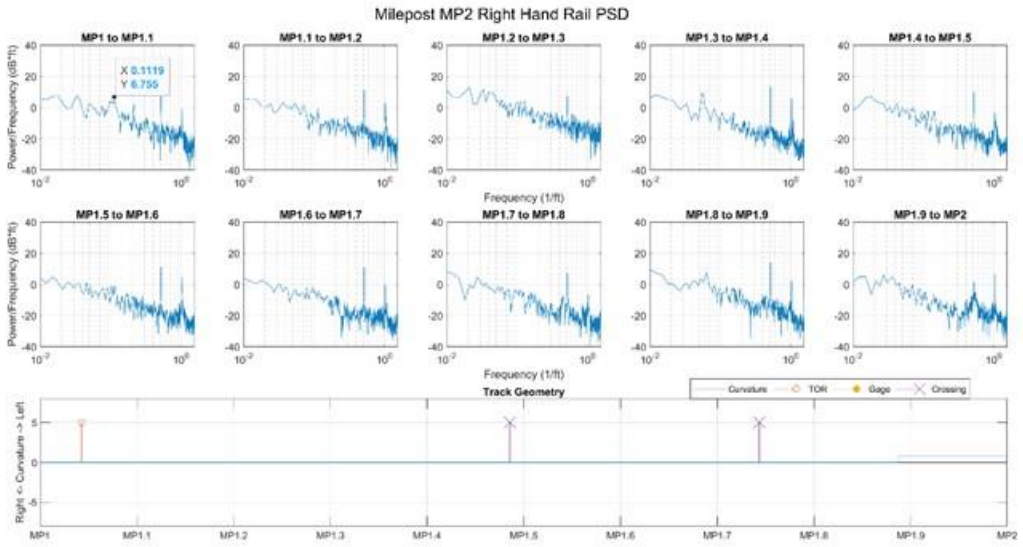

Figure 5-50 Calculated Gloss Ratio Block PSD Plots for the Geometry Train on the Right hand rail on Milepost Block 2

Because the fluorescence signal is less sensitive to frequency content, the fluorescent signal for milepost block 2 for the geometry train does not have any rail wheel beat frequency content even at the TOR applicator. The time domain signal clearly shows the effects of the TOR applicator at this site so there is an indication that the applicator is working correctly even though the frequency content is lacking.

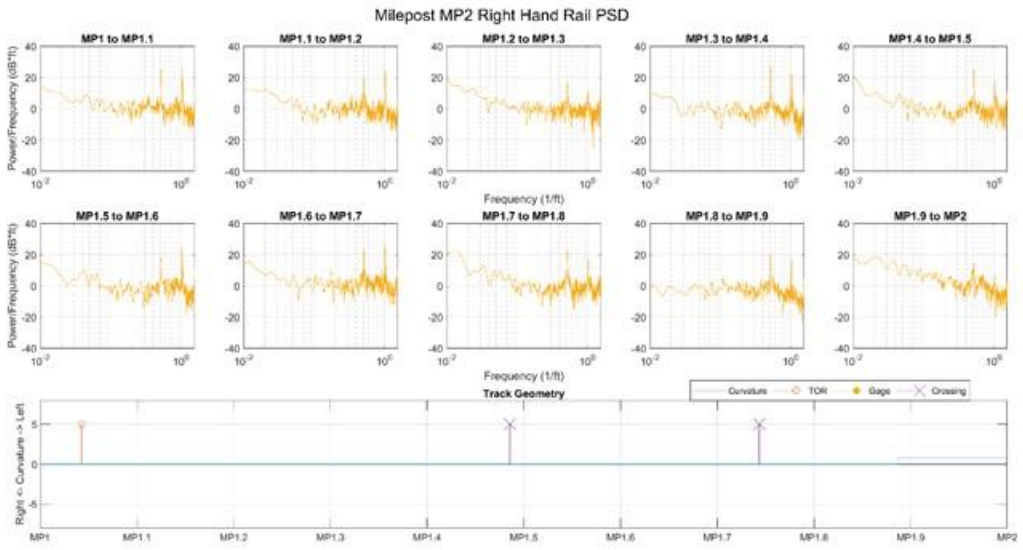

Figure 5-51: Fluorescence Block PSD Plots for the Geometry Train on the Left hand rail on Milepost Block 2

In milepost block 3, the frequency content from the rail wheels is completely absent until the wayside applicators at MP 2.7. This is a good indication that the TORFM condition is becoming

uniform. The rail wheel beat frequency is prominent through the entire sharp left hand curve. The visual effect of this interval patchy behavior of the TORFM could be witnessed during the field survey and can be clearly seen in Figure *5-12*. In response to this, it is suggested that the TOR applicator be moved farther back west. Moving the applicator back west would allow for less phase coherence of the rail wheels and more uniform spreading of the TORFM in the curve. A longer wiper application bar could also help spread the TORFM to a larger part of the rail wheel and provide a more even application of TORFM with a shorter coherence length.

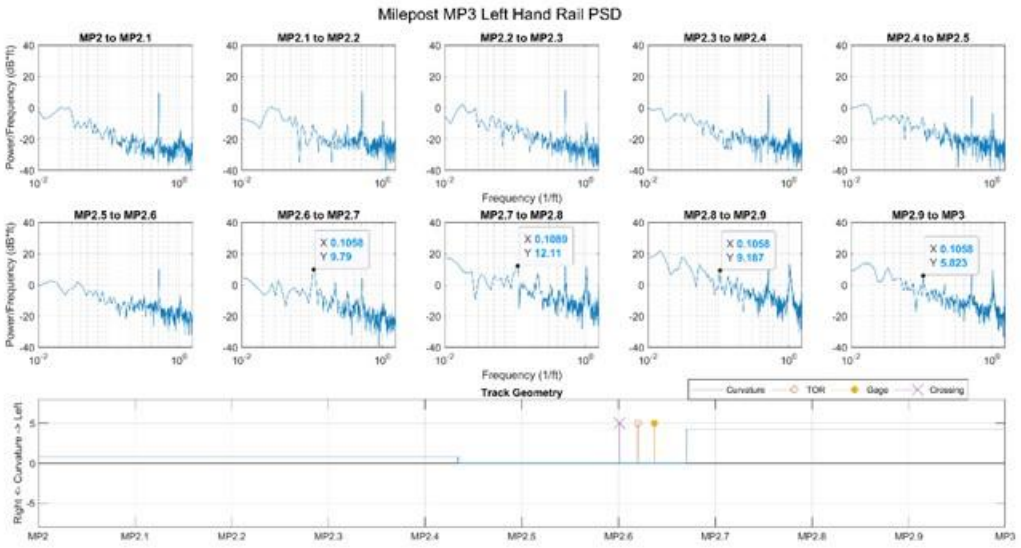

Figure 5-52: Calculated Gloss Ratio Block PSD Plots for the Coal Train on the Left hand rail on Milepost Block 3

Consistent with previous applicator sites, the fluorescent rail wheel beat frequency is only present at the TOR applicator at MP 2.7.

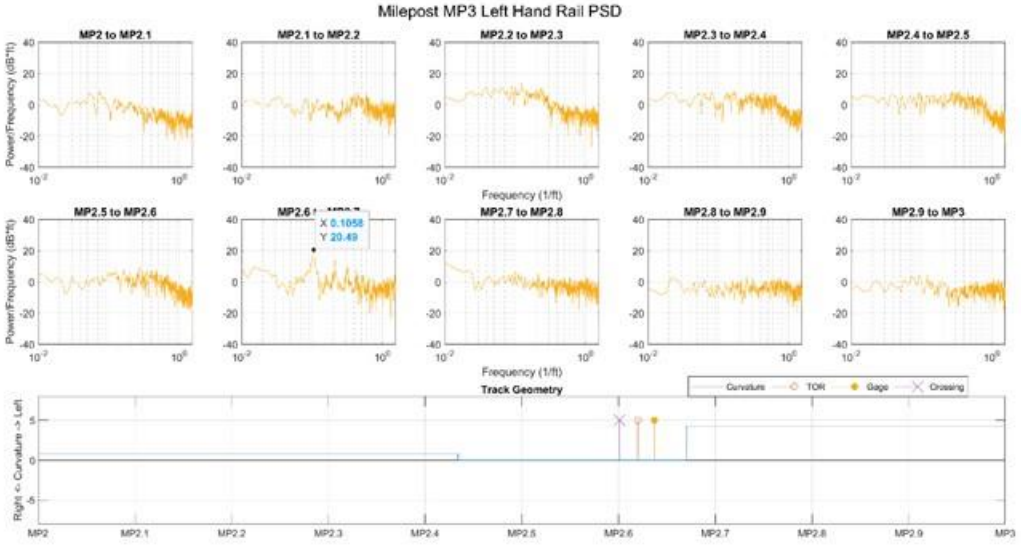

Figure 5-53: Fluorescence Block PSD Plots for the Coal Train on the Left hand rail on Milepost Block 3

For the geometry train in milepost block 3, the beat frequency is prevalent for both the PSD block with the TOR applicator and also the block following. The lubricity signal was very strong at this site so the increased amount of lubricity on the wheels may have helped prolong the beat frequency longer. The rail wheel frequency does, however, quickly fade out.

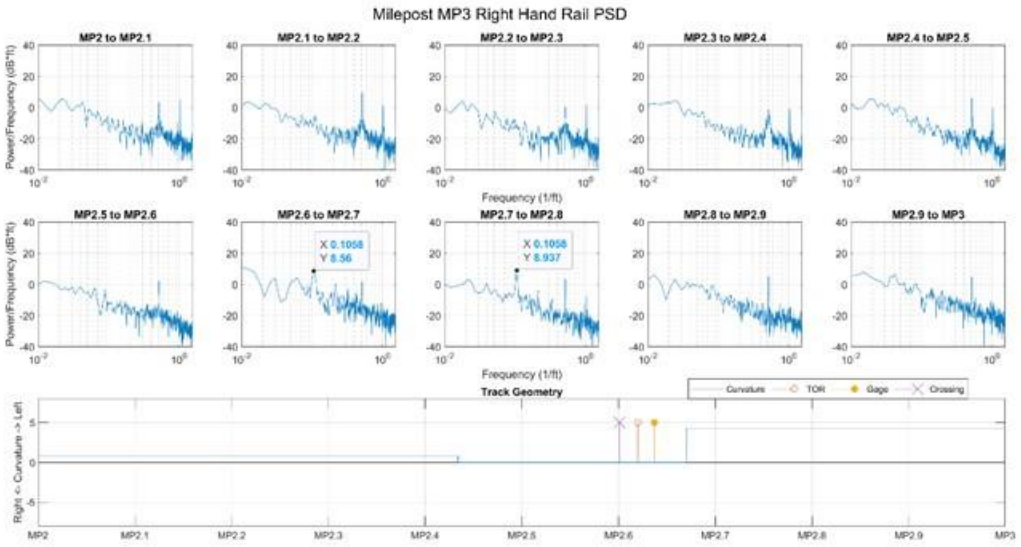

Figure 5-54: Calculated Gloss Ratio Block PSD Plots for the Geometry Train on the Right hand rail on Milepost Block 3

In milepost block 3, the geometry train once again does not have a fluorescent rail wheel beat frequency even at the applicator site. This is somewhat unexpected because the time series data showed a significant amount of fluorescent signal. This fluorescent signal was from flange grease migration to the top-of-rail surface. The wheel flanges wipe past the gage corner of the rail which helps to spread the flange grease around the wheel circumference more effectively than the spot applications of TORFM. For that reason, the lack of rail wheel beat frequency when present with a high amount of flange grease migration follows logically.

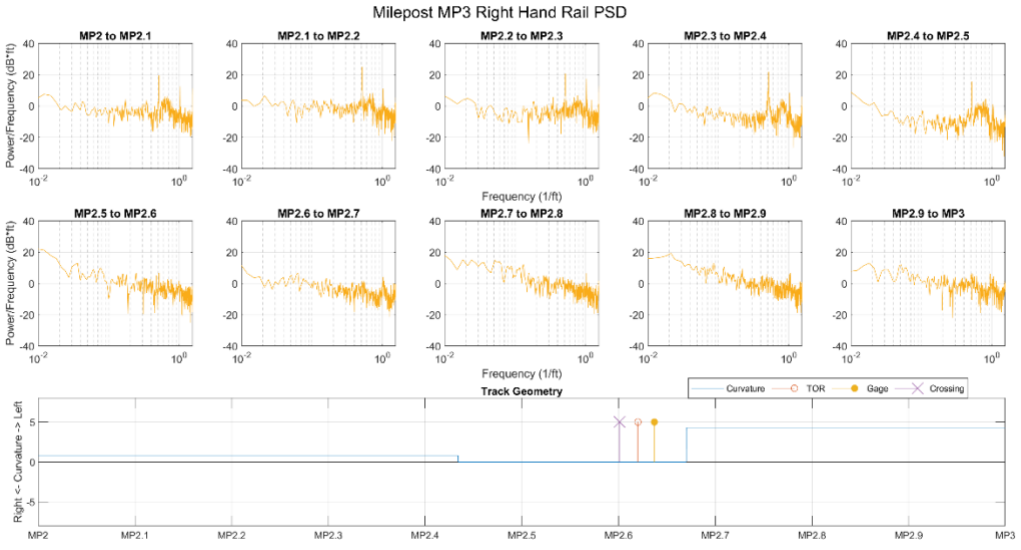

Figure 5-55: Fluorescence Block PSD Plots for the Geometry Train on the Right hand rail on Milepost Block 3

The beat frequency of the rail wheels reappears in the long right hand curve in milepost block 4. This particular section warrants some deeper investigation. The mechanics for the reappearance of the lubricity beat frequency are not completely understood. In previous sections, it was suggested that although the TORFM spreads around the wheel circumference, the spot where it was applied has a larger TORFM reservoir. As the TORFM begins to wear off around the wheel, eventually the application spot is far more lubricated than the rest of the wheel. This behavior would mesh with the observation that the lubricity levels are falling in this curve and the beat frequency is becoming prominent again.

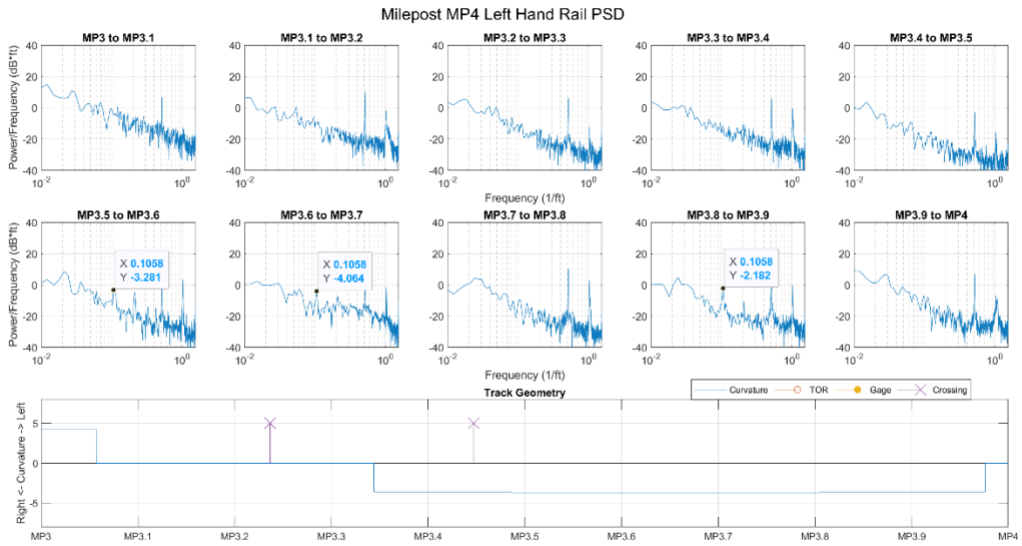

Figure 5-56: Calculated Gloss Ratio Block PSD Plots for the Coal Train on the Left hand rail on Milepost Block 4

The beat frequency that reappeared for the calculated gloss ratio does not have the same effect for the frequency content of the fluorescence sensor. This is expected based on the lower frequency capacity of the fluorescent channel. This also indicates that the resurgence of the beat frequency in the gloss ratio data is significantly less prominent than the behavior at a wayside applicator.

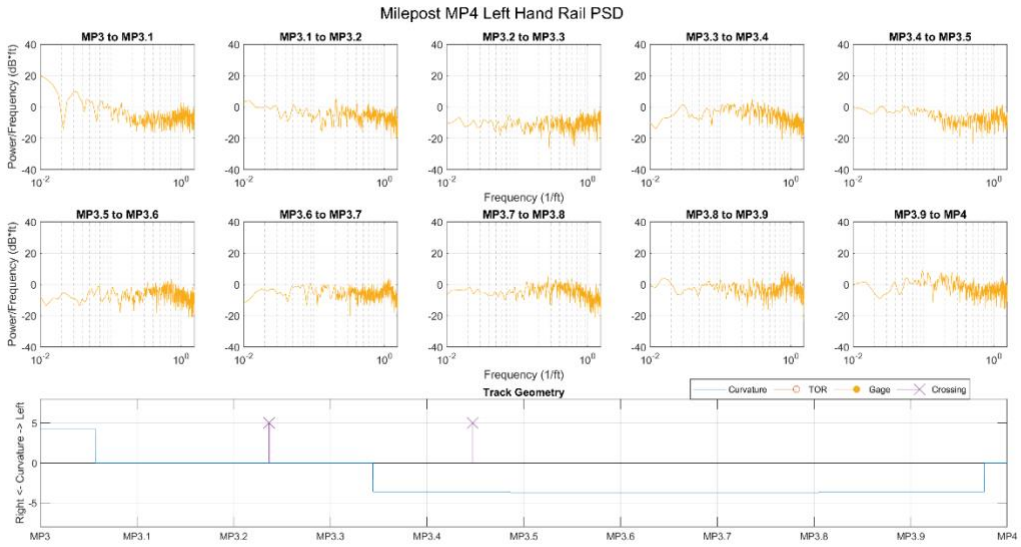

Figure 5-57: Fluorescence Block PSD Plots for the Coal Train on the Left hand rail on Milepost Block 4

In milepost block 4, the hand off between the geometry train and the grain train occurs at MP 3.45 on the right hand rail. This occurs in the middle of a 1/10th mile PSD block which is an issue that will not be present when runs are longer and continuous in the future. For this entire block, there was little expectation on observance of the rail wheel beat frequency. From MP 3 to MP 3.45, the geometry train had been demonstrated to be a poor at exciting the beat frequency in the rail wheel data. From MP 3.45 onward, the grain train both had insufficient wheel conditioning from successive TOR applicators and also was far enough down track from the applicator at MP 2.7 to still be carrying a beat frequency. This far down track it would be expected that the wheels would no longer be in phase. The lack of beat frequency resurgence in the long right hand curve demonstrates a difference in the manner in which TORFM is being spread both from left to right rail and also from coal train to grain train.

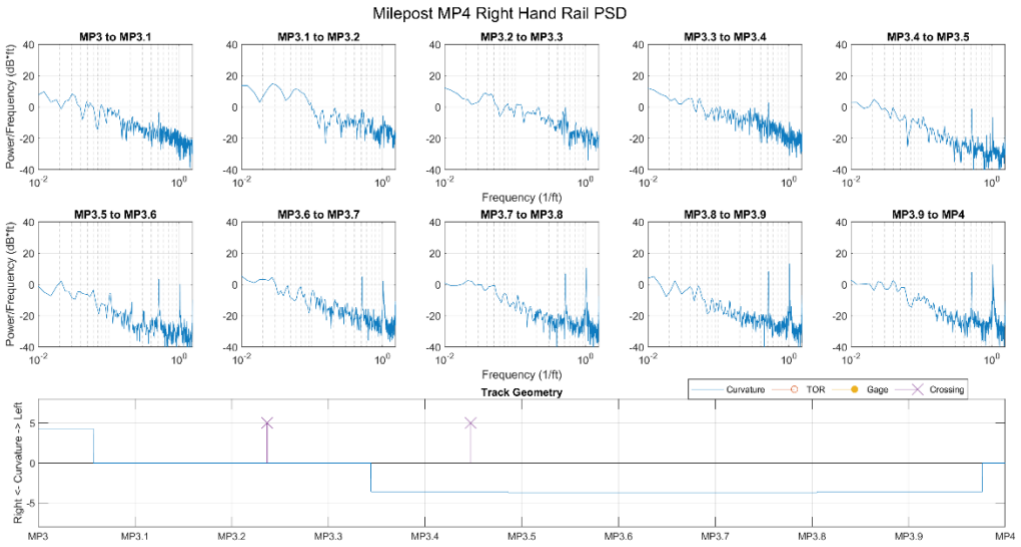

Figure 5-58: Calculated Gloss Ratio Block PSD Plots for the Geometry Train (MP 3 to MP 3.45) and Grain Train (MP 3.45 to MP 4) on the Right hand rail on Milepost Block 4

Oddly, the fluorescent channel showed a beat frequency for a single 1/10th mile block PSD between MP 3.1 and MP 3.2. This could be due to the phantom applicator effect exiting the sharp left hand curve but the lack of frequency peak in the gloss ratio PSD is surprising. The general trend has been that the gloss ratio is more sensitive to frequency content than the fluorescence channel. With this limited set of runs, this remains an anomaly that will have to be observed in future tests to draw any concrete conclusions and the presence of this anomaly does not challenge any of the conclusions drawn.

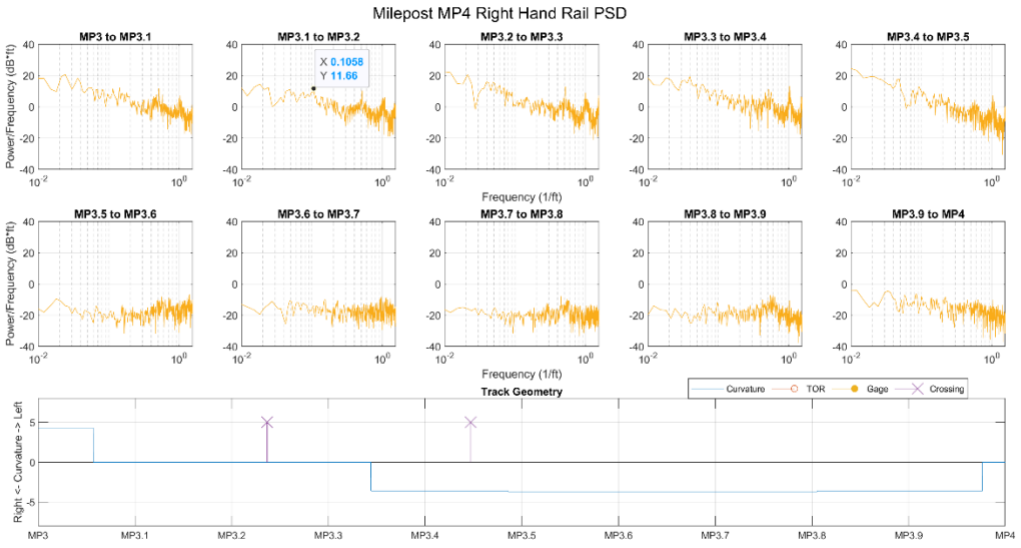

Figure 5-59: Fluorescence Block PSD Plots for the Geometry Train (MP 3 to MP 3.45) and Grain Train (MP 3.45 to MP 4) on the Right hand rail on Milepost Block 4

During the field survey of the curve at MP 4.2, signs of track lubricants were found but they were also determined to be spotty and this section of track as a whole was determined to be less lubricated as a whole. The sporadic resurgence of the rail wheel beat frequency continues for much of this 5th milepost block. As a result, this research shows that at lower lubricated conditions the rail wheel frequency can become prominent again. For the mechanics of TORFM propagation, this suggests that the theory about a TORFM reservoir remaining at the application spot on the wheel long after the TORFM spread to the rest of the wheel has worn off has potential. At different points

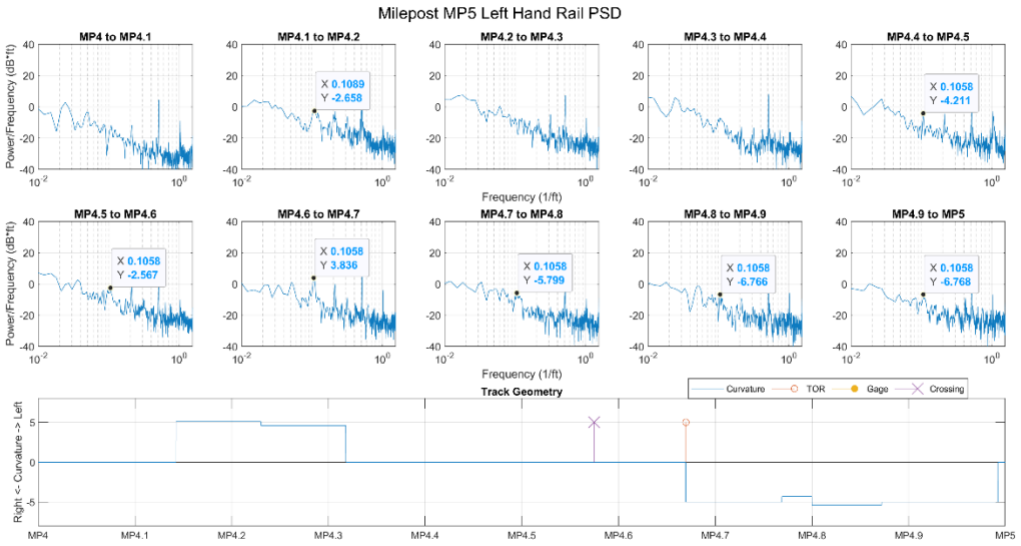

Figure 5-60: Calculated Gloss Ratio Block PSD Plots for the Coal Train on the Left hand rail on Milepost Block 5

in this research project it has been suggested that investigating the rail is only one half of the picture. This result would indicate that a study of the TORFM distribution around the wheel would also be valuable to better understand the contact mechanics of TORFM and the manner in which TORFM carries down track.

The left hand rail did not have strong evidence of the TOR applicator signal at MP 4.7 in the time series data. The frequency response of the gloss ratio does, however, have a peak at the applicator

site but the following peaks are far more subdued. The fluorescent signal does not have significant frequency content from the rail wheel beat frequency for a peak to be visible.

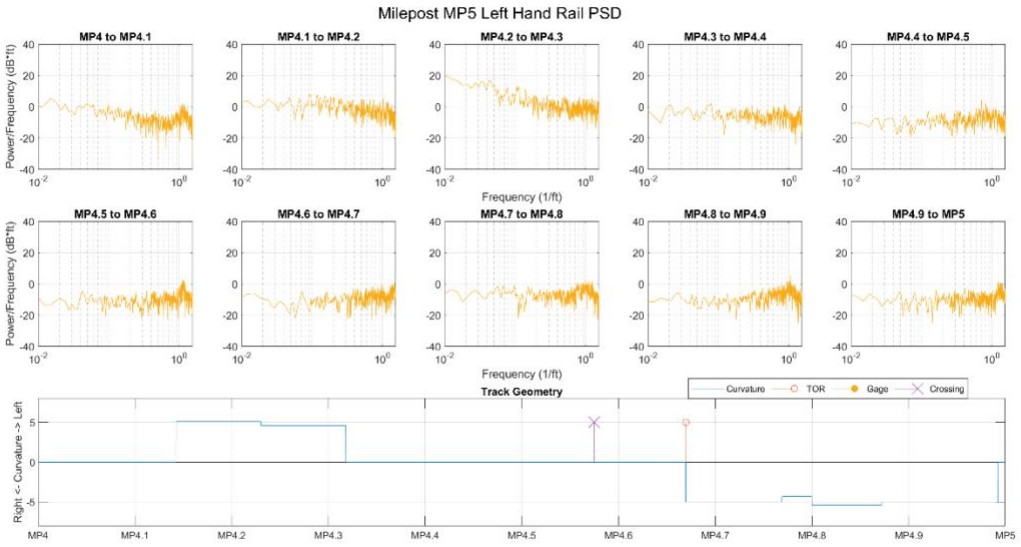

Figure 5-61: Fluorescence Block PSD Plots for the Coal Train on the Left hand rail on Milepost Block 5

The frequency content of the grain train is very similar to that of the coal train in milepost block 5. Since both are long revenue trains this makes sense although other plots have shown some differences caused by the grain train coming to a stop over the wayside applicators at MP 2.7

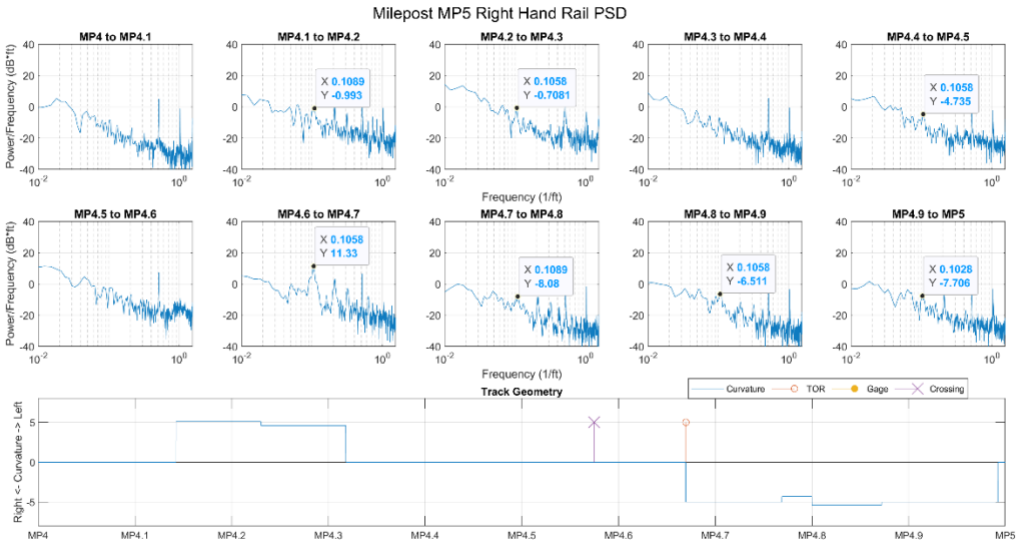

Figure 5-62: Calculated Gloss Ratio Block PSD Plots for the Grain Train on the Right hand rail on Milepost Block 5

At the applicator site, the gloss ratio has a strong rail wheel beat frequency that continues through the end of the frequency domain evaluation. The fluorescent signal also has a strong beat frequency at the applicator site which continues a significant distance down track. This 0.3 mile prevalence of the rail wheel beat frequency is the farthest distance observed in the fluorescence data. The time series data showed that the lubricity condition was very high at this location and the strong frequency performance in the fluorescent signal confirms this observation.

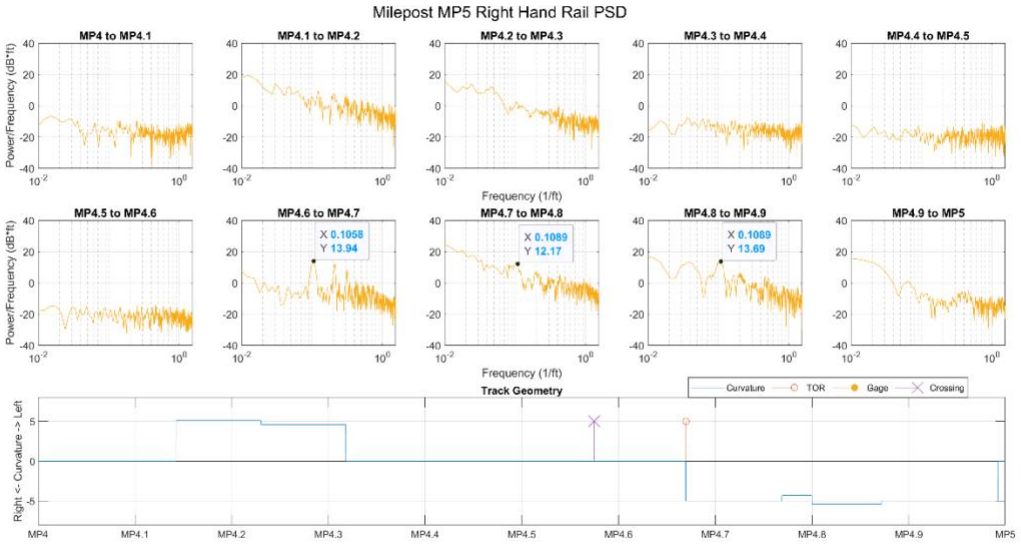

Figure 5-63: Fluorescence Block PSD Plots for the Grain Train on the Right hand rail on Milepost Block 5

6. Conclusions and Future Steps

In this chapter, all previous sections of the report will be summarized. An overview of all of the work conducted for this research will be presented. Next, all of the significant findings will be compiled. Finally, there will be a section on suggestions for future steps of the research.

6.1 Summary

During this study, an existing optical instrument, the second-generation Rail Lubricity Sensor, was modified from its designed spot testing configuration to trial collecting moving, spatial lubricity data down track from a wayside applicator. From that first trial, moving field test, several conclusions were drawn based on the performance of the current optical instrument and the ability to quickly, effectively, and safely collect optical lubricity data of an adequate amount of track in the allotted amount of time.

From these lessons, a new third generation Rail Lubricity Sensor was designed, built, and commissioned. This new sensor solved many of the issues uncovered when adapting the second generation sensor for moving testing. Primarily, the new sensor used a blue laser diode with a significant increase in optical scattering which had the result of lowering the angle sensitivity between the optical instrument and the head slope of the rail. Additionally, the new sensor discarded the highly angle specific specular reflection channel in favor of a lubricity metric that was only reliant on diffuse scattering reflections further reducing the dependency on precise angle alignment. Finally, the electronics and filters allowed the box to have a significant increase in stability at different device temperatures allowing the instrument to more effectively reject abject environmental conditions.

The new third generation sensor was tested to verify that it continues to build on the optical detection principals built though the past years and iterations of rail lubricity sensors designed and tested by RTL. This included preliminary design testing and commissioning on an optical test bench where precise test configurations could be implemented with short sections of rail removed from revenue service and donated to RTL. Once the device was constructed the sensor could then be tested in motion on the laboratory track panel in conditions that more precisely mimic actual field conditions. This included mounting the third generation sensor to the remote control rail cart for the first time bringing them together into a complete Lubricity Assessment System. Once mounted on the cart, tests could be conducted in motion as they would be in the field on the track panel in lab.

For the second round of field testing on a moving platform, a new rail cart was constructed completely with a propulsion system and the necessary braking, emergency stop, and other safety systems needed to be safely operated on mainline track. This new remote control rail cart dramatically increased the amount of testing that was able to be accomplished with no observed detrimental effects to the data integrity. Further, the remote-control rail cart allows the test engineers to be located inside of a Hyrail vehicle increasing safety when moving around on track structures. The remote control rail cart on its own is a useful tool in the arsenal of research equipment owned and operated by the Railway Technologies Laboratory, and its modular design will allow the cart to be adapted and used for a wide variety of future research projects.

Finally, after collecting several miles of field test data on revenue service track, the raw data was processed using a variety of digital signal processing techniques. This signal processing step helps improve the readability of the field test data and also helps to extract useful signal traits to better yield conclusive lubricity assessments. Through a recursive process, existing test data was analyzed and the results were used to identify additional signal processing techniques. These additional filters were applied to the test data to attempt to answer questions and uncertainties from previous analysis steps.

6.2 Significant Findings and Conclusions

The results of this research have yielded several significant findings. This includes once again demonstrating the ability of optical based methods to detect the presence or absence of rail lubricants. For this study, this conclusion is more specific to the third generation Rail Lubricity Sensor and the moving testing methods. The moving testing on revenue service track also identified several significant signal traits representative of different rail lubricity conditions. Further study of these characteristic signals will be essential in building a larger overall signal in the manner in which rail lubricants propagate down track and the overall effective carry distance from a wayside applicator.

6.2.1 Demonstration of ability to detect flange grease crossover

During the shakedown run on the passing siding, the optical measurements were able to clearly identify a point in the curve where the flange grease was present on the top-of-rail surface. With the fluorescent detector channel, it has often been suggested that this was a capability of the instrument, but this is the first time this ability had been demonstrated with the Rail Lubricity Sensor on revenue service track.

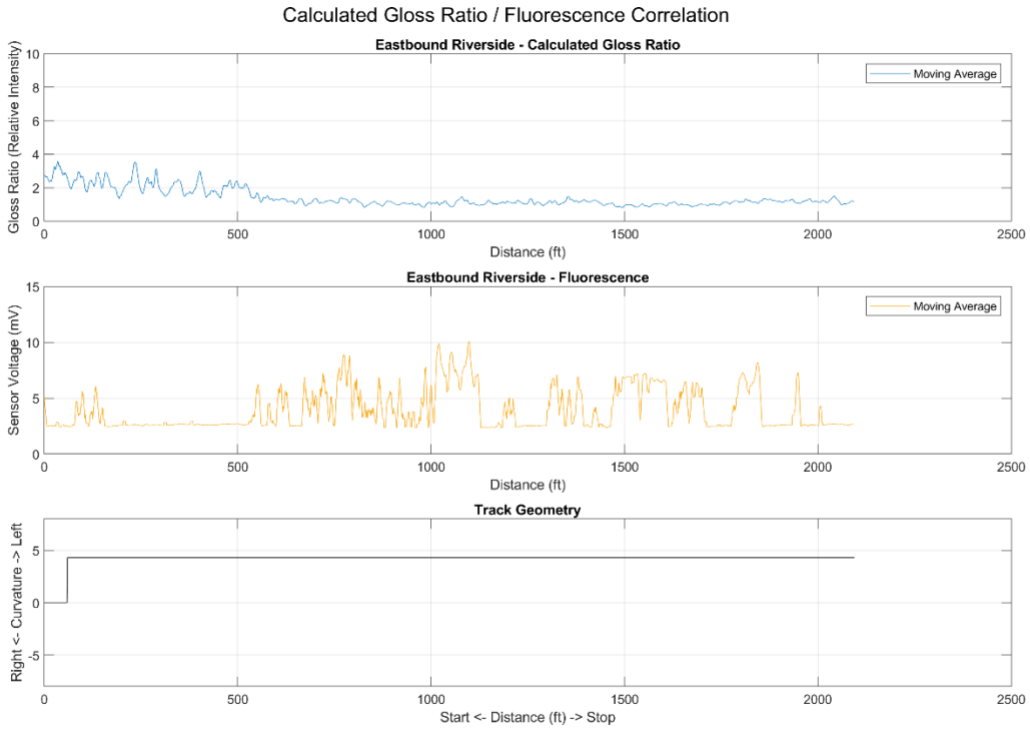

Figure 6-1: Flange grease crossover effects on Calculated Gloss Ratio and Fluorescence signal

The above plot is from the shakedown run on the passing siding. The passing siding only has a flange grease applicator so any residual effect from TORFM is strongly reduced by this point. The drop in the gloss ratio channel and the spike in the fluorescent signal is a clear indication that the flange grease is migrating to the top-of-rail surface.

6.2.2 Significant lubricity signal response at wayside applicator

During revenue service track testing, the signal performance at wayside applicators was of particular significance as this was one section where there was no doubt that TORFM would be present. Based on the data collected, a unique signal formation was present at the applicator site. This unique signal serves to further demonstrate that the optical instrument is able to identify heavy lubricated conditions on revenue service track and is an effective instrument at identifying rail lubricity condition. This is clearly demonstrated at the applicators in the plot below. Both of the gloss ratio plots dip to a heavy TORFM condition right at the applicators before the curve effects take place. This is even more pronounced in the fluorescence data for the left hand rail where there is a clear rise in fluorescence at the applicator. For the right hand rail, the fluorescent signal is already close to its maximum value so the effect is diminished.

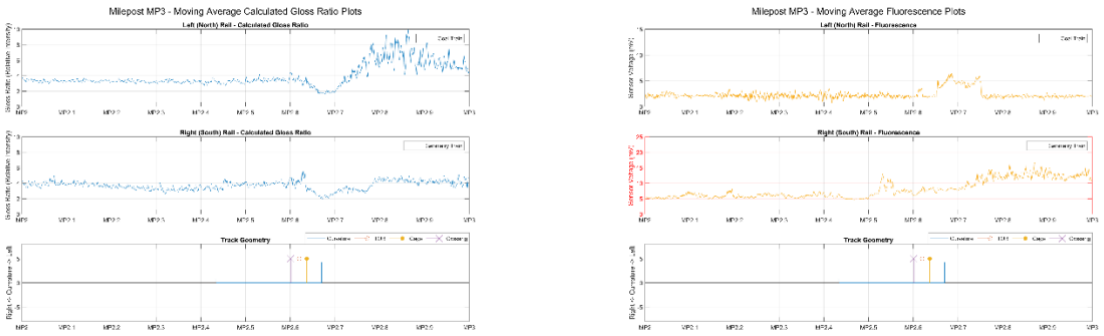

Figure 6-2: Lubricity signal effects near a wayside applicator site

Based on this characteristic signal, the test data would suggest that there was an issue with the final TOR applicator on the left rail at MP5. During a follow up field survey, it was confirmed that this applicator was functioning correctly which contradicts the reading from the Rail Lubricity Signal. Given the small sample size, it is difficult to make any conclusive evaluation about this one anomaly. Wayside applicators are programmed to pump a set amount of lubricant for a set number of axles. It is possible that for this particular test, the remaining TORFM at the applicator site was exceptionally low but that the applicator was very close in axle count to being commanded to pump more TORFM out.

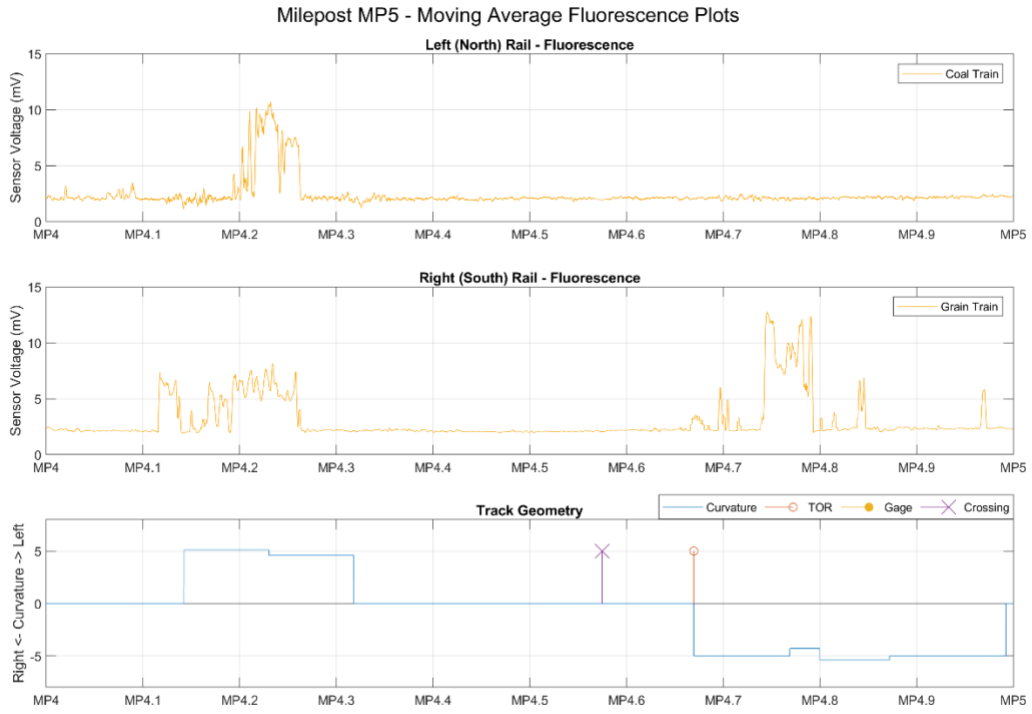

Figure 6-3: Present lubricator effect on right hand rail and errant absent lubricator effect on left hand rail

6.2.3 Discovery of Phantom Applicator effect at curve transitions

While identifying wayside applicator characteristic signals in the test data, a similar signal was observed frequently at the entrance and exit of curves, particularly sharper curves. The prevailing theory is that because the TORFM is applied to the outside of the wheel a TORFM reservoir builds on the outside surface of the wheel with the TORFM being drawn down to the contact patch. Because the wheels are tapered, both the gage and field side of the wheel tread has sections that are not in contact with the rail. The TORFM on these sections is also not in contact with the rail and is therefore not subject to the same forces that consume the TORFM from the wheel surface.

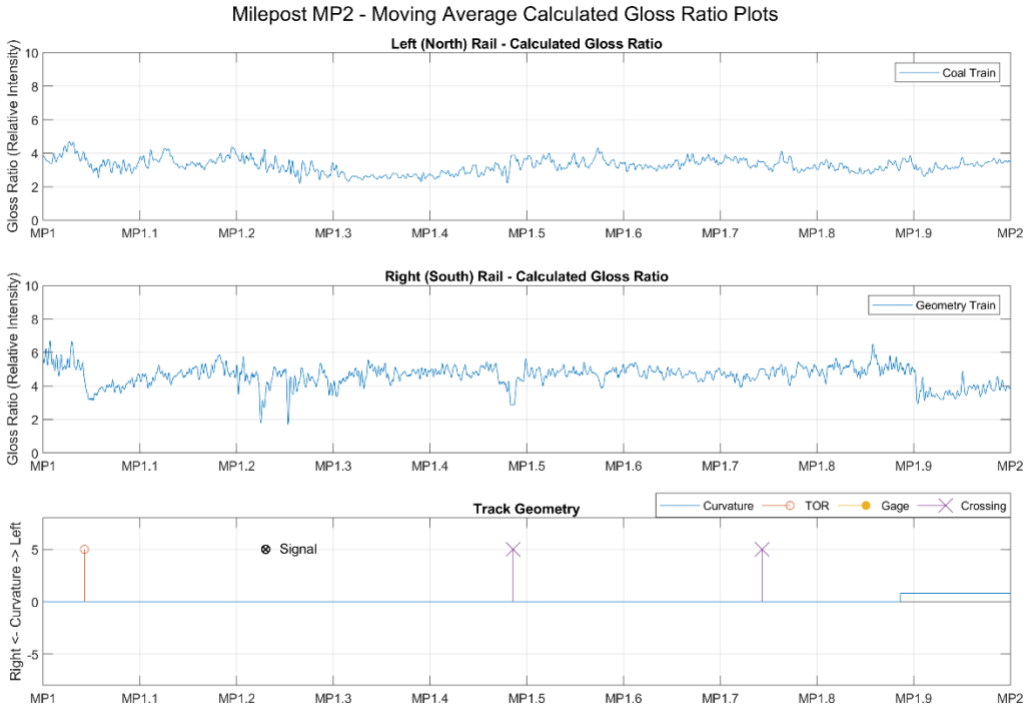

Figure 6-4: Physical wayside applicator effect at MP1.05 and Phantom applicator effect at MP1.9 in Calculated Gloss Ratio Moving Average Filtered Plots

This is most evident on the right hand rail on the figure above. There is a corresponding drop in calculated gloss ratio at the entrance to the curve that is a very similar shape and dip to the one right at the applicator. When the wheelset enters or exits a curve it shifts laterally to a different point of contact on the wheel tread. That new part of the wheel tread can have TORFM on it that has been lying "dormant" and not in contact with the rail until this point. As new TORFM is placed in contact with the rail, it acts as a "phantom applicator" and causes a change in the lubricity signal on the rail that looks similar to that of the signal at a wayside applicator. This appears to be a novel observation and could have significant impacts on the way TORFM propagation is understood and modeled in the future.

6.2.4 Lubricity signal dependency on preceding traffic

During the mainline TORFM study, the test trials were conducted with 3 very different preceding train consists. This covered both the condition of a very short, low tonnage train in the track geometry train, a long, high tonnage train in the coal train, and a long train which had come to a stop in the middle of the test run for the grain train. This benefitted the research study be creating three very different test conditions to evaluate the viability of optical based measurements as a whole but also restricted the ability to compare run-to-run conditions as the lubricity results were noticeable different.

As previously mentioned, two different FRA reports had different conclusions on the TORFM lubricity condition after a passing train. The first concluded that the TORFM was consumed by the end of the train while the second determined that the TORFM was still effective in lowering lateral forces in the strain gage equipped curve for successive trains not utilizing TORFM. This testing would indicate that there is still TORFM remaining on the track following even a long high tonnage train like the loaded coal train but that the lubricity signal is significantly reduced. A lateral force study would be necessary to conclude if this trailing level of lubricity is effective in lowering lateral forces or not.

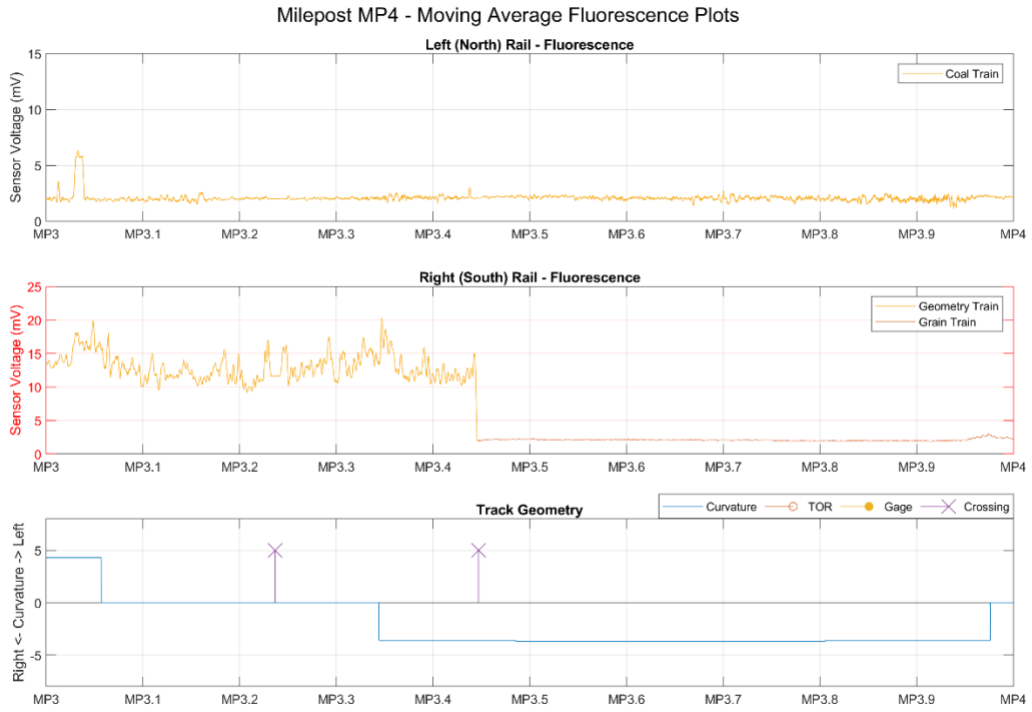

Figure 6-5: Demonstration of variation in lubricity signal magnitudes between three different preceding traffic conditions

The figure above shows the fluorescent trace at the switchover point between the geometry train and thee grain train. This plot clearly shows the large difference in signal magnitude between the two and the change is immediate demonstrating that it is not a difference between the physical left

and right rails. While the y axis scales are different, the overall signal magnitude of the grain train is almost identical to that of the coal train showing that the track geometry train has a significantly different amount of track lubricity on the track after it passes.

From this we can conclude that knowledge of the preceding traffic is an important piece of information that needs to be documented with the test data. If mounted on a research train like the track geometry train test, this would ensure that the preceding traffic is always the same and would allow the sensor to take advantage of the significant increase in signal level as a result of the shorter, lower tonnage train.

6.2.5 Non-uniform spatial TORFM lubricity distribution

In MP3, there is a sharp left hand curve directly following a TOR and gage face applicator. Based on the proximity to the applicator, there is a high degree of confidence that the curve is receiving TORFM to reduce lateral forces; however, the lubricity data indicates that the curve appears to be unlubricated. The gloss ratio also shows a high degree of variance in this section of the curve.

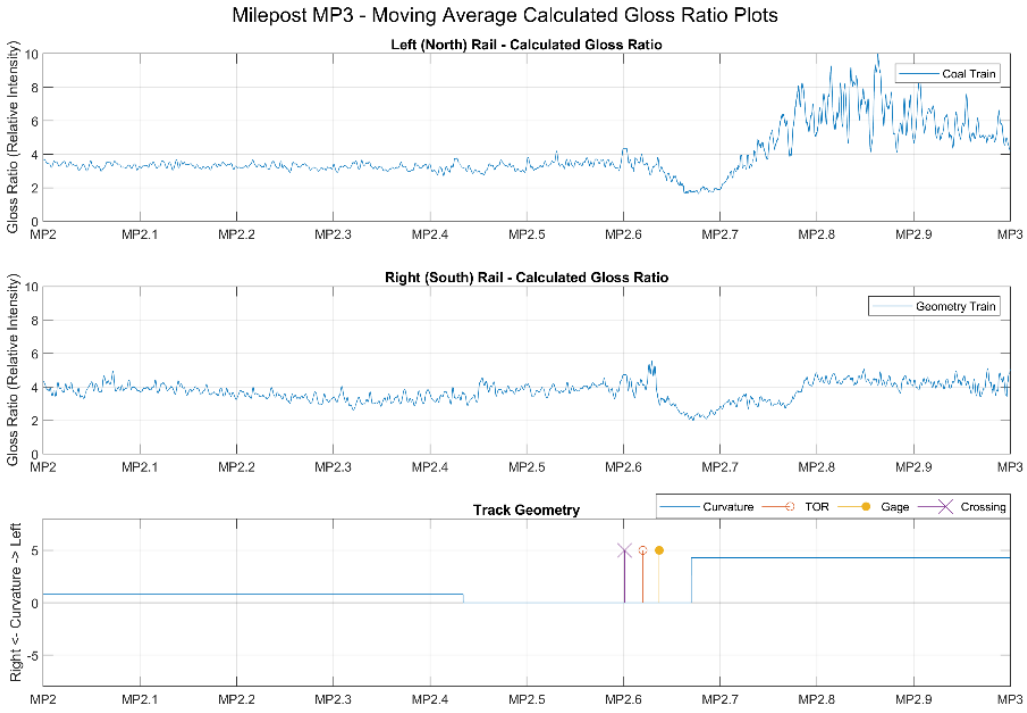

Figure 6-6: High variation in top-of-rail lubricity condition on left hand rail in a tight curve

During a field survey that was conducted as a follow up to the field testing, it was observed that there was signs of TORFM on the left hand rail contradicting the assumption that the rail was clean but these signs of TORFM were patchy and erratic. Based on this, the conclusion then became that the high points in the gloss ratio represented sections of clean rail and the low points were sections still treated with TORFM.

Figure 6-7: Non-uniform, "patchy" distribution of TORFM on the top-of-rail surface in a sharp curve

In the figure above, in the center of the image there is a shiny section of rail with darker sections surrounding it. There is no doubt that this is a high wear curve and as a result the rail is shinier as a result of higher surface wear. This patchy distribution of TORFM was observed by the optical sensor while on a moving platform but would pose serious challenges to any instrument that relies on spot measurements to evaluate rail lubricity. Without testing longer sections of track, it would be very easy to collect only a lubricated or a clean spot and draw a conclusion that is not representative of the track section as a whole. Multiple spot tests could alert the user to the issue by returning contradicting results but this could also further drive confusion as to whether the conflict was due to device operation error or representative of actual track conditions. As a result, moving testing like that performed in this study is more beneficial moving forward to avoid the local effects.

For this specific curve, the lubricity data shows clearly that the applicator is working but also that a large amount of the TORFM is being worn away in the curve. This reading could suggest to a maintenance-of-way engineer that increasing the application rate of the wayside applicator may provide added benefit to reducing the wear in the curve. The phantom applicator effect exiting the curve and the curves further down the track indicate that although much of the TORFM is being worn away on the specific contact patch for this curve, sufficient TORFM is continuing to spread down track and armed with the observations from the field survey the applicators appear to be working as intended.

6.2.6 Curve Fitting and Conditioning Effect

Visually looking at the data indicated that the trends for the data were roughly piecewise linear where the linear slope of the linear could be estimated to be proportional to the wear rate of the TORFM. The slopes of the linear curve fits decreased for both the left and right rail in MP2 following the second lubricator once the conditioning effect observed in a 2014 AREMA publication [32] had taken effect. This serves to confirm the behavior observed during the Norfolk Southern Corporation testing.

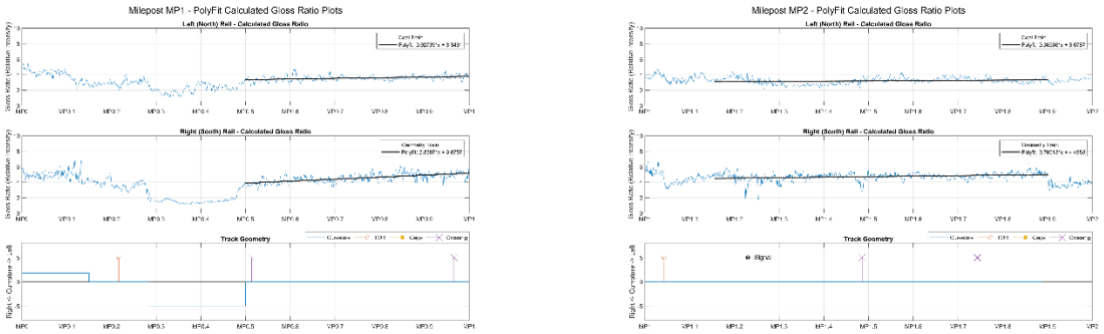

Figure 6-8: Comparison in trend line slope trailing the first TOR applicator (Left) and the second TOR applicator (Right)

When extending linear curve fits to predict carry distance, the results were less successful for the revenue service trains but may be predicative following the research track geometry train. After the first applicator, the trend line predicted about 1.38 miles of carry distance. After the second applicator, this distance extended to 3.64 miles of carry distance. After consulting with industry experts, these values are close to the carry distances that are expected. With only two data points, it is entirely possible that these are coincidental results and that trend line data is not predictive of carry distance. This is something that will need to be investigated further.

When looking farther down track, it was observed that the trend lines on MP4 and MP5 had different slopes despite being directly adjacent to each other. In response, a polynomial fit was applied to both sections and the following plot was created.

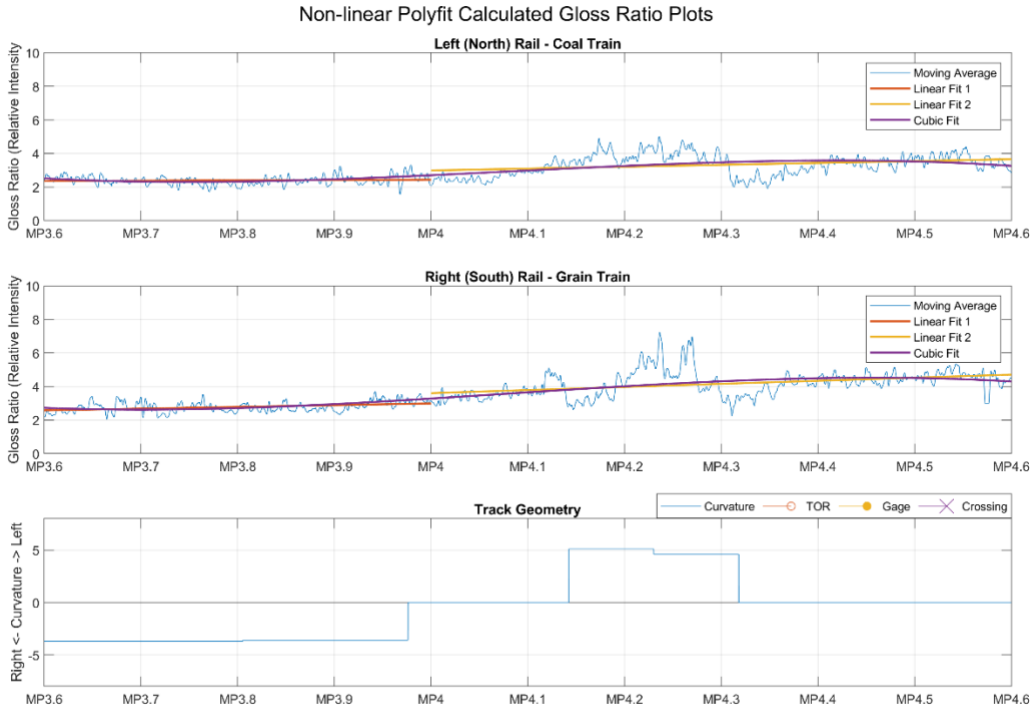

Figure 6-9: Various curve fits applied to Moving Average Filtered Calculated Gloss Ratio data

An odd order polynomial fit was selected to better fit the overall trend of the data at the ends and a cubic fit was chosen to minimize the order of the curve fit. A higher order fit will better fit the data but will be artificial and specific only to the data that it was fitted to. The cubic fit matches the data well but performs worse at the ends. The behavior of the data is closer to that of a sigmoid which has horizontal asymptotes at either end. The task of generating the shape of a predictive sigmoid curve highlights a strong need for more modeling of the propagation behavior of TORFM to build an accurate model.

6.2.7 Freight car wheel spatial frequency in Lubricity Data

At this point in the data processing, basic frequency domain analysis has been performed but there is significant potential for a much deeper dive into the frequency content of the lubricity data. The key findings in the frequency domain are peaks representing the wheel circumferences of the remote control rail cart and of a common diameter freight car wheel.

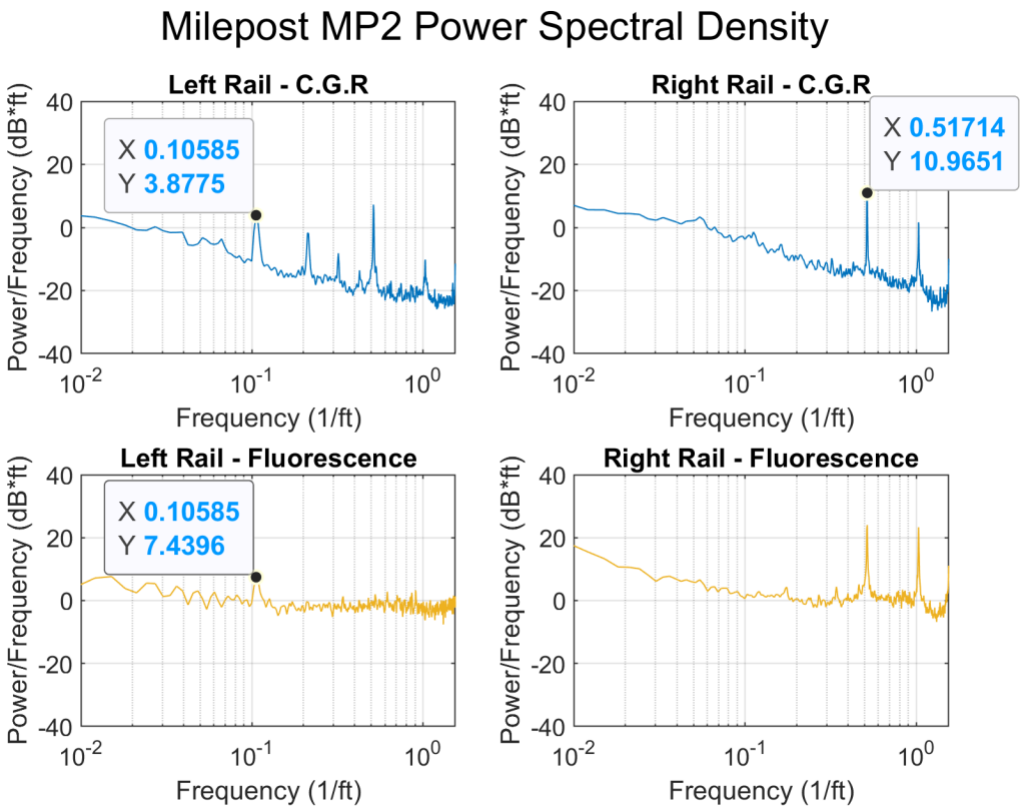

Figure 6-10: Power Spectral Density Plot of Lubricity Signals for Milepost 2 with Data Tips applied to Freight Car Wheel Frequency

The 0.5171 ft^{-1} frequency correlates to the circumference of the 23.25-inch diameter remote control rail cart wheels and are present in the majority of the PSD plots. Due to the low overall signal, the fluorescence PSD plots have limited frequency response especially when the overall fluorescent signal is near the noise floor. Under this operating condition, there is insufficient signal from the rail to couple a frequency response into the optical detector. The 0.10585 ft^{-1} peak correlates to the 36-inch diameter freight car wheel used on the majority of railroad rolling stock in the United States. For this frequency, the peak only appears on the left hand rail following the coal train. The coal train has a sufficient number of 36-inch wheel sets to inject frequency content into the lubricity signal whereas the track geometry train on the right hand rail does not. The lack of signal on the right hand rail when compared to the left is further evidence that the frequency content is the direct result of the third body TORFM layer on the top-of-rail surface rather than some physical phenomenon of the material surface of the top-of-rail surface. This TORFM propagation mode has been assumed based on the point application of TORFM at the applicator sites but, from the literature review for this study, has never been measured making this another novel discovery of the project.

The PSD can also be broken down into smaller blocks to track how the frequency content of the signal changes as a function of distance down track. Future analysis could make a moving PSD window and could extract and plot the magnitude of specific frequency bins to better describe the

change in frequency content down track. For this study, 1/10th mile blocks were used, and the results are beneficial in describing some of the dynamics of the frequency signal.

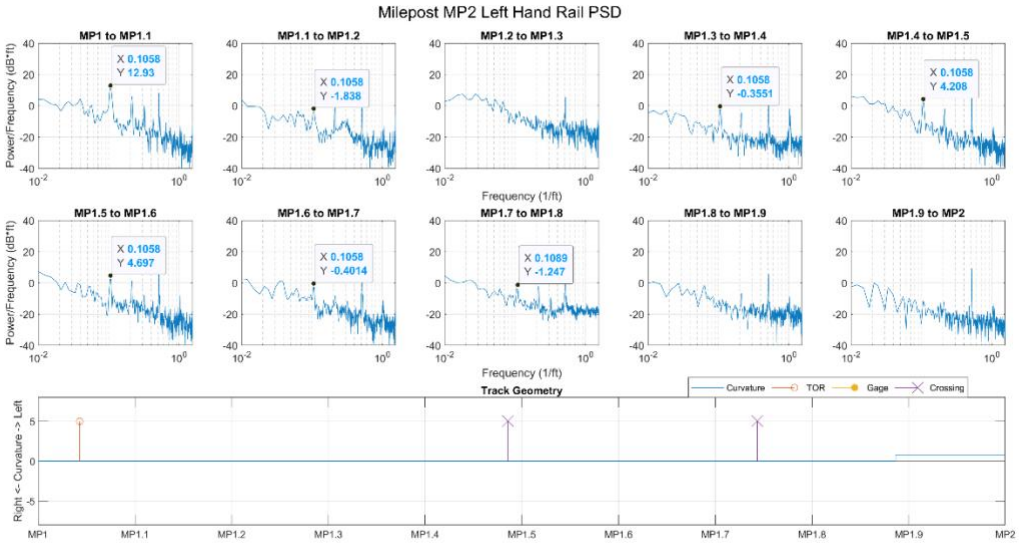

Figure 6-11: 1/10th milepost block Calculated Gloss Ratio Power Spectral Density Plots for Milepost 2 with Data Tips applied to Freight Car Wheel Frequencies

The left hand rail block PSD shows that while following the coal train the rail wheel frequency content is high for 0.8 miles down track from the applicator. There is one block 0.2 miles from the applicator that did not have significant excitation at the rail wheel frequency but the frequency returns immediately in the following block. This information was presented to industry experts who supported the idea of increasing the length of the wiper bar to more evenly deposit the TORFM around the wheel circumference.

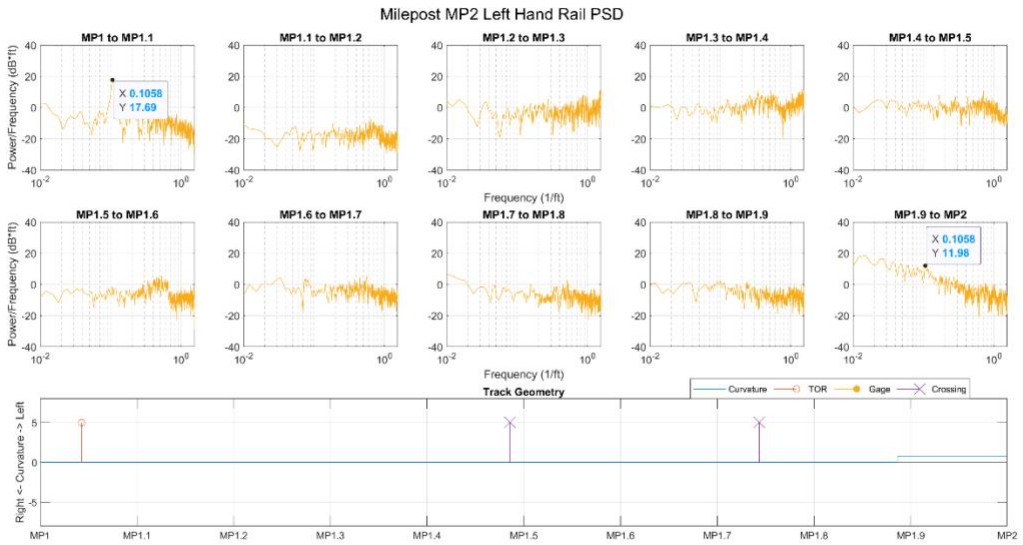

Figure 6-12: 1/10th milepost block Fluorescence Power Spectral Density Plots for Milepost 2 with Data Tips applied to Freight Car Wheel Frequencies

The fluorescence data remains less responsive to frequency excitation but has a corresponding peak at the applicator site in the first block. The frequency content quickly diminishes into the background until it reappears right at the entrance to the left hand curve at the end of the milepost. This recurrence of the rail wheel frequency also supports the concept of a phantom applicator effect from fresh TORFM lying dormant on the wheels coming into contact with the rail as the train shifts laterally through curves.

The lubricity signal is very feature rich and has components from a wide array of different extraneous factors beyond rail lubricity. This creates challenges when identifying the lubricity component of the system and rejecting outside interference. There is a significant amount of frequency domain analysis techniques that can be applied to this data and should be applied in future studies. This research also strongly recommends trialing longer wiper bars to disrupt the phase coherence of the passing rail wheels.

6.2.8 Conclusions

In conclusion, this research first and foremost affirms that moving optical testing of rail lubricity is effective and viable in monitoring the lubricity condition of the track. The optical instruments have been demonstrated as capable of identifying track lubricants by variations in the optical scattering power and fluorescent performance of the top-of-rail surface. Further, moving platform is essential in avoiding the inconsistencies inherent to spot analysis techniques. The resulting data signal is very feature rich and has some complications when it comes to isolating the optical signal. As a result, the data requires analysis of trends and is lubricity assessment is less successful in making specific evaluations at a spot without comparing to a cleaned rail condition. This also means that the data can be filtered and processed in a myriad of ways to isolate other useful component signals that have yet to be identified. This could include analyzing the normal and

diffuse scattering channels independently to access the surface roughness of the rail. The measurement of the phantom applicator effect is a novel discovery and the frequency analysis that can identify the beat frequency of a railroad wheel while distributing TORFM is also a feature that, from our review, has not been measured before.

This research demonstrates a conclusive need for a deeper understanding into the physical mechanics of the spreading of TORFM down rail. The linear curve fitting demonstrated strong piecewise linear curve fits but non-linearity over longer distance. With a deeper understanding of TORFM propagation and an increased test sample set it will be possible to begin constructing predicative models of TORFM propagation and wear behavior and overall effective carry distance. The correlation of other sensor types, namely lateral force sites, will also greatly improve the discrete levels of TORFM evaluation this sensor can provide.

This sensor corroborates the conditioning effect described in the 2014 AREMA paper on "Considerations on choosing a Top-of-Rail (TOR) Material" [32] and demonstrates the different amounts of TORFM that are left behind after different types of rail traffic. Based on this testing, in the future a Rail Lubricity Sensor can easily be mounted on a track research car and take advantage of the higher overall lubricity signal levels behind a research car to increase the detectivity of the sensor. In this configuration, the frequency content of the rail wheel beat frequency is diminished but the trade off on overall signal magnitude is an advantage. Finally, this research would strongly suggest trailing a longer applicator bar to limit the phase coherence of the rail wheels when spreading the TORFM down track.

6.3 Future Steps

The key takeaway from this research is the validity and viability of conducting moving top-of-rail lubricity evaluation with custom optical systems. Moving forward, the key future step will be to conduct more moving testing. The moving analysis has demonstrated how the stochastics of rail surface condition and lubricant propagation down track restrict the viability of point based measurements such that they are not necessarily representative of lubricity trends. Additional moving testing on the same section of track will allow for a better understanding of the actual lubricity conditions. There are a couple different tests that could shed some valuable insight into the specific mechanics that govern the propagation of rail lubricants down track. The lubricators along the section of track tested in this research could be shut off for a short period until all of the TORFM is worn away. A definitive clean rail assessment could be collected and then successive measurements could be collected after the applicators are reactivated. This could also be conducted in tandem with the rail grinding schedule for that line. The rail grinding process will remove all TORFM that may be entrained into surface figure of the rail leaving a definitive clean rail condition behind. Another test could be conducted on a long straight section of rail with a single applicator present at the start point. Under these conditions, the extinction mechanics of TORFM could be more precisely evaluated and a baseline understanding of the optimal carry distance could be gathered.

Both of these suggested test conditions hint at the underlying need for future research into the contact mechanics, propagation, and fade out behavior of TORFM during railroad operations. Visual observations with camera systems, seeding the TORFM with fluorescent dye, simulation

studies, and others may be necessary to better understand this aspect of TORFM and its effectiveness in railroad operations. A roller rig, like the VT-FRA roller rig at RTL, could be an ideal candidate to study, at a small scale, the contact and spreading dynamics of TORFM and also the extinction models and changes in lateral forces during fade out of the TORFM. This knowledge and understanding will be fundamental when it comes to creating predicative models for TORFM effectiveness and carry distance.

In chapter 5 during the signal processing and data analysis, it was observed that the lubricity conditions were different between each of the runs as a function of the train traffic that came before. This was very fortunate during this research study as it highlighted several different lubricity modes from the different traffic that runs on this section of track. Unfortunately, this strongly limits the amount of run-to-run comparisons that can be made which in turn limits the ability to create accurate models of rail lubricity behavior. Additional test runs will allow for the collection of different rail conditions due to the stochastic manner in which the TORFM is applied to the rail.

Testing new sections of track is also an important future step. New sections of track are important for verifying that lubricity assessments are not specific to local track geometry. While selecting new sections of track to test, it would be advantageous to conduct lubricity assessment at a lateral force site equipped with strain gages. Currently, optical measurements are only a relative measures of track lubricity. Optical methods have so far been determined to be capable of assessing the presence or absence of track lubricants and, to a more limited degree, a qualitative assessment to the magnitude of the lubricity on the rail head. By combining lateral force site measurements with optical lubricity data it will be possible to correlate qualitative optical measurements with quantitative amounts of lateral force reduction. This correlation will go a long way to providing a definitive point where the lubrication on the top-of-rail surface is no longer providing an adequate reduction in lateral forces and is insufficient.

The remote control rail cart will continue to be a useful tool in collecting test data for intermediate speed / intermediate range lubricity testing; however, it has always been a goal of this project to develop a sensor that can be meshed into existing track metrology vehicles. The third generation Rail Lubricity Sensor is a strong candidate for mounting on a track geometry car for high speed / long distance testing. This round of field testing showed that even if the axle count of the geometry train was not sufficient to inject a strong rail wheel related spatial frequency into the lubricity data, the overall signal levels were much higher following the track geometry car increasing the detectivity of the sensor. Combining and correlating the optical data with other rail metrics will provide for a holistic view of the rail lubricants and their effectiveness. Evaluating lubricated rail in comparison with wear data for untreated sections will go a long way to defining the benefit and return on investment that the railroads are looking for. A long term final sensor would be able to couple into existing track metrology measurements and the “big data” methods used to develop predicative maintenance models. Combining lubricity measurements with rail wear and profile data can provide a robust and holistic look at quantifying the performance and benefit of track lubricity programs.

References

[1] Tuzik, B., 2018, "Getting a Grip on Friction: Causes and Cures," Railway Track and Structures, December 2018.
[2] Kumar, S., Kumar, U., Chattopadhyay, G., and Reddy, V., "Issues and challenges with logistics of rail maintenance," Proc. International Intelligent Logistics Systems Conference: 22/02/2006-23/06/2006, Australian Society for Operations Research, pp. 16.11-16.19.
[3] Diamond, S., and Wolf, E., 2002, "Transportation for the 21st century," TracGlide Top-of-Rail Lubrication System, Department of Energy, USA.
[4] Neighborgall, C., Mast, T., Peterson, A., Ahmadian, M., and Holton, C., "Development of Laser/LED-Based Instrument for Optical Detection of Railroad Top-of-Rail (ToR) Friction Modifiers and Lubricity Conditions," Proc. 2019 Joint Rail Conference, American Society of Mechanical Engineers Digital Collection.
[5] Iwnicki, S., Spiryagin, M., Cole, C., and McSweeney, T., 2019, Handbook of railway vehicle dynamics, CRC press.
[6] Plotkin, D., 2000, "Evaluation of a Top-of-Rail Lubrication System."
[7] Reiff, R., Pena, R., Davis, K., and Clifton, M., 2004, "Locomotive-Based Top of Rail Friction Control Implementation Results and Issues. Phase 1: Atomized Spray/Friction Control Product."
[8] Eadie, D., and Santoro, M., 2006, "Top-of-rail friction control for curve noise mitigation and corrugation rate reduction," Journal of sound and vibration, 293(3-5), pp. 747-757.
[9] Eadie, D. T., Santoro, M., and Kalousek, J., 2005, "Railway noise and the effect of top of rail liquid friction modifiers: changes in sound and vibration spectral distributions in curves," Wear, 258(7-8), pp. 1148-1155.
[10] Akira Matsumoto, Y. S., Hiroyuki Ohno, Masao Tomeoka, Kousuke Matsumoto, Tomohisa Ogino, Masuhisa Tanimoto, Yasushi Oka, Masayuki Okamo, 2005, "Improvement of bogie curving performance by using friction modifier to rail/wheel interface," Wear(258), p. 9.
[11] Oldknow, K., and Reiff, R., 2006, "Use of Dynamic Rail Deflection as a Means of Determining Changes in Top of Rail Friction."
[12] Cortis, D., Giulianelli, S., Malavasi, G., and Rossi, S., 2017, "Self-diagnosis method for checking the wayside systems for wheel-rail vertical load measurement," Transport Problems, 12.
[13] Lundberg, J., Rantatalo, M., Wanhainen, C., and Casselgren, J., 2015, "Measurements of friction coefficients between rails lubricated with a friction modifier and the wheels of an IORE locomotive during real working conditions," Wear, 324, pp. 109-117.
[14] Alarcón, G. I., Burgelman, N., Meza, J. M., Toro, A., and Li, Z., 2015, "The influence of rail lubrication on energy dissipation in the wheel/rail contact: a comparison of simulation results with field measurements," Wear, 330, pp. 533-539.
[15] Harmer Steel, 2014, "136-lb/yd AREMA Rail,"http://www.harmersteel.com/tee-rails/136-lb-yd-arema-rail/.
[16] Public Domain, 2011, "Graphical List of Track Gauges," Wikimedia Commons, https://commons.wikimedia.org/wiki/File:Track_gauge.svg.
[17] Esveld, C., Markine, V. L., and Shevtsov, I. Y., 2006, "Shape optimisation of a railway wheel profile," Global Railway Review https://www.globalrailwayreview.com/article/2222/shape-optimisation-of-a-railway-wheel-profile/.
[18] Redtenbacher, F. J., 1855, Die Gesetze des Lokomotiv-Baues, Mannheim : Bassermann.

[19] Iwnicki, S., 2006, Handbook of Railway Vehicle Dynamics, CRC Press, Boca Raton.
[20] Klingel, W., 1883, "Uber den Lauf der Eisenbahnwagen auf gerader Bahn," Organ fur die Fortschritte des Eisenbahnwesens in technischer Beziehung.
[21] Reynolds, O., 1875, "On the efficiency of belts or straps as communicators of work," Journal of the Franklin Institute, 99(2), pp. 142-145.
[22] Carter, F., "The Electric Locomotive (Including Appendix and Plate at Back of Volume)," Proc. Minutes of the Proceedings of the Institution of Civil Engineers, Thomas Telford-ICE Virtual Library, pp. 221-252.
[23] Dukkipati, R. V., 2000, Vehicle dynamics, CRC Press.
[24] LB Foster, "Wayside TOR Applicator Figure,"https://www.lbfoster.eu/perch/resources/solutions/lbfoster-keltrack-tor-friction-modifier-datasheet.pdf.
[25] Association of American Railroads, 2013, "Total Annual Spending 2013 Data," https://blog.midwestind.com//wp-content/uploads/2017/11/2013-AAR_spending-graphic-fact-sheet.pdf.
[26] Donald T. Eadie. Dave Elvidge, K. O., Richard Stock, Peter Pointner, Joe Kalousek, Peter Klauser, 2008, "The effects of top of rail friction modifier on wear and rolling contact fatigue: Full-scale rail-wheel test rig evaluation, analysis and modelling," Wear(265), p. 8.
[27] S. Kumar, G. C., V. Reddy, U. Kumar, 2006, "Issues and Challenges with Logisitics of Rail Maintenance," Second International intelligent Logistics Systems Conference.
[28] Plotkin, D., 2000, "Evaluation of a Top-of-Rail Lubrication System," Federal Railroad Administration.
[29] Matsumoto, A., Sato, Y., Ohno, H., Tomeoka, M., Matsumoto, K., Ogino, T., Tanimoto, M., Oka, Y., and Okano, M., 2005, "Improvement of bogie curving performance by using friction modifier to rail/wheel interface: Verification by full-scale rolling stand test," Wear, 258(7-8), pp. 1201-1208.
[30] Waara, P., 2000, "Wear reduction performance of rail flange lubrication," Luleå tekniska universitet.
[31] Singh, D. L., 2018, "The Application of Laser Technology for Railroad Top of Rail (TOR) Friction Modifier Detection and Measurements," Masters of Science in Mechanical Engineering, Virginia Polytechnic Institute and State University, Blacksburg, Virginia, USA.
[32] Chiddick, K., Kerchof, B., and Conn, K., "Considerations in Choosing a top-of-rail (TOR) Material," Proc. AREMA Annual Conference and Exposition, Chicago, IL, pp. 1-21.
[33] Matsumoto, A., Sato, Y., Ohno, H., Shimizu, M., Kurihara, J., Tomeoka, M., Saitou, T., Michitsuji, Y., Tanimoto, M., and Sato, Y., 2012, "Continuous observation of wheel/rail contact forces in curved track and theoretical considerations," Vehicle system dynamics, 50(sup1), pp. 349-364.
[34] Lu, X., Cotter, J., and Eadie, D., 2005, "Laboratory study of the tribological properties of friction modifier thin films for friction control at the wheel/rail interface," Wear, 259(7-12), pp. 1262-1269.
[35] Tomberger, C., Dietmaier, P., Sextro, W., and Six, K., 2011, "Friction in wheel–rail contact: a model comprising interfacial fluids, surface roughness and temperature," Wear, 271(1-2), pp. 2-12.
[36] Rajpal S. Sirohi, F. S. C., 1999, Optical Methods of Measurement, New York.

[37] Hasan, A. M., 2016, "Quantitative Laser-based Assessment of Top of Rail Friction Modifiers for Railroad Application," Doctor of Science, Virginia Polytechnic Institute and State University.
[38] Xie, J., and Kar, A., 1999, "Laser welding of thin sheet steel with surface oxidation," WELDING JOURNAL-NEW YORK-, 78, pp. 343-s.
[39] Stone, R. A., 1994, "Roughness and Relection in Machine Vision," Doctor of Philosophy, Carnegie-Mellon University.
[40] Michael R. Cohen, L. J. S., III, "Diffuse Reflectance Measurements of Standard Diffusers," https://www.4physics.com/tn3/lambertian.htm.
[41] Orellana, G., 2006, "Fluorescence-based sensors," Optical Chemical Sensing, A. N. C. F. Baldini, J. Homola, S. Martellucci, ed., Springer, p. 535.
[42] Sharma, A., and Schulman, S. G., 1999, Introduction to fluorescence spectroscopy, Wiley New York.
[43] Smith, W. J., 2008, Modern optical engineering, Tata McGraw-Hill Education.
[44] A. Kapoor, F. J. F., S.K. Wong, M. Ishida, 2002, "Surface roughness and plastic flow in rail wheel contact," Wear(253), p. 8.
[45] Torrance, K. E., and Sparrow, E. M., 1967, "Theory for off-specular reflection from roughened surfaces," Josa, 57(9), pp. 1105-1114.
[46] Kiely, A. B., Lettieri, T. R., and Vorburger, T. V., 1992, "A model of an optical roughness-measuring instrument," International Journal of Machine Tools and Manufacture, 32(1-2), pp. 33-35.
[47] Fresnel, A., 1868, Oeuvres complètes d'augustin Fresnel, Imprimerie impériale.
[48] Freeman, J., 2013, "Gloss Samples," Wikipedia, https://commons.wikimedia.org/wiki/File:Gloss-samples.gif.
[49] Kerchof, B., 2019, "Adverse High Rail Profiles," Railway Track and Structures, December 2019.
[50] Hasan, A. M., 2016, "Quantitative Laser-based Assessment of Top of Rail Friction Modifiers for Railroad Application," Doctor of Philosophy in Mechanical Engineering, Virginia Polytechnic Institute and State University, Blacksburg, VA, USA.
[51] Mast, T., Neighborgall, C., Taheri, M., Holton, C., and Ahmadian, M., "Considerations for Sensor Selection for Detecting Top-of-Rail (TOR) Lubrication " Proc. 2020 Joint Rail Conference, American Society of Mechanical Engineers Digital Collection.
[52] Holton, C., 2020, "Rail Lubricity Gloss Ratio Sensor Unit: February, 2020," Technical Note No. TN 20-01, Railway Technologies Laboratory.
[53] Holton, C., 2019, "Results of TOR Thickness Testing: December 2019," Technical Note No. TN 19-03, Railway Technologies Laboratory.
[54] Association of American Railroads, 2019, "AAR Freight Rail Fact Sheet 2019," https://www.aar.org/wp-content/uploads/2019/01/AAR-Freight-Rail-Fact-Sheet-2019.pdf.
[55] Shannon, C. E., 1949, "Communication in the presence of noise," Proceedings of the IRE, 37(1), pp. 10-21.
[56] The MathWorks Inc., 2020, "Increase Precision of Numeric Calculations," https://www.mathworks.com/help/symbolic/increase-precision-of-numeric-calculations.html.
[57] Schlessinger, M., 1995, "Infrared Technology Fundamentals: Revised and Expanded," Optical Engineering-New York-Marcel Dekker Incorporated-, 49, pp. 46-46.
[58] Smith, S. W., 1997, "The scientist and engineer's guide to digital signal processing."
[59] Solomon Jr, O., 1991, "PSD computations using Welch's method," STIN, 92, p. 23584.

ACKNOWLEDGEMENTS

The authors wish to thank and acknowledge the US Department of Transportation, University Transportation Center Program (RailTEAM UTC) for funding support for this research.

ABOUT THE AUTHORS

Mehdi Ahmadian, J. Bernard Jones Chair and Director

Dr. Mehdi Ahmadian is a Dan Pletta Professor of Mechanical Engineering at Virginia Tech, where he also holds the position of Director of Center for Vehicle Systems and Safety (CVeSS), and the Railway Technologies Laboratory (RLT). Dr. Ahmadian has authored more than 130 archival journal publications and more than 250 conference publications, including a number of keynote lectures. He has served as Editor or Editor-in-Chief for four journals on Vehicle System Dynamics, Vibration and Control, Shock and Vibration and Automobile Engineering. Dr. Ahmadian is Fellow of American Society of Mechanical Engineers of the American Institute for Aeronautics and Astronautics (AIAA). He has received many distinguished scholar awards.

Timothy E. Mast

Mr. Timothy Mast was a Graduate Research Assistant in mechanical engineering working on this project. He served as the Locomotives Chair for the ASME Rail Transportation Division Progress Reports Committee. He was also a Controls and Dynamics Engineer with a strong interest in Locomotives, Track Geometry Cars, and the rail industry in general. He obtained his Bachelor of Science in Mechanical Engineering from Messiah University and master's degree in mechanical engineering from Virginia Tech.